

**Synthesis, structure-activity relationships and biological evaluation of optimised terminally alkylated (bis)urea and (bis)thiourea polyamine analogues as antiplasmodial agents**

By  
Ethan Besaans

---

Submitted in partial fulfilment of the requirements for the degree:

*Magister Scientiae* Biochemistry

In the Faculty of Natural and Agricultural Sciences

University of Pretoria

Pretoria

November 2016



UNIVERSITEIT VAN PRETORIA  
UNIVERSITY OF PRETORIA  
YUNIBESITHI YA PRETORIA

Plagiarism declaration:

University of Pretoria

Faculty of Natural and Agricultural Sciences

Department of Biochemistry

Full name: **Ethan Besaans** Student number: **u10111442**

Title of work: **Synthesis, structure-activity relationships and biological evaluation of optimised terminally alkylated (bis)urea and (bis)thiourea polyamine analogues as antiplasmodial agents**

Declaration:

I understand what plagiarism entails and am aware of the University's policy in this regard.

I declare that this thesis is my own, original work. Where someone else's work was used (whether from a printed source, the internet or any other source due acknowledgement was given and reference was made according to departmental requirements.

I did not make use of another student's previous work and submit it as my own.

I did not allow and will not allow anyone to copy my work with the intention of presenting it as his or her own work.

Signature: \_\_\_\_\_



Date: \_\_\_\_\_

## Acknowledgments

I would like to thank my supervisor, Prof. Lyn-Marie Birkholtz for her guidance, patience and faith in my capabilities. I would like to thank my co-supervisor Dr. Natasha October for her advice and guidance while synthesising the compounds. I would like to thank Dr. E. Palmer for assistance with NMR analysis, Dr. D. Koontz for MS and UPLC analysis and Dr. A. Andayi for his advice and support with the synthesis of the compounds. Thanks to the students of the Malaria group and the staff at the Department of Biochemistry (University of Pretoria). I would like to thank Dr. Bianca Verlinden for her support and guidance, Dr. Dina Coertzen for culturing parasites for the study.

I would like to acknowledge, the South African National Research Foundation and the University of Pretoria for funding this project and the bursary provided by the DST/NRF South African Research Chair (SARChI) programme.

I would like to thank my mother, for her support and editing services. I would like to thank all my friends for putting up with me and finally I would like to thank my wife without you, life would be like a broken pencil.

## Summary

The sustained control and elimination of malaria requires novel approaches to combat the emergence of drug resistance. *Plasmodium falciparum* causes the most lethal form of human malaria. Current therapeutics have shown decreased efficacy as a result of *P. falciparum* developing resistance to them. Consequently, novel antimalarial agents with new mechanisms of action are urgently needed to aid in the control and ultimate eradication of this disease and should display low resistance indices and high selectivity indices. Polyamines are involved in a variety of cellular functions including cell differentiation and proliferation and have been shown to be essential to malaria parasites *in vitro*. However, these analogues lacked drug-like properties, negating their use in malaria disease models *in vivo*. The objective of this study was to develop novel polyamine analogues based on a previous generation of compounds and to determine their antiplasmodial activity *in vitro*. Consequently, a novel series of (bis)urea and (bis)thiourea polyamine analogues were designed and synthesised with moderately high yields and purity. *In silico* evaluation of drug-likeness of these compounds indicated low oral bioavailability overall, although the predicted values were improved over the parent series. The antiplasmodial activity of the novel analogues indicated that halogenation generally decreases activity except for bromination, which did improve *in vitro* activity. Cheminformatics analysis enabled in-depth analysis of the structure-activity relationships (SAR) of this class of compounds, allowing structural features to be identified that are important for activity. Complementing the SAR with quantitative structure-activity relationships (QSAR) allowed the determination of a descriptor that weakly correlates with the analogues' activities. The structural requirements for activity were found to be based on representations of the polyamine analogues molecular structures by means of circular atom neighbourhood's. This work therefore contributed to the further development of the polyamine analogues as potential antimalarial drugs.

## TABLE OF CONTENTS

<b>Acknowledgments</b> .....	<b>iii</b>
<b>Summary</b> .....	<b>iv</b>
<b>TABLE OF CONTENTS</b> .....	<b>v</b>
<b>LIST OF FIGURES</b> .....	<b>vii</b>
<b>LIST OF TABLES</b> .....	<b>x</b>
<b>LIST OF ABBREVIATIONS</b> .....	<b>xi</b>
<b>Chapter 1: Introduction</b> .....	<b>1</b>
1.1 Malaria .....	1
1.2 Life cycle of <i>P. falciparum</i> parasites.....	3
1.3. The control of malaria .....	5
1.4. Polyamine properties and functions .....	10
1.5. Polyamine metabolism and transport.....	11
1.6 Polyamine metabolism as a drug target.....	15
1.7 Hypothesis .....	24
1.8 Research Objectives.....	24
<b>Chapter 2: Materials and Methods</b> .....	<b>25</b>
2.1 Synthesis of Polyamino(bis)ureas and Polyamino(bis)thioureas.....	25
2.2 Antiplasmodial activity determination .....	28
2.3 Cheminformatic analysis of Polyamino(bis)ureas and Polyamino(bis)thioureas .....	31
<b>Chapter 3: Results</b> .....	<b>34</b>
3.1 Synthesis of Polyamino(bis)ureas and Polyamino(bis)thioureas.....	34
3.1.1 Synthesis of analogues based on the 3-5-3 backbone .....	34
3.1.2 Synthesis of analogues based on the 3-piperaziny-3 backbone .....	48
3.2 Antiplasmodial activity determination .....	52
3.3 Cheminformatic analysis of Polyamino(bis)ureas and Polyamino(bis)thioureas polyamine analogues .....	59

<b>Chapter 4: Discussion .....</b>	<b>71</b>
<b>Chapter 5: Conclusion .....</b>	<b>82</b>
<b>Chapter 6: References .....</b>	<b>83</b>
<b>Appendix:.....</b>	<b>92</b>

## LIST OF FIGURES

Figure 1.1: World map showing the global malaria transmission areas, areas with limited risk and areas with no malaria transmission. ....	2
Figure 1.2: The lifecycle of <i>P. falciparum</i> parasites. ....	4
Figure 1.3: Chemical structures of antimalarials .....	6
Figure 1.5: The chemical structures of the three main polyamines. ....	10
Figure 1.6: Polyamine biosynthetic pathways and transport systems present in the human host and <i>P. falciparum</i> parasites. ....	13
Figure 1.7: Structures of symmetrically substituted bis(alkyl) polyamine analogues. ....	17
Figure 1.8: Structures of symmetrically substituted bis(alkyl) polyamine analogues. ....	18
Figure 1.9: Structure of MDL 27695. ....	18
Figure 1.10: Structure of BW-1. ....	19
Figure 1.11: Structures of XBI-54-12C, XBI-54-13D and XBI-54-13B. ....	20
Figure 1.12: Structures of (bis)urea and (bis)thiourea analogues. ....	20
Figure 1.13: Structure of the lead (bis)urea alkylated polyamine analogues. ....	21
Figure 1.14: Preliminary antiplasmodial structure-activity relationships for symmetrical substituted polyamines. ....	23
Scheme 1: Synthetic scheme of (bis)ureas and (bis)thiourea analogues based on the 3-5-3 backbone. ....	34
Figure 3.1: TLC chromatogram of <i>1,13-dinitrile-4,10-diazotridecane</i> (2) .....	35
Figure 3.2: <sup>1</sup> H NMR spectrum of <i>1,13-dinitrile-4,10-diazotridecane</i> (2) .....	36
Figure 3.3: Mass spectrum of <i>1,13-Dinitrile-4,10-diazotridecane</i> (2) .....	36
Figure 3.4: TLC chromatogram of <i>1, 13-dinitrile-4, 10-(di-tert-butyloxycarbonyl)-4, 10-diazotridecane</i> (3) A and column chromatography purification B, C and D .....	37
Figure 3.5: <sup>1</sup> H NMR spectrum of <i>1, 13-dinitrile-4, 10-(di-tert-butyloxycarbonyl)-4, 10-diazotridecane</i> (3) .....	38
Figure 3.6: Mass spectrum of <i>1, 13-dinitrile-4, 10-(di-tert-butyloxycarbonyl)-4, 10-diazotridecane</i> (3) .....	38
Figure 3.7: TLC chromatogram of <i>1, 13-diamino-4, 10-di(tert-butyloxycarbonyl)-4, 10-diazotridecane</i> (4) .....	39
Figure 3.8: <sup>1</sup> H NMR spectrum of <i>1, 13-diamino-4, 10-(di-tert-butyloxycarbonyl)-4, 10-diazotridecane</i> (4) .....	40
.....	41

Figure 3.9: Mass spectrum of 1, 13-diamino-4, 10-(di-tert-butyloxycarbonyl)-4, 10-diazotridecane (4).....	41
Figure 3.10: TLC chromatogram of 1,13-bis-[3-(4-chlorophenyl)thioureido]-4,10-di(tert-butyloxycarbonyl)-4,10-diazatridecane (E1SB) and column chromatography purification.....	42
Figure 3.11: <sup>1</sup> H NMR spectrum of 1,13-bis-[3-(4-chlorophenyl)thioureido]-4,10-di(tert-butyloxycarbonyl)-4,10-diazatridecane (E1SB) .....	43
Figure 3.12: Mass spectrum of 1,13-bis-[3-(4-chlorophenyl)thioureido]-4,10-di(tert-butyloxycarbonyl)-4,10-diazatridecane (E1SB) .....	44
Figure 3.13: TLC chromatogram of 1,13-bis-[3-(4-chlorophenyl)thioureido]- 4,10-diazatridecane (E1SD). .....	45
Figure 3.14: <sup>1</sup> H NMR spectrum of 1,13-bis-[3-(4-chlorophenyl)thioureido]- 4,10-diazatridecane (E1SD) .....	46
Figure 3.15: Mass spectrum of 1,13-bis-[3-(4-chlorophenyl)thioureido]-4,10-diazatridecane (E1SD).....	46
Figure 3.16: UPLC purity determination chromatogram of 1,13-bis-[3-(4-chlorophenyl)thioureido]-4,10-diazatridecane (E1SD).....	47
Scheme 2: Synthetic scheme of (bis)ureas and (bis)thiourea analogues based on the 3-piperazinyl-3 backbone. ....	48
Figure 3.17: TLC chromatogram of 1,4-bis{3-[3-(4-fluorophenyl)thioureido]propyl}-piperazine (A3S). ....	49
Figure 3.18: <sup>1</sup> H NMR spectrum of 1,4-bis{3-[3-(4-fluorophenyl)thioureido]propyl}-piperazine (A3S). ....	50
Figure 3.19: Mass spectrum of 1,4-bis{3-[3-(4-fluorophenyl)thioureido]propyl}-piperazine (A3S) .....	51
Figure 3.20: Dose-response curve of <i>P. falciparum</i> parasites after treatment with the 3-5-3 polyamine analogues. ....	53
Figure 3.21: <i>P. falciparum</i> (3D7) parasites after treatment with the 3-5-3 polyamine analogues.....	55
Figure 3.22 as on page 57: Dose-response curve of <i>P. falciparum</i> parasites after treatment with the 3-piperazinyl-3 polyamine analogues.....	58
Figure 3.23: Principle component analysis of the polyamine analogues chemical space using Chem-GPS. ....	63



Figure 3.24: Molecular similarity analysis of the chemical space of the polyamine analogues. Self-organizing map depicting structural-activity landscape. ....	64
Figure 3.25 as on page 66: Matched molecular pair activity cliff analysis of the polyamine analogues. A) Separated on backbone, B) separated on internal substituents and C) separated on terminal groups. ....	67
Figure 3.26: Matched molecular pair activity cliff analysis of the 3-5-3 backbone compounds in the data set. ....	68
Appendix figure 1: <sup>1</sup> H NMR spectrum of <i>1,13-dinitrile-4,10-diazotridecane</i> (2) showing integration. ....	92
Appendix figure 2: <sup>1</sup> H NMR spectrum of <i>1,13-dinitrile-4,10-(di-tert-butyloxycarbonyl)-4,10-diazotridecane</i> (3) showing integration. ....	92
Appendix figure 3: <sup>1</sup> H NMR spectrum of <i>1,13-diamino-4,10-(di-tert-butyloxycarbonyl)-4,10-diazotridecane</i> (4) showing integration. ....	93
Appendix figure 4: <sup>1</sup> H NMR spectrum of <i>1,13-bis-[3-(4-chlorophenyl)thioureido]-4,10-di(tert-butyloxycarbonyl)-4,10-diazatridecane</i> (E1SB) showing integration. ....	93
Appendix figure 5: <sup>1</sup> H NMR spectrum of <i>1,13-bis-[3-(4-chlorophenyl)thioureido]-4,10-diazatridecane</i> (E1SD) showing integration. ....	94

## LIST OF TABLES

Table 1.1: Antimalarial drugs.....	9
Table 3.1: Analogue synthesis summary of compounds E1SB-E4OB. ....	44
Table 3.2: Analogue synthesis summary of compounds E1SD-E4OD.....	47
Table 3.3: Analogue synthesis summary of compounds A1S-A5O.....	51
Table 3.4: Antiplasmodial activities of the 3-5-3 backbone polyamine analogues....	55
Table 3.5: Antiplasmodial activities of the 3-piperazinyl-3 backbone polyamine analogues.....	58
Table 3.6: ADMET prediction of 3-5-3 polyamine analogues. ....	59
Table 3.7: Drug-likeness prediction of 3-5-3 polyamine analogues. <i>In silico</i> physiochemical predictors were obtained using the Discovery Studio Modelling Environment program.....	60
Table 3.8: ADMET prediction of 3-piperazinyl-3 polyamine analogues .....	61
Table 3.9: Drug-likeness prediction of 3-piperazinyl-3 polyamine analogues.....	62
Table 3.10: Training set models summary. ....	69
Table 3.11: Test set models summary .....	70
Appendix Table 1. Database of polyamine analogues .....	95
Appendix Table 2A: Top 20% SALI summary MMP analysis of polyamine analogues separated on backbone.....	97
Appendix Table 2B: Top 20% SALI summary MMP analysis of polyamine analogues separated based on internal substituents.....	98
Appendix Table 2B: Top 20% SALI summary MMP analysis of polyamine analogues separated based on internal substituents continued. ....	99
Appendix Table 2C: Top 20% SALI summary MMP analysis of polyamine analogues separated on terminal.....	100
Appendix Table 3: Top 20% SALI summary MMP analysis of polyamine analogues of the 3-5-3 backbone. ....	100

## LIST OF ABBREVIATIONS

ACTs	Artemisinin-based combination therapies
ADMET	Absorption, Distribution, Metabolism, Excretion and Toxicity
AdoMet	S-adenosylmethionine
AdoMetDC	S-adenosylmethionine decarboxylase
CLogP	Calculated LogP
dcAdoMet	decarboxylated S-adenosylmethionine.
DFMO	<i>DL-<math>\alpha</math>-difluoromethylornithine</i>
DIPEA	<i>N,N-Diisopropylethylamine</i>
ECFPs	Extended connectivity fingerprints
GMAP	Global Malaria Action Plan
LLE	Ligand-lipophilicity efficiency
LLINs	Long-lasting insecticidal nets
LSD1	Lysine-specific demethylase 1
MAE	Mean absolute error
MGBG	Methylglyoxalbis(guanylhydrazone)
MOA	Mode of action
MSA	Molecular similarity analysis
NPP	Newly formed permeation pathways
ODC	Ornithine decarboxylase
PCA	Principal Component analysis
QED	Quantitative Estimate of Drug-likeness
R <sup>2</sup>	Squared correlation coefficient
RMSE	Root mean square error
SALI	Structure-activity landscape index
SAR	Structure-activity relationship
TLC	Thin layer chromatography
WHO	World Health Organization

# Chapter 1: Introduction

## 1.1 Malaria

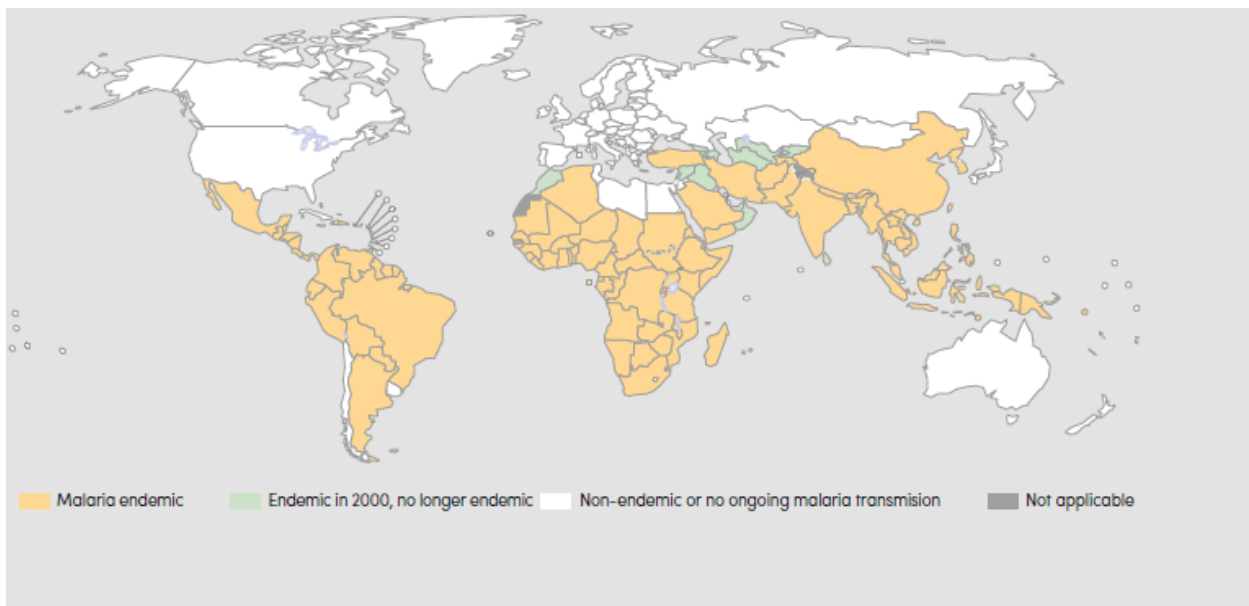
Malaria is an ancient disease and has afflicted mankind through the ages and continues to affect our society [1]. The first symptomatic description of malaria dates back to Chinese medical writings (2700 B.C.), which described several of the symptoms such as fever, headache, nausea, vomiting and fatigue. Other early descriptions include clay tablets with cuneiform writing from Mesopotamia (2000 B.C.), Egyptian Ebers papyri (1570 B.C.) and Hindu texts as far back as the sixth-century B.C. The so-called “father of modern medicine” Hippocrates (470-370 B.C.) recorded the chief symptoms of the disease and described the *quartan* (every fourth day) and *tertian* (every third day) periodic fevers associated with the disease. The Romans noted that the disease was linked to swamp and marshlands, and the disease became known as the Roman fever. By the Middle Ages, the word malaria (“mal” meaning bad and “-aria” meaning air) was used, thought to have been used first by Francisco Torti (1658), in reference to the miasmas produced from the swamp and marsh waters.

Currently, malaria is considered the most devastating of all parasitic diseases. In 2015, 97 countries had on-going malaria transmission, occurring mostly in the tropical and sub-tropical regions as is shown in Figure 1.1. The World Health Organization estimated that 3.3 billion persons were at risk of malaria in 2015. An estimated 214 million malaria cases and 438 000 deaths due to malaria were reported in 2015, 89% of these occurred in Africa [2].

There are five species of the genus *Plasmodium* that are known to infect humans namely: *P. falciparum*, *P. vivax*, *P. ovale*, *P. malariae* and *P. knowlesi*. Almost all deaths and severe disease are caused by the tertian *P. falciparum* species of the malaria parasite. This species has been considered to be the most pathogenic *Plasmodium* parasite as it is capable of adhering to endothelium linings during the erythrocytic stage of the infection [3]. It accounted for 89% of the 2015 malaria cases, occurring in the tropical regions of sub-Saharan Africa, Southeast Asia and the Western Pacific areas which share the Amazon rainforest [2]. *P. vivax* and possibly *P. ovale* can cause relapsing malaria by remaining dormant in the liver as hypnozoites, which makes infection with these parasites challenging to eradicate [4, 5]. The *P. vivax* species of the malaria parasite occurs mostly

in Asia and Latin America while *P. ovale* is mainly distributed in West Africa. *P. malariae* is distinct from the other species as it can persist in infected individuals for very long periods of time at low parasitaemia if not properly treated [6]. *P. knowlesi* was recently identified as capable of infecting humans by zoonotic transfer from Macaque monkeys, occurring in Southeast Asia [7, 8].

The *Plasmodium* parasite is transmitted to the human host by passing into the blood when a female mosquito of the genus *Anopheles* takes her blood meal. There are over thirty *Anopheline* mosquito species capable of acting as transmitters; however; only three species are considered the chief transmitters namely: *An. funestus*, *An. arabiensis* and *An. Gambiae* [9].



**Figure 1.1: World map showing the global malaria transmission areas, areas with limited risk and areas with no malaria transmission.**

Malaria is widespread in the tropical and sub-tropical regions of sub-Saharan Africa, Southeast Asia and countries sharing the Amazon rainforest. Malaria was eradicated from North America and Europe [2].

## 1.2 Life cycle of *P. falciparum* parasites

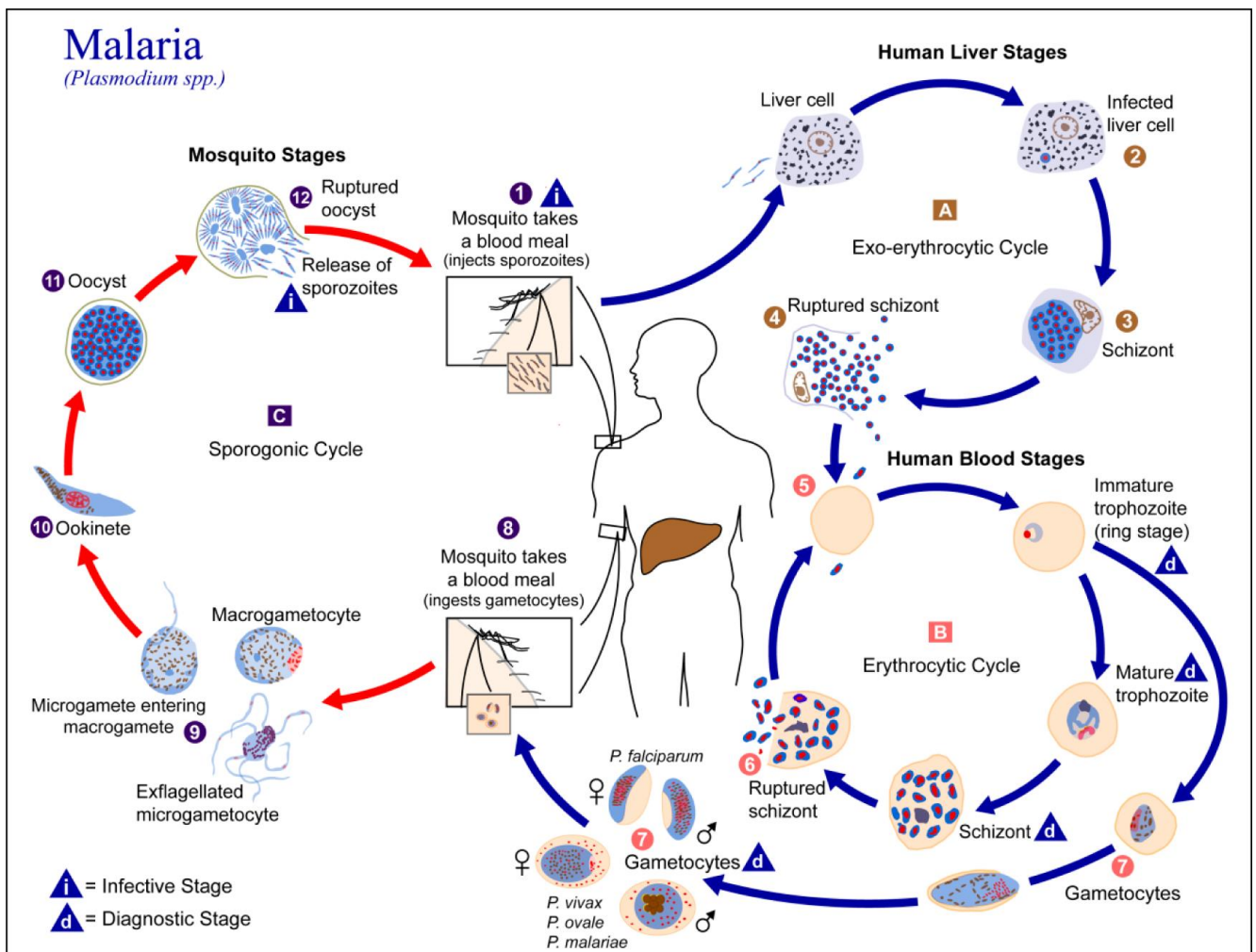
All human malaria parasites are known to undergo both sexual and asexual development stages in their insect and human host, respectively, as is illustrated in Figure 1.2. Initially, the transmittance of *P. falciparum* sporozoites takes place as the infected female *Anopheles* mosquito takes a blood meal from the human host and inoculation of the peripheral blood-flow takes place with sporozoites from the mosquito's salivary gland [9]. The sporozoites then invade hepatocytes and a 5-15 day asexual, exo-erythrocytic schizogony takes place. During this period, no clinical symptoms of malaria are seen and the sporozoites develop into exo-erythrocytic merozoites that are released into the bloodstream.

The merozoites consequently invade erythrocytes and the parasite spreads itself into a bi-concave disc, yielding the characteristic "ring shape" seen in Giemsa stained blood smears [10]. The ring-stage parasite feeds on haemoglobin and other nutrients taken up from the plasma. As the ring stage enlarges, adherence molecules are synthesised and are exported for presentation on the erythrocyte membrane to allow adherence to blood vessel, visceral and placental linings [3]. Further development of the ring stage into either the trophozoite stage during schizogony or leaving the asexual cycle and entering sexual gametocyte differentiation then takes place.

The trophozoite stage further modifies the erythrocyte, allowing additional endothelial adhesion. The parasite continues to feed on haemoglobin, and the haem by-products are crystallised into dark pigmented haemozoin within the food vacuole. Further maturation of the trophozoite stage causes a series of nuclear divisions, intense synthesis and assembly of molecules that are needed for erythrocyte invasion. This form is referred to as the schizont; and the nuclei and molecules produced form merozoite buds on the schizont's periphery. Subsequently, after 48-72 hours the schizont erupts in a protease dependent lysis process and releases as many as 36 daughter merozoites per schizont into the blood [11]. The synchronous eruption of the schizonts is associated with the quartan and tertian fevers seen in malaria [12].

Small numbers of committed parasites leave the asexual cycle and enter the sexual pathway, forming male and female gametocytes [13]. Gametocytogenesis, the formation of gametocytes, has been shown to vary and is influenced by numerous stress factors,

including parasite density, host immune response and drug treatment [14]. Gametocytes are taken up by mosquitoes when a blood meal is taken from an infected individual, and this allows the transmittance of the parasite. These gametocytes release female macrogametes and flagellated male microgametes that fuse, forming a zygote. The zygote undergoes development into an ookinete, which adheres to; and then penetrates the midgut wall of the mosquito. The ookinete develops into an oocyst that eventually forms numerous sporozoites that invade the salivary glands of the mosquito and allow further transmittance [9].



**Figure 1.2: The lifecycle of *P. falciparum* parasites.**

The main phases in the liver; the red blood cells (asexual and sexual erythrocytic stages) of the human host; gut and the salivary glands of the mosquito host are depicted. (<http://www.dpd.cdc.gov/dpdx>, Public Health Image Library, provided by CDC-DPDx, Alexander J. da Silva and Melanie Moser).

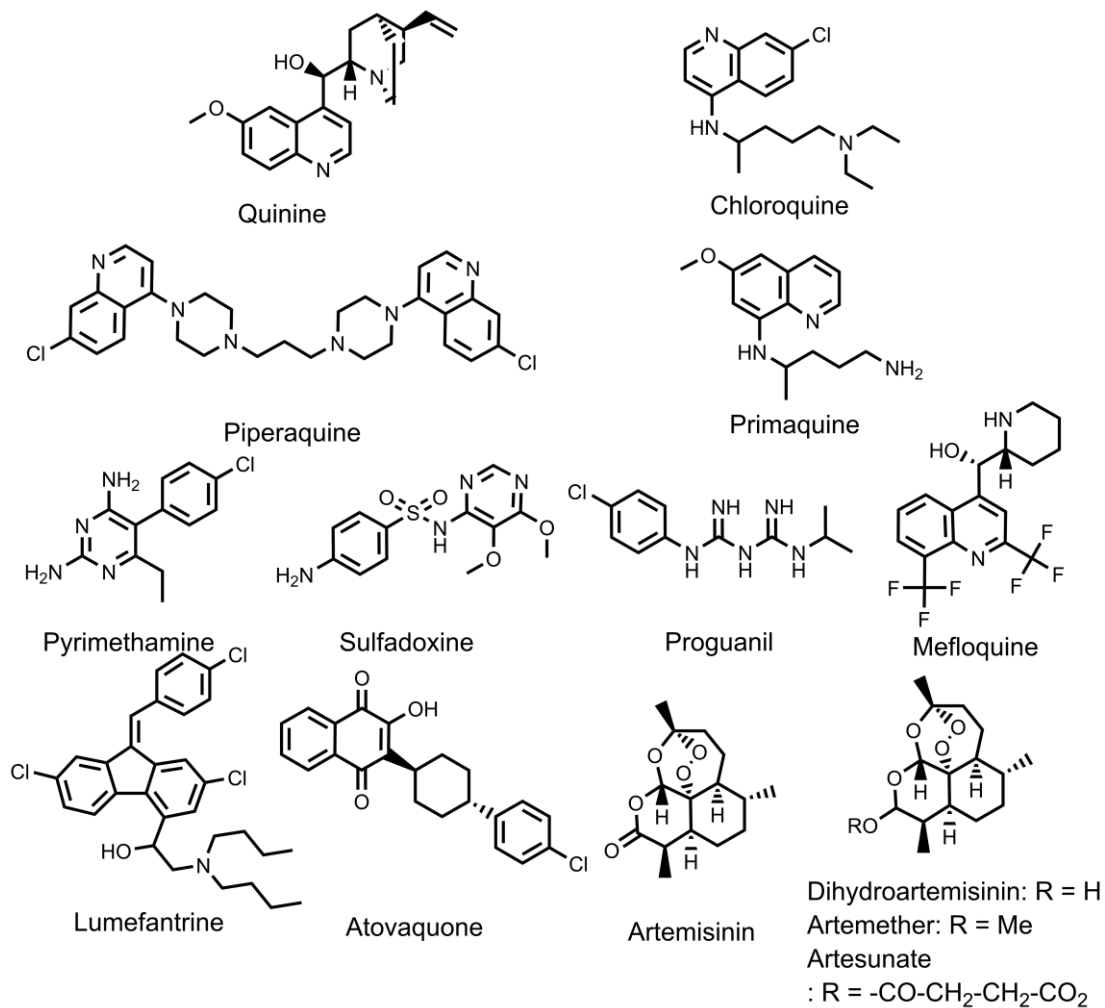
### 1.3. The control of malaria

In addition to the high mortality associated with malaria, it also impacts on the social and economic well-being of societies in affected areas. This occurs as the disease drains already scarce health and human resources interfering with educational achievement [2]. In Africa, the economic burden is estimated at \$12 billion a year [15]. In an effort to curtail the burden that the disease imposes, numerous international initiatives have been set up with the aim to coordinate efforts for the control, elimination and ultimately the eradication of the disease. Consequently, the Global Malaria Action Plan (GMAP) was adopted in 2007, which is supported by the WHO/Roll Back Malaria Partnership. To achieve the goals set out in the GMAP, a combination of long-lasting insecticidal nets (LLINs), indoor residual spraying and other vector control measures (e.g. larviciding and environmental management) have been proposed in addition to medicinal treatment and diagnostics for malaria case management [16]. In terms of medicinal treatment of infected individuals, Artemisinin-based combination therapies (ACTs) are currently recommended for treatment against *P. falciparum* malaria and chloroquine [17] and primaquine (PQ) are the treatments of choice against sensitive *P. vivax* malaria [16, 18].

The GMAP strategy has been applied quite successfully in Rwanda, Zanzibar, Zambia and São Tomé and Príncipe [19]. Although malaria can be drastically reduced using IRS and LLINs, increased resistance against the insecticides used and mosquito behavioural changes are threatening the usage of vector control measures against malaria [20]. There is optimism for efficacious malaria vaccine, which holds promise in aiding malaria control strategies, but they are still lacking the required efficacy. Presently, the first ever Phase III clinical trials are being conducted on a vaccine against malaria; however, the RTS, S/AS01 vaccine is only 55% effective in adults and 31% effective in babies [21]. Another vaccine, the PfSPZ vaccine, is also under development and has shown promising results [22].

At present, the primary component of parasite control is the use of currently available antiparasitic drugs as chemotherapy or chemoprophylaxis, which is considered the most effective public health tool against malaria [16]. The currently used antimalarials can be divided into sets based on their mode of action (MOA) and chemical scaffolds (Figure 1.3).





**Figure 1.3: Chemical structures of antimalarials**

Artemisinin and derivatives, combined with lumefantrine or piperazine and previous first-line therapies (sulfadoxine–pyrimethamine and chloroquine). Preferred drugs for the elimination of hypnozoites (primaquine), combination for prophylaxis (atovaquone–proguanil). Redrawn from [23].

The first effective antimalarial was in the form of Bark extracts from the Cinchona tree, which has been used to treat malaria since at least 1632. The active compound was isolated and named quinine and was widely used until a better derivative chloroquine, was introduced in 1945. The quinolones and their derivatives have a MOA based on their ability to interfere with haemozoin synthesis, which is an essential detoxification process during the parasites catabolism of haemoglobin in the food vacuole [24] (Table 1.1). Consequently, the parasite is exposed to cytotoxic oxidative stress due to the accumulation of free haem, resulting in parasite death. Chloroquine resistance was observed in 1957 on the Thai-Cambodian border, the resistance was found to be as a result of a mutated ATP-dependent efflux pump. The mutated chloroquine resistance transporter (*PfCRT*) actively removes chloroquine from the food vacuole [25]. Following

the spread of chloroquine resistance, sulfadoxine–pyrimethamine was adopted as the first-line antimalarial treatment.

The antifolate class of antimalarials block the biosynthesis of folate and consequently halt the biosynthesis of nucleotides [26] (Table 1.1). Dihydrofolate reductase (DHFR) is inhibited by proguanil or pyrimethamine while dihydropteroate synthase (DHPS) is inhibited by sulfadoxine. Sulfadoxine and pyrimethamine work synergistically by inhibiting sequential enzymes in the biosynthesis of folate. Resistance to the antifolates emerged quickly and is the result of mutations in DHFR and DHPS leading to reduced enzyme inhibition [26]. The naphthoquinone, atovaquone, is an inhibitor of the mitochondrial cytochrome bc 1 complex [27]. The inhibition of the parasites electron transport chain leads to the inhibition of dihydro-orotate dehydrogenase (DHODH), which is required for pyrimidine nucleotide biosynthesis. Atovaquone resistance is due to a point mutation in the cytochrome b gene [28]. Atovaquone is used as a combination with proguanil for treatment and prophylaxis of malaria. Although proguanil by itself is considered ineffective, its metabolic activation by hepatic cytochrome P450 results in the metabolite cycloguanil, which is a DHFR inhibitor [29].

The artemisinin series and its derivatives, MOA is associated with the bio-activation of the endoperoxide bridge by  $Fe^{2+}$  or heme resulting in free radicals [30], which are consequently responsible for the alkylation of proteins and free haem [31] (Table 1.1). Artemisinin and its derivatives are fast-acting antimalarials and are cleared rapidly [32]. Consequently, they are combined with slower clearing drugs such as lumefantrine and piperazine to eliminate residual parasites. The ACTs have supplanted the previously recommended sulfadoxine–pyrimethamine combination, which in turn replaced chloroquine. Unfortunately, as is illustrated in Table 1.1, resistance to antimalarial medicines is a recurring problem and resistance to almost all classes of drugs have been observed [33-35]. This includes resistance to ACTs that was first observed at the Thai-Cambodia border. Artemisinin resistance was initially suggested to be due to mutation of *PfATP6*, however, this hypothesis could not be corroborated in later studies [36, 37]. The copy number of *Pfmdr1* has also been associated resistance [38]. More recently mutations in the kelch propeller domain of the *PfK13* protein has been shown as a molecular marker indicating resistance [39]. Artemisinin resistant parasites can enter a state of quiescence conferring resistance to numerous antimalarials and allowing

recrudescence of parasites after drug treatment [40]. Thus, the last therapy capable of treating multi-drug resistant *P. falciparum* malaria will most likely lose its efficacy as resistance begins to spread, as it already has across mainland Southeast Asia, undermining malaria control efforts [41, 42]. Consequently, the goals of eradication campaigns such as the GMAP cannot be accomplished without the discovery of novel antimalarials, which are capable of exploiting new MOAs [43].

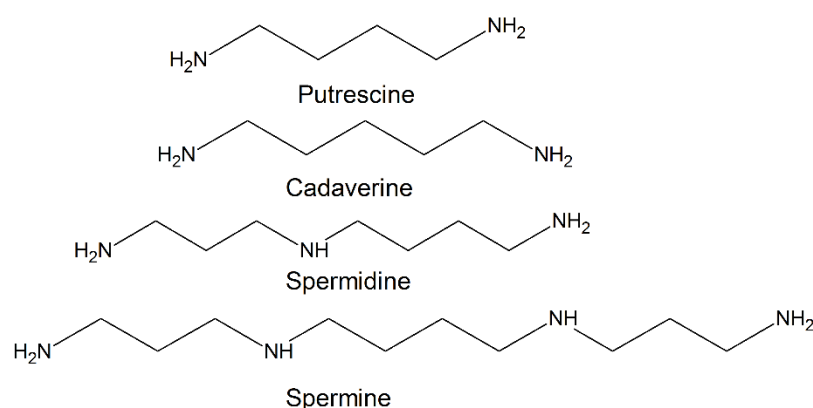
**Table 1.1: Antimalarial drugs**

Antimalarial drug	Chemical class	Year of introduction	Resistance emergence	Mode of action	Mechanism of resistance
<b>Quinine</b>	Amino alcohol	1645	1910	Inhibition of heme detoxification	Mutations in <i>PfCRT</i> and <i>PfMDR1</i>
<b>Chloroquine</b>	4-Amino-quinoline	1945	1957	Inhibition of heme detoxification	Mutations in <i>PfCRT</i> and <i>PfMDR1</i>
<b>Primaquine</b>	4-Amino-quinoline	1952	Unknown	Unknown ( active against liver hypnozoites and gametocytes)	Unknown
<b>Piperaquine</b>	Bisquinoline	1960	1980	Inhibition of heme detoxification	Mutations in <i>PfCRT</i> and <i>PfMDR1</i>
<b>Mefloquine</b>	4-Methanolquinoline	1977	1982	Inhibition of heme detoxification	Mutations in <i>PfCRT</i> and <i>PfMDR1</i>
<b>Lumefantrine</b>	Aryl aminoalcohol	1970	Unknown	Inhibition of heme detoxification	Mutations in <i>PfCRT</i> and <i>PfMDR1</i>
<b>Sulphadoxine</b>	Aminosulphonamide	1967	1967	DHFR-TS inhibitor	Mutations in DHFR domain of DHFR-TS protein
<b>Pyrimethamine</b>	Diaminopyrimidine	1967	1967	DHFR inhibitor	Mutations in DHFR domain of DHFR-TS protein
<b>Proguanil</b>	Bi-guanidine	1948	1949	DHFR inhibitor	Mutations in DHFR domain of DHFR-TS protein
<b>Atovaquone</b>	Naphthoquinone	1996	1996	Mitochondrial cytochrome bc1 complex inhibitor	Mutations in cytochrome bc1 complex catalytic domain
<b>Artemisinin's</b>	sesquiterpene lactone	1970	2006	Protein and heme alkylation, free radical formation	Copy number of <i>Pfmdr1</i> , Mutation of the <i>PfK13</i> propeller domain and quiescent state

Abbreviations used; chloroquine resistance transporter (*PfCRT*), Multi-drug resistance protein (*PfMDR*), Dihydrofolate reductase (DHFR), Dihydropteroate synthase (DHPS), Kelch protein 13(*PfK13*)  
 Compiled from [20, 23, 34, 44].

## 1.4. Polyamine properties and functions

Polyamines are a class of biological compounds that are aliphatic, low molecular weight nitrogenous bases, which possess an overall cationic charge at physiological pH due to their high pKa values. The structures of these molecules consist of repeating methylene moieties that separate 2-4 amine groups [45]. The representative biological polyamines are illustrated in Figure 1.5 namely; putrescine (1, 4-diaminobutane), cadaverine (1, 5-diaminopentane), spermidine (*N*-(3-aminopropyl)-1, 4-diaminobutane) and spermine (*N*, *N*-bis(3-aminopropyl)-1,4-diaminobutane).



**Figure 1.5: The chemical structures of the three main polyamines.**

The names and structure of the three representative biological polyamines; putrescine, spermidine, spermine and cadaverine the polyamine formed during protein hydrolysis. Redrawn from [45, 46].

Polyamines have been found in almost all organisms examined, except for certain orders of the Archaea namely, *Methanobacteriales* and *Halobacteriales* [47]. Polyamines have been suggested to be similar to bivalent inorganic cations such as magnesium or calcium; however, polyamines are unique in that their positive charge is spread over the molecule's backbone in a particular spatial orientation. Additionally, their homeostasis is controlled by metabolism and transport [48]. The cationic nature of the polyamines allows them to bind electrostatically to negatively charged biological macromolecules. The stabilising effects of these interactions within cells promote cell growth [45, 49].

The growth of cells is therefore explicitly linked to the presence of polyamines and it has been shown that the polyamines and their biosynthetic enzymes are present at higher concentrations in rapidly growing cells such as cancerous and parasitic cells. In addition, their uptake by means of polyamine transport mechanisms is increased in these cellular environments [50-52]. Therefore, targeting polyamine metabolism or transport as a drug target holds great promise for treating rapidly proliferative diseases [53]. The polyamines

have been shown to be involved in a myriad of biological processes including replication; transcription; translation; post-translational modification; ion channel gating; and membrane stability. Additionally, they have been shown to regulate cellular proliferation; transformation; differentiation; apoptosis; autophagy; and tumorigenesis [54]. Consequently, the polyamines have been found to be essential for cell survival and depletion of the polyamine pool in mammalian cells has been shown to stop translation and cell growth [55, 56].

## **1.5. Polyamine metabolism and transport**

### **1.5.1 The biosynthesis of polyamines in mammalian cells**

The correct metabolism of polyamines is critical as they are required for cellular growth and if depleted could cause death, whereas over-production could be toxic [50]. Thus, the cell exerts tight control of polyamine biosynthesis, catabolism and transport. The biosynthesis of polyamines in mammalian cells (Figure 1.6), is carried out initially by the enzymatic decarboxylation of ornithine by ornithine decarboxylase (ODC, EC 4.1.1.17). Thus, this enzyme catalyses what could be referred to as the “bottle neck” of biosynthesis of the polyamines. The amount of the enzyme ODC is ordinarily the limiting factor in the production rate of putrescine; however, the supply of the aminopropyl donor decarboxylated *S*-adenosylmethionine (dcSAM) influences the rate of conversion of putrescine as well. The conversion of putrescine to higher polyamines is catalysed by aminopropyl transferases. The synthesis of spermidine occurs by the decarboxylation of *S*-adenosylmethionine (SAM) by the enzyme *S*-adenosylmethionine decarboxylase (AdoMetDC, EC 4.1.1.50) to form the aminopropyl donor. This is transferred to the primary amine group of putrescine by means of spermidine synthase (EC 2.5.1.16) to form spermidine. This is followed by the addition of another aminopropyl group to the primary amine group of spermidine by means of the enzyme spermine synthase (EC 2.5.1.22) to form spermine [46, 57, 58].

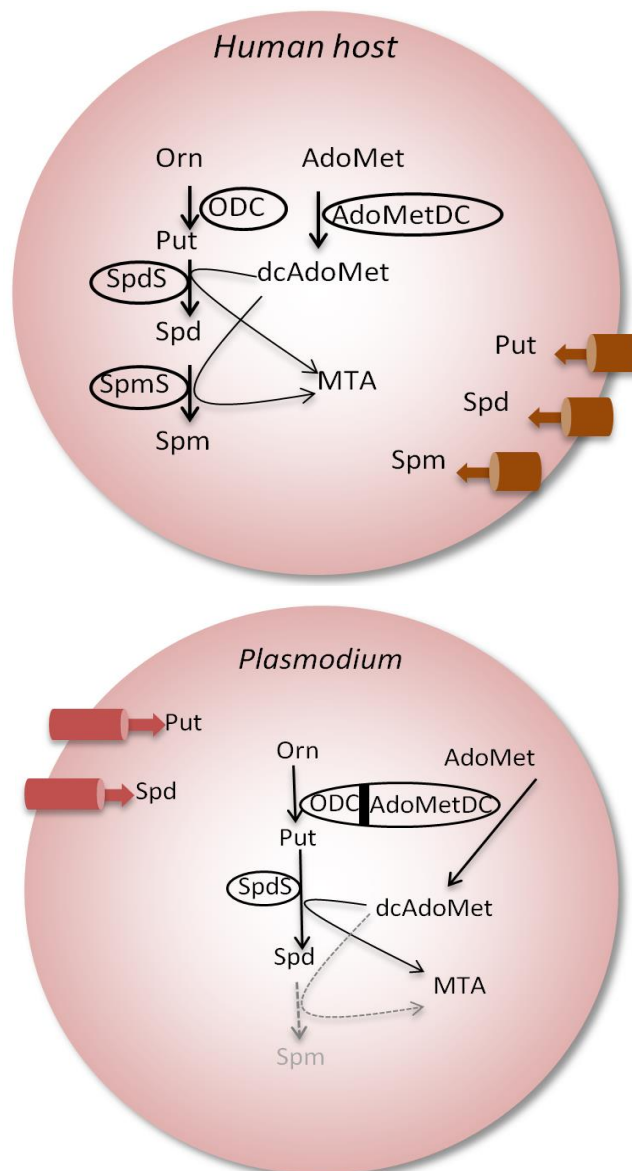
The control of the biosynthesis of polyamines occurs by regulating ODC on the levels of mRNA synthesis, mRNA translation and stability, and protein degradation affecting the amount of the enzyme but not its activity. Degradation occurs by a non-ubiquitin pathway involving two proteins termed antizyme (AZ) and antizyme inhibitor, the rate of degradation is increased by high levels of polyamines [46]. AdoMetDC is regulated by a

pro-enzyme processing step, mRNA translation and protein turnover. The regulation of spermine and spermidine formation by the action of the aminopropyl transferases is determined by the availability of the substrates [59, 60].

### **1.5.2 The biosynthesis of polyamines in *P. falciparum* parasites**

The presence of polyamines in the asexual intra-erythrocytic form of *P. falciparum* parasites has been found to be in the high mM concentrations making up 14% of the total metabolome of isolated parasites [61]. Consequently, it has been shown that the rapid proliferation of the parasite is dependent on the availability of high quantities of polyamines [62].

The biosynthesis of polyamines in *Plasmodium* species is quite different to mammalian cells as is illustrated in Figure 1.6 below, with three key differences. Firstly, the ODC enzyme of the parasite forms a bifunctional complex with AdoMetDC, which is found on a single peptide. This property is unique to the plasmodia and has been implicated in polyamine biosynthesis control [51, 63]. Secondly, the synthesis of low amounts of spermine is thought to be carried out by the parasite's spermidine synthase as no spermine synthase activity has been described in the parasite [64]. Thirdly, the parasite's polyamine biosynthesis differs from mammalian cells in terms of catabolism; to date the inter-conversion of polyamines to their acetylated intermediates for catabolism has not been shown [65].



**Figure 1.6: Polyamine biosynthetic pathways and transport systems present in the human host and *P. falciparum* parasites.**

ODC: ornithine decarboxylase. SpdS: spermidine synthase. AdoMetDC: S-adenosylmethionine decarboxylase. AdoMet: S-adenosylmethionine. dcAdoMet: decarboxylated S-adenosylmethionine. MTA: 5'-methylthioadenosine. Put: putrescine. Spd: spermidine. Adapted from [66].

The regulation of polyamine biosynthesis in *P. falciparum* parasites is exerted by means of a feedback inhibition mechanism of ODC by putrescine with no stimulation of AdoMetDC, and the expression of the bifunctional enzyme [67]. The activity of spermidine synthase and the rate of polyamine transport form part of the regulation of polyamine levels in the parasite [67, 68]. The bifunctional AdoMetDC/ODC has been indicated to be the rate-controlling enzyme in the parasite's pathway, based on previous studies. Consequently, inhibition of this enzyme and enzymes responsible for polyamine synthesis, could result in polyamine pool depletion and cell death. Inhibition studies have been performed using *DL-α-difluoromethylornithine* (DFMO), which irreversibly alkylates



the ODC enzyme, thus inactivating it [69]. This resulted in arrested growth of *P. falciparum* parasites in the early trophozoite stage. The halt in parasite proliferation was only cytostatic, likely due to the existence of a compensatory mechanism in the form of polyamine uptake [70, 71].

### 1.5.3 Polyamine transport in intra-erythrocytic *P. falciparum* parasites

Erythrocytes do not contain significant quantities of polyamines and show no activity in polyamine biosynthetic enzymes, with low quantities of spermidine and spermine [72]. Thus far, the uptakes of putrescine by normal erythrocytes from the extracellular content have been shown to be a diffusive process; however, a membrane transport process dependant on concentration gradients have been reported for putrescine and spermidine in normal erythrocytes [73].

Upon infection by malaria parasites the quantity of polyamines in the erythrocyte units rise dramatically and polyamine biosynthetic enzyme activity increases [72]. Newly formed permeation pathways (NPP) appear in infected erythrocytes whose properties are entirely different to the normal permeation pathways of uninfected erythrocytes [74, 75]. Putrescine transport have been characterised in Rhesus monkey erythrocytes infected by *P. knowlesi* indicating an increase of 11-fold after infection [76]. The use of sulfhydryl blocking reagents on *P. knowlesi* infected erythrocytes showed a large decrease in putrescine uptake indicating that its uptake is carrier mediated. Additionally, the uptake of putrescine was shown to be affected by spermidine and spermine, implying a shared transport system [76]. More recently, detailed biochemical data indicated that the parasite-infected erythrocyte facilitates the uptake of putrescine via a diffusive process. Furthermore, upon infection of the erythrocyte NPP's induced by the parasite allowed spermidine uptake to occur by the erythrocyte [77]. Characterisation of polyamine transport into isolated parasites indicated that putrescine and spermidine are taken up via a temperature dependent process. Polyamine uptake was affected by putrescine, spermidine and spermine in a cross-competitive manner, suggesting a shared transport system. Polyamine uptake was also partially inhibited by basic amino acids. Polyamine biosynthesis inhibition resulted in an increase in putrescine and spermidine uptake. The uptake was shown to be dependent on concentration gradients, as well as on the parasite's membrane potential. This was indicated by the increasing polyamine uptake rates during membrane depolarisation and decreasing polyamine uptake rates during

hyper-polarisation. This signified an electrogenic uptake process, hypothesised to be due to the parasite's inwardly negative membrane potential [77].

## 1.6 Polyamine metabolism as a drug target

The targeting of polyamine metabolism as a chemotherapeutic means to treat hyper-proliferative diseases such as cancer, has become a key research topic due to its essential role in cellular replication [46]. Perturbation of polyamine metabolism has proven itself as a clinically viable treatment of West African sleeping sickness caused by *Trypanosoma brucei gambiense* [17]. The significance of polyamines in the proliferation of the *P. falciparum* parasite as well as the distinct differences in polyamine metabolism in this parasite has made it a viable drug target in the fight against antimalarial resistance [78].

Initially, the focus of polyamine-targeted therapy in cancer cells was to inhibit the biosynthetic enzymes ODC and AdoMetDC. One of the first irreversible inhibitors of ODC, DFMO, was shown to have antitumorigenic activity [79]. The activity observed *in vitro* was as a result of DFMO's ability to deplete putrescine and spermidine; depletion of the intracellular polyamine pools resulted in a cytostatic growth response. Further testing of DFMO on human small cell lung cancer *in vivo* and *in vitro* resulted in cytotoxic effects and clinical trials for DFMO as a single agent were commenced [69]. Inhibition studies have been performed against *P. falciparum* using DFMO, which resulted in arrested growth of *P. falciparum* parasites in the early trophozoite stage. However, this again was only cytostatic due to a compensatory polyamine uptake [70, 71]. More recent inhibitors of ODC such as *3-aminooxy-1-aminopropane* (APA), CGP54169A, and CGP52622A showed effective *in vitro* inhibition of *P. falciparum* proliferation, however inhibition remained cytostatic [80]. Single enzyme inhibitors directed against AdoMetDC were also synthesised such as methylglyoxalbis(guanylhydrazone) (MGBG). MGBG was used as a treatment for leukaemia before it was demonstrated to be a competitive inhibitor of AdoMetDC [81]. Following this, a class of nucleoside type inhibitors were synthesised based on the structure of AdoMet. An effective representative of this class *5-[(Z)-4-amino-2-butenyl]methylamino-5-deoxyadenosine* (MDL 73811), acted as an irreversible inactivator of AdoMetDC and showed efficacy in treating trypanosomiasis in animal models, however, it was shown to act cytostatically on L1210 cells [82, 83]. AdoMetDC inhibitors tested against *in vitro P. falciparum* such as CGP48664A, CGP40215A and

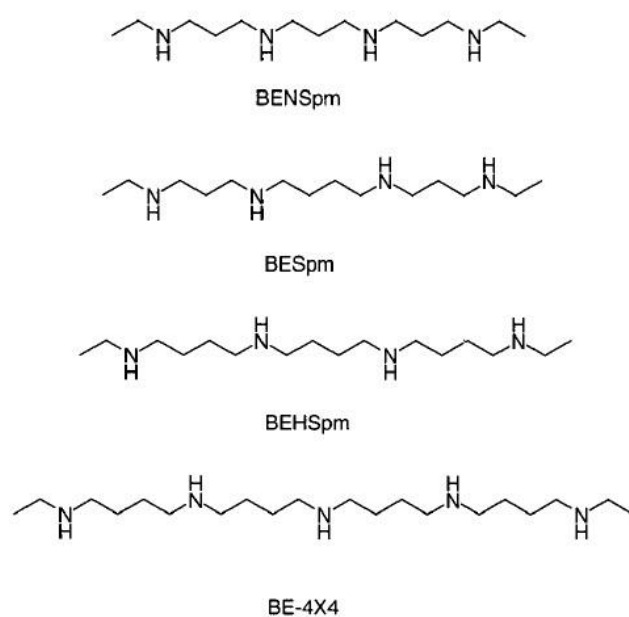
MDL73811 showed inhibition of proliferation; however, the inhibition was shown to be cytostatic. A series of derivatives of MDL73811 have recently been assayed against *in vitro* *P. falciparum* with Genz-644131 proving the most active. Additionally, nano-encapsulation of Genz-644131 potentiated its inhibitory effects [84]. Unfortunately, all of these compounds suffered from similar problems in that singular inhibition of either ODC or AdoMetDC of *P. falciparum in vitro* causes cytostatic inhibition in the trophozoite stage of the parasite and they are not able to cure *P. berghei* infected mice [70, 85].

### 1.6.1 Terminally alkylated polyamine analogues

Due to the failed clinical efficacy of single enzyme inhibitors as chemotherapeutic agents, a strategy aimed at exploiting the self-regulatory nature of the polyamine pathway using polyamine analogues was proposed by Porter and Bergeron [86]. Their proposal was based on the possibility of polyamine analogues interfering at multiple sites in the polyamine pathway, thus preventing or minimising the compensatory mechanisms previously seen with the single enzyme inhibitors. Polyamine analogues are compounds that structurally mimic polyamines and can be considered functionally either as (1) anti-metabolites – that function by depleting intracellular polyamine concentrations, or (2) polyamine mimetics – that function by displacing the natural polyamines from their binding sites, but are not able to substitute in function [87]. In addition, these analogues can act as antagonists interfering with polyamine transport systems that are essential for continued proliferation [88].

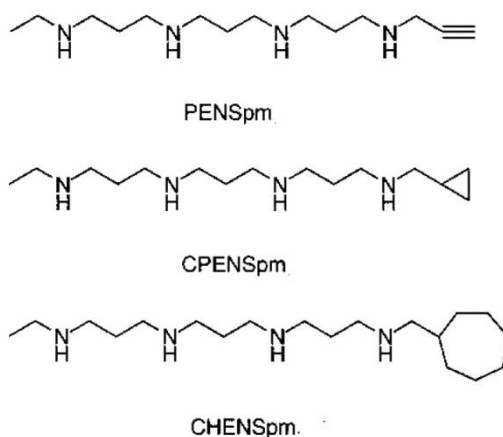
The first set of analogues that were developed were symmetrical and terminally substituted bis(alkyl)polyamines. The focus of these studies involved modifying the terminal amines'  $pK_a$  values. The latter were made more basic in comparison to the naturally occurring polyamines and amine terminal ends were protected by symmetrical bis(alkyl) groups, thereby preventing their oxidation by polyamine oxidase. The analogues were derivatives of either spermine or spermidine and included: *bis(ethyl)norspermine* (BENSpm), *bis(ethyl)spermine* (BESpm), *bis(ethyl)homospermine* (BEHSpm) and *1,20-(ethylamino)-5,10,15-triazanona-decane* (BE-4x4) as shown in Figure 1.7. BENSpm underwent Phase II clinical trials as a treatment for various human solid tumours; however, it was shown to be ineffective as a single agent but showed synergism with other standard chemotherapeutic agents in further studies [89]. Additionally, BE-4x4 has been shown to be effective against various cancer cell lines [90].

Their mechanism of action was linked to polyamine biosynthetic pathway regulation and production of free radicals. They were shown to be promising anti-tumour agents [91]. In general, terminally alkylated polyamines lead to a decrease in all three of the naturally occurring polyamines found in mammalian cells, by down-regulating both ODC and AdoMetDC through a combination of mechanisms, resulting in cytotoxicity or a cytostatic response [46]. The analogues' efficacy was most pronounced in the 3-3-3, 4-4-4 and 4-4-4-4 carbon backbone derivatives. It was observed that alkylation of internal amines' as well as substituents larger than ethyl substituents, led to a reduced *in vitro* activity. These analogues are taken up by cells via polyamine transport systems and the presence of terminal amine groups play an important part in the transport selectivity [92].



**Figure 1.7: Structures of symmetrically substituted bis(alkyl) polyamine analogues.**  
 Adapted from [93].

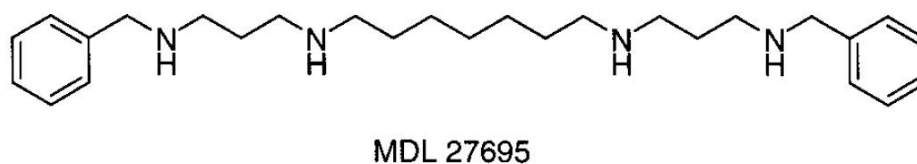
To expand on the effects of the terminal substituents on activity, unsymmetrically substituted alkylpolyamines analogues were evaluated [94]. These analogues were based on the spermine and norspermine backbone. The analogues PENSpm, CPENSpm and CHENSpm as illustrated in Figure 1.8 below, proved to be more active than BENSpm against cancerous cells. Although CPENSpm showed lower toxicity and greater therapeutic efficacy, its clinical results were similar to those obtained with the BENSpm. CPENSpm was shown to have little cell cycle inhibitory effects, however CHENSpm and IPENSpm were shown to block the cell cycle [46, 93].



**Figure 1.8: Structures of symmetrically substituted bis(alkyl) polyamine analogues.**

Adapted from [93].

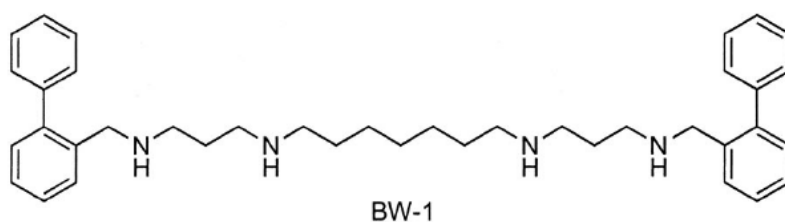
Due to the previously shown efficacy of PA's, a series 3-7-3 polyamine backbone and terminal benzyl groups compounds were synthesised. The most promising of these, MDL 27695 (Figure 1.9), was shown to have marked antimalarial and antileishmanial activity [95, 96]. The activity of this analogue was hypothesised to be due to its rapid oxidation by polyamine oxidase within mouse erythrocytes resulting in oxidative stress [97]. In *P. berghei* mice models, the analogue in combination with DFMO resulted in an additive effect and successfully cured infections as well as provided immunity upon re-infection [96]. Co-treatment of the analogue with amine oxidase inhibitors could not elicit the same curative effect. The success of these analogues led them to be evaluated against *Leishmania donovani*, against which they showed activity *in vivo* and *in vitro* [95].



**Figure 1.9: Structure of MDL 27695.**

Adapted from [93].

A second series of analogues with a 3-7-3 carbon backbone were shown to possess promising antitrypanosomal and antimicrosporidia effects [98]. A representative of these analogues is 1,15-bis{N-[o-(phenyl)benzylamino]}-4,12-diazapentadecane (BW-1) as illustrated in Figure 1.10. The analogue showed effective inhibition of AdoMetDC in *Onchocerca volvulus* with a 10-fold selectivity versus human AdoMetDC [99]. Additionally, BW-1 was shown to interfere with *Encephalitozoon cuniculi* polyamine oxidase activity by acting as a substrate [100].

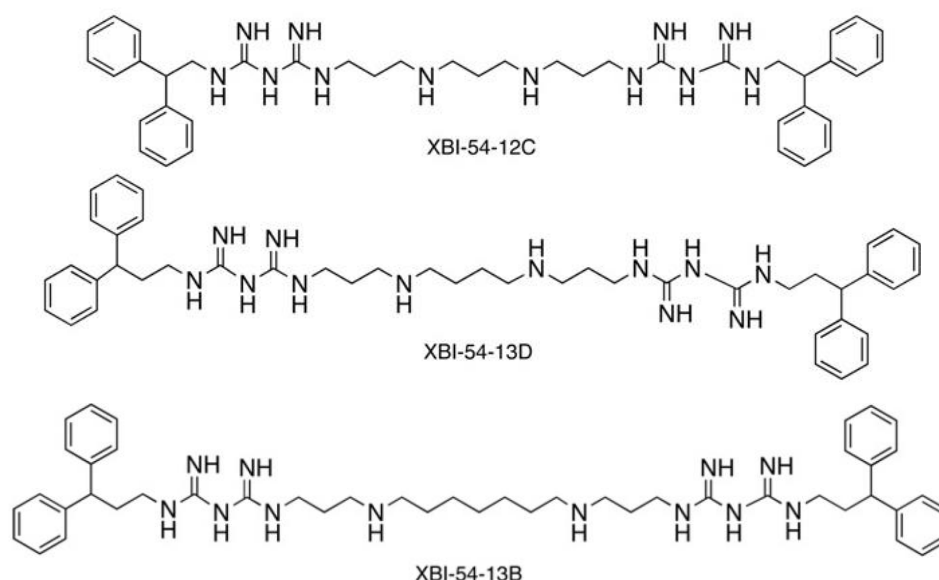


**Figure 1.10: Structure of BW-1.**

Adapted from [100].

### 1.6.2 Polyamino(bis)guanidines and polyaminobiguanides

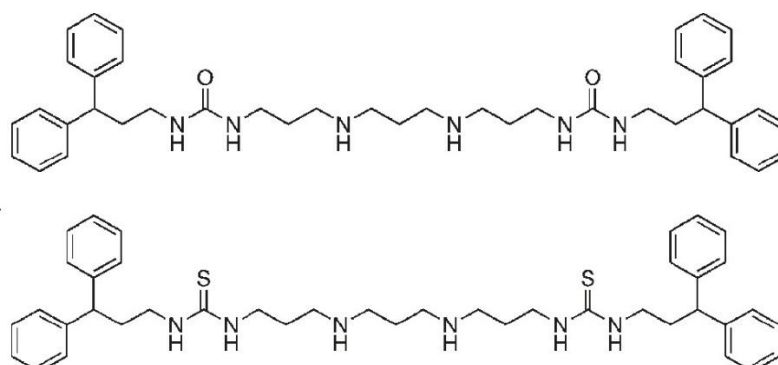
The effectiveness that terminally (bis)alkylated polyamine analogues showed towards cancer prompted the synthesis of substituted polyaminoguanidines. This was done as the biguanide functionality was hypothesised to increase the basicity of the polyamine analogues. Additionally, the biguanide functional group is found in various non-polyamine amidine therapeutics including chlorhexidine and the antimalarial chlorguanide [101]. The series was based on the 3-7-3 carbon backbone with substituted terminal guanidines or biguanides as illustrated in Figure 1.11. These analogues were shown to possess potent antibacterial and antitrypanosomal effects [102]. From these, the most potent biguanides had a 3-3-3 or 3-4-3 carbon backbone additionally the 3-7-3 carbon backbone also demonstrated potency. The biguanides XBI-54-12C and XBI-54-13D were the first reported biguanides with antitrypanosomal activity, attributed to trypanothione reductase inhibition. The analogues were also shown to inhibit the growth of *Yersinia pestis*, due to the analogues ability to prevent the organism from producing a biofilm [102]. The analogue XBI-54-13B has been shown to act as a potent epigenetic modulator acting as an inhibitor of lysine-specific demethylase 1 (LSD1). LSD1 is implicated in gene expression and repression, inhibition of LSD1 results in increased gene expression as a result of the recruitment of transcriptional activation complexes to the induced gene [103, 104]. These analogues were shown to inhibit human colon carcinoma and human breast cancer cell growth, affecting the re-expression of multiple, aberrantly silenced genes [103].



**Figure 1.11: Structures of XBI-54-12C, XBI-54-13D and XBI-54-13B.**

Adapted from [101, 102].

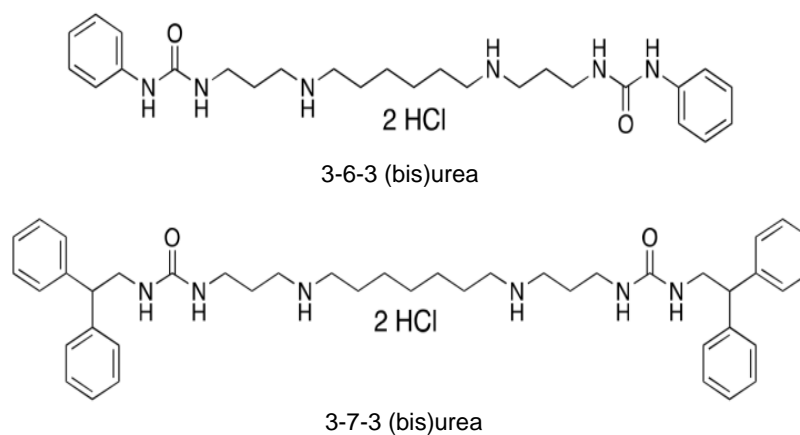
Due to the promising outcome obtained with the XBI-45-13B analogue, it was used as a scaffold for the development of isosteric ureas and thioureas polyamine analogues that were also potent inhibitors of LSD1 and could also inhibit cancer cell growth. The novel (bis)urea and (bis)thiourea based polyamine analogues as illustrated in Figure 1.12. The study revealed that replacement of the imine NH functionality of the terminal guanidine present in the previous series with oxygen or sulphur was a tolerable isosteric change, as active analogues in both the urea and thiourea series were shown, however, the thiourea analogues were shown to be more active. Additionally, it was revealed that bulkier aromatic substituents on the terminal nitrogen improved activity, however, no predictable differences in activity between analogues with varying carbon backbone linkages was shown, but the 3 carbon backbone did show slightly increased activity [105].



**Figure 1.12: Structures of (bis)urea and (bis)thiourea analogues.**

Adapted from [105].

Recently, a series of terminally alkylated (bis)urea and (bis)thiourea analogues were synthesised and evaluated for their antimalarial properties, based on the previous lead compounds [106]. These analogues contained 3-3-3, 3-4-3, 3-6-3 or 3-7-3 carbon backbone structures and were combined with a variety of terminal urea/thiourea substituents. They were all symmetrical analogues containing arylalkyl terminal substituents. This series was tested for possible inhibitory activity against *P. falciparum* parasites, most showed *in vitro* IC<sub>50</sub> values below 500 nM against *P. falciparum* [106]. The lead compound of this series as shown in Figure 1.13, had potent inhibitory activity against *P. falciparum*. It was also found that 3-3-3 and 3-4-3 carbon backbones were not effective against the parasite, whereas 3-7-3 carbon backbones were effective in the nM range. The 3-7-3 carbon backbone compounds possessed the greatest activity against the parasite with the (bis)urea compounds and diphenylethyl terminal substituted analogues being the most active. These analogues were shown to be involved in a cytotoxic response in the parasite measured by a decrease in cell viability. The mode of action of these analogues was shown to be due to inhibition of the parasites ability to replicate its DNA, which resulted in life cycle halts in schizogony. The inhibitory effect seen with these analogues was irreversible upon treatment with exogenous polyamines implying that the analogues could be blocking binding sites of natural polyamines, displacing the latter from their binding sites.



**Figure 1.13: Structure of the lead (bis)urea alkylated polyamine analogues.**

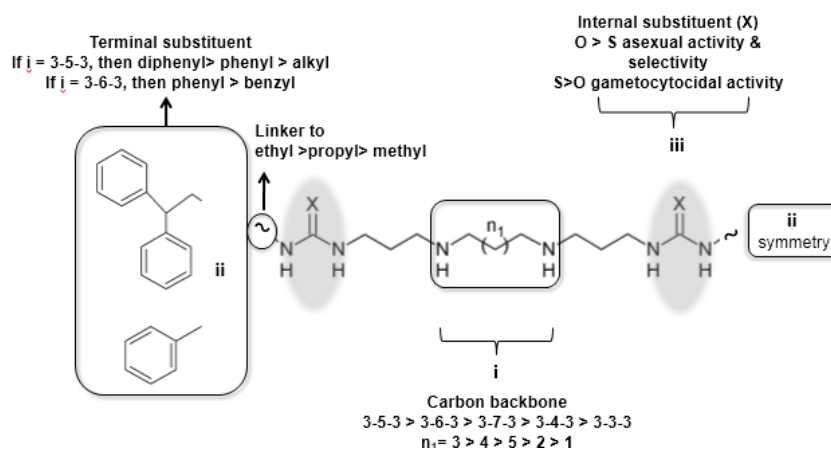
Adapted from [106].

The 3-5-3 backbone architecture polyamine analogues were previously found to have the best antitrypanosomal activity [101]. Consequently, based on the success of both first generation and second generation polyamine analogues, third generation symmetrically alkylated (bis)thiourea and (bis)urea polyamine analogues with 3-5-3 carbon backbones



were assessed [107]. Additionally, fluorinated derivatives of the (bis)urea polyamines analogues based on the previous lead compounds were synthesised with the goal of improving pharmacokinetic properties by enhancing metabolic stability and absorption. The analogues were shown to possess potent antimalarial activity *in vitro*. The analyses performed on the analogues indicated average solubility, permeation of cellular membranes and metabolic stability. However, the compounds showed no *in vivo* antimalarial activity against murine malaria in a Peters 4-day suppressive test model, which was attributed to poor oral bioavailability, as concentrations of the analogue were low during the *in vivo* pharmacokinetic evaluation [108]. This could be attributed to low absorption or rapid metabolism.

The compounds possessing terminal phenyl rings were the most active, while diphenylethyl, benzyl rings and diphenylmethyl substituted analogues showed decreasing activity. Analogues with small alkyl or without terminal alkyl groups were the least effective. The preliminary structure-activity relationship (SAR) obtained is illustrated in Figure 1.14. The SAR indicates that the spacing of amines and the pKa of the terminal amines influence the analogues biological activity. This can be explained in terms of the cationic interactions of the protonated amino groups with targets [109]. Based on the previously obtained results, there is a need to synthesise analogues with improved absorption and metabolic stability by fine-tuning the known structure-activity relationships to develop novel antimalarials that are active *in vivo*.



**Figure 1.14: Preliminary antiplasmodial structure-activity relationships for symmetrical substituted polyamines**

Adapted from [107].

### 1.6.3 Rational drug design and lead optimisation

The lack of antimalarial activity against murine malaria of the previous lead compound was attributed to low oral bioavailability. To optimise the known structure-activity relationships previously reported and overcome the suspected low absorption or rapid metabolism, optimisation of the analogues with regard to pharmacokinetic properties should be implemented.

This project aims to synthesise novel analogues based on the previously obtained SARs for polyamine analogues against *P. falciparum* parasites [107]. Novel analogues of the reported lead compounds will be designed to incorporate structural features that enhance metabolic stability, increase permeability and increase log D to less than 5 [110]. An attractive strategy to improve metabolic stability is to block the metabolically labile sites present in the analogues with a fluorine or halogen substituents [111], due to hydroxylation in Phase I metabolism that occurs at the *para*-position of the aromatic ring. Therefore, halogenated analogues are expected to be more metabolically stable as the C-X bond is considerably stronger [112]. This strategy has been applied successfully to a large range of previously inactive compounds [113]. Substitution at the *para*-position with a trifluoromethyl group could also aid in increasing the metabolic stability of the analogues by blocking oxidation at the *para*-position in addition to deactivating the  $\pi$  system of the benzene ring [114]. Further modification of the polyamine backbone to reduce the number of rotatable bonds by using a conformationally restrained cyclic ring such as a piperazine, could also lead to increased bioavailability. The observations made by Veber *et al* that orally active compounds have less than 10 rotatable bonds [151].

Additionally, the cyclic ring would drastically decrease the basicity of the amine functionalities.

The proposed structural modifications to enhance metabolic stability are therefore presented as: 1) *para*-substitution on the terminal phenyl rings with various halogens and trifluoromethyl groups and 2) reducing the number of rotatable bonds via incorporation of a structurally rigid polyamine backbone i.e. piperazine.

## 1.7 Hypothesis

The structural modification of novel 3-5-3 carbon backbone (bis)urea and (bis)thiourea polyamine analogues with *para*-substituted phenyl rings containing various halogens and trifluoromethyl groups, additional modification of the backbone to piperazine, will have potent *in vitro* antiplasmodial activity against the human malaria parasite, *P. falciparum* and possess greater drug-like properties.

## 1.8 Research Objectives

1. Synthesis of (bis)urea and (bis)thiourea substituted polyamines based on previous series of lead compounds.
2. Characterisation of polyamine analogues, Absorption, Distribution, Metabolism, Excretion and Toxicity (ADMET) characteristics and their drug-likeness *in silico*.
3. *In vitro* antiplasmodial activity determination of the polyamine analogues against drug sensitive and -resistant strains of *P. falciparum*.
4. Development of structure-activity relationship based on the current and previous series of polyamine analogues.
5. Development of predictive quantitative structure-activity relationships based on the current and previous series of polyamine analogues.

Publications containing work presented in this dissertation:

Verlinden, Bianca K., Marna de Beer, Boobalan Pachaiyappan, Ethan Besaans, Warren A. Andayi, Janette Reader, Jandeli Niemand *et al.* "Interrogating alkyl and arylalkylpolyamino (bis) urea and (bis) thiourea isosteres as potent antimalarial chemotypes against multiple lifecycle forms of *Plasmodium falciparum* parasites." *Bioorganic & Medicinal Chemistry*, Volume 23, Issue 16, 15 August 2015, Pages 5131-5143.

## Chapter 2: Materials and Methods

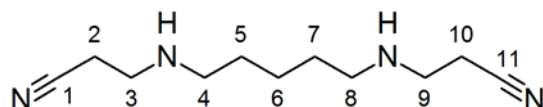
### 2.1 Synthesis of Polyamino(bis)ureas and Polyamino(bis)thioureas

All chemical reagents and dry solvents were purchased from Sigma Aldrich Chemical Co. (Milwaukee, WI) and were used without further purification. For reaction purposes, dry solvents were used, which were stored over molecular sieves. Thin layer chromatography (TLC) was performed on Merck pre-coated silica gel 60 F-254 plates, visualisation was by UV lamp, iodine stain and ninhydrin stain. Column chromatography was performed on Sigma Aldrich silica gel 60, 230–440 mesh. All  $^1\text{H}$  and  $^{13}\text{C}$  NMR spectra were recorded on a Bruker Avance 400 MHz spectrometer, and all chemical shifts are reported as  $\delta$  values referenced to TMS. Splitting patterns are indicated as follows: s, singlet; d, doublet; t, triplet; m, multiplet; b, broad peak. In all cases,  $^1\text{H}$  NMR and  $^{13}\text{C}$  NMR were consistent with assigned structures. **In some cases, the protons of amines were not seen in the  $^1\text{H}$  NMR, likely as a result of deuterium exchange due to hygroscopic NMR solvents.** Infrared spectra were recorded on a Bruker Alpha ATR-IR spectrophotometer and are referenced to polystyrene. Prior to biological testing, the target molecules as depicted in Scheme 1 and 2 were determined to be 95% pure or greater by UPLC-MS chromatography (ESI-time-of-flight) using a Waters H-series chromatograph fitted with a C18 reversed-phase column (Acquity UPLC BEH C18 1.7  $\mu\text{M}$ , 2.1  $\times$  50 mm). A gradient elution (95%  $\text{H}_2\text{O}$ /5% acetonitrile to 20%  $\text{H}_2\text{O}$ /80% acetonitrile) over 10 min was used. The specific synthetic procedures and spectral analysis for each intermediate and target molecule is included in Appendix 1.

#### 2.1.1 Synthesis of analogues based on the 3-5-3 backbone

##### 2.1.1.1 Synthesis and spectral analysis of compounds 2-4

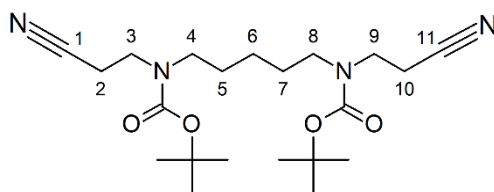
###### **1,13-dinitrile-4,10-diazotridecane (2)**



To a solution of **pentane-1,5-diamine (1)** (1.00 g, 9.79 mmol) in anhydrous ethanol (90 ml) was added acrylonitrile (10.38 g, 19.57 mmol) and the resulting solution was stirred at room temperature for 48 hrs. The completion of the reaction was confirmed by TLC (40% MeOH in  $\text{CH}_2\text{Cl}_2$ ) (Figure 3.1). The solvent was evaporated to yield a viscous yellow oil (1.75 g, 85% yield).  $R_f$ : 0.33.  $^1\text{H}$  NMR ( $\text{CDCl}_3$ , 300 MHz):  $\delta$  2.76 (t, 4H,  $J = 5$  Hz, H-3,

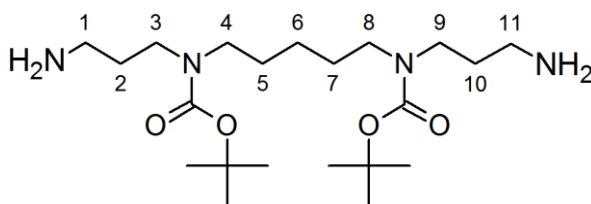
H-9), 2.47 (t, 4H,  $J=9.3$  Hz, H-2, H-10), 2.34 (t, 4H,  $J=6.8$  Hz H-4, H-8), 1.39 (m, 4H, H-5, H-7), 1.24. (m, 2H, H-6).  $^{13}\text{C}$  NMR ( $\text{CDCl}_3$ ):  $\delta$  119.25 (2C), 47.67 (2C), 44.93 (2C), 27.87 (2C), 25.55 (2C), 18.56 (1C). FT-IR: 3310 (N-H st), 2928, 2853, 2245 (CN st), 1642, 1469, 1419, 1363, 1124, 867, 749. MS (EI  $m/z$ ) calculated for  $\text{C}_{11}\text{H}_{20}\text{N}_4$  [ $\text{M}^+$ ] = 208.17; found 208.07 [ $\text{M}^+$ ].

### 1, 13-dinitrile-4, 10-(di-tert-butylloxycarbonyl)-4, 10-diazotridecane (3)



To a solution of **1,13-Dinitrile-4,10-diazotridecane (2)** (2.00 g, 9.60 mmol) in  $\text{CHCl}_3$  (150 ml) was added *N,N*-Diisopropylethylamine (DIPEA) (3.34 ml) and the reaction mixture was stirred at  $0^\circ\text{C}$  for 10 min, followed by which Di-tert-butyl dicarbonate (4.19 g, 19.2 mmol) was added. The resulting mixture was stirred at room temperature for 24 hrs. When the completion of the reaction was confirmed by TLC ( $\text{CH}_2\text{Cl}_2/\text{MeOH}/\text{NH}_4\text{OH}$  89:10:1) (Figure 3.4), the solvent was removed under reduced pressure, diluted with ethyl acetate and washed with 1 N HCl and a saturated brine solution. The organic layer was then dried with anhydrous  $\text{MgSO}_4$  and filtered. The dried organic layer was concentrated and subjected to purification using silica gel chromatography ( $\text{CH}_2\text{Cl}_2/\text{MeOH}/\text{NH}_4\text{OH}$  89:10:1) to yield a yellow viscous oil (1.73 g, 54% yield).  $R_f$ : 0.8,  $^1\text{H}$  NMR ( $\text{CDCl}_3$ ):  $\delta$  3.42 (t, 4H,  $J = 8.9$  Hz, H-3, H-9), 3.22 (t, 4H,  $J = 9.8$  Hz, H-2, H-10), 2.58 (bs, 4H, H-4, H-8), 1.50 (m, 4H, H-5, H-7), 1.41 (m, 18H, Boc), 1.23 (m, 2H, H-6).  $^{13}\text{C}$  NMR ( $\text{CDCl}_3$ ):  $\delta$  146.68 (2C), 118.36 (2C), 80.3 (2C), 48.50 (2C), 47.38 (2C), 28.16 (8C), 25.23 (1C), 17.51. (2C). FT-IR: 3054, 3005, 2988, 2348, 1690, 1276, 1263, 769, 747, 706. MS (EI  $m/z$ ) calculated for  $\text{C}_{21}\text{H}_{36}\text{N}_4\text{O}_4$  [ $\text{M}^+$ ] = 408.27; found 409.30 [ $\text{M}^+$ ].

### 1, 13-diamino-4, 10-di(tert-butylloxycarbonyl)-4, 10-diazatridecane (4)



To a Parr-hydrogenator bottle was added **1, 13-dinitrile-4, 10-(di-tert-butylloxycarbonyl)-4, 10-diazotridecane (3)** (2.09 g, 5.1 mmol) and 1 g of Raney Cobalt-2724 (50% w/v in  $\text{H}_2\text{O}$ ) in anhydrous ethanol (120 ml) and concentrated  $\text{NH}_4\text{OH}$  (5 ml).

The mixture was shaken on a Parr-Hydrogenator at room temperature for 96 hrs at 55 psi. The reaction mixture was filtered over celite and the filtrate was concentrated *in vacuo*. The sample was then dissolved in water (50 ml), basified with concentrated NH<sub>4</sub>OH and extracted three times with CH<sub>2</sub>Cl<sub>2</sub> (50 ml), the organic layers were combined, dried over MgSO<sub>4</sub> and the solvent was removed *in vacuo* to yield a viscous yellow oil (1.956 g, 91.6% yield) which was used without further purification. *R*<sub>f</sub>: 0.09 (CH<sub>2</sub>Cl<sub>2</sub>/MeOH/NH<sub>4</sub>OH 89:10:1), <sup>1</sup>H NMR (CDCl<sub>3</sub>): δ 3.15 (t, 4H *J* = 5 Hz, H-3, H-9), 3.09 (t, 4H *J* = 5.1 Hz, H-2, H-10), 2.50 (bs, 4H, H-4, H-8), 1.89 (bs, 4H, NH<sub>2</sub>), 1.65 (m, 4H, H-1, H-11), 1.51 (m, 4H, H-5, H-7), 1.37 (m, 18H, Boc), 1.28 (m, 2H, H-6). <sup>13</sup>C NMR (CDCl<sub>3</sub>): δ 154 (2C), 78.06 (2C), 48.05 (2C), 46.19 (2C), 38.87 (2C), 29.82 (2C), 28.18 (6C), 27.42 (2C), 23.40 (1C). FT-IR: 2970, 2930, 2864, 1676, 1585, 1477, 1417, 1389, 1364, 1304, 1250, 1157, 1018, 879, 770. MS (EI *m/z*) calculated for: C<sub>21</sub>H<sub>44</sub>N<sub>4</sub>O<sub>4</sub> [M<sup>+</sup>] = 416.34; found 439.32 [M+Na].

#### A. General method for the synthesis of compounds E1SB-E4OB

An ice-cold stirred solution of **1,13-diamino-4,10-di(tert-butyloxycarbonyl)-4,10-diazatridecane (4)** in 20 ml anhydrous HPLC grade CH<sub>2</sub>Cl<sub>2</sub> was prepared under nitrogen. To this was added the corresponding aryl isocyanate or aryl isothiocyanate solution in 5 ml anhydrous HPLC grade CH<sub>2</sub>Cl<sub>2</sub> in a drop-wise fashion. The reaction mixture was allowed to stir at room temperature for 24 hrs. During this time, the formation of product was monitored by TLC (75% EtOAc in hexane). After the completion of the reaction, the solvent was removed *in vacuo* and the crude product was purified using chromatography on silica gel (75% EtOAc in hexane) to afford the final product in moderate yields. Please refer to Chapter 3 for detailed NMR data for compounds E1SB-E4OB.

#### B. General method for the synthesis of compounds E1SD-E4OD

To a stirred solution of N-Boc protected (bis)urea or (bis)thiourea derivative was added HPLC grade EtOAc (20 ml) under a stream of nitrogen followed by 6 molar equivalents of 1.25 M HCl in MeOH. The reaction mixture was allowed to stir at room temperature overnight and formation of the product was monitored by TLC. The product precipitated as a crystalline solid during the course of the reaction. After the completion of the reaction, the solvent was removed *in vacuo* followed by the addition of fresh EtOAc, which was then stirred for 15 min. The solution was then filtered and the precipitate was washed several times with EtOAc and anhydrous HPLC grade CH<sub>2</sub>Cl<sub>2</sub>. The solid so obtained was

dried at 80°C for 30 min to afford the final pure product in good yields. Please refer to Chapter 3 for detailed NMR data for compounds E1SD-E4OD.

## 2.1.2 Synthesis of analogues based on the 3-piperaziny-3 backbone

### C. General method for the synthesis of compounds A1S-A5O

An ice-cold stirred solution of **1,4-bis(3-aminopropyl)piperazine** in 20 ml anhydrous HPLC grade CH<sub>2</sub>Cl<sub>2</sub> was prepared under nitrogen. To this was added the corresponding aryl isocyanate or aryl isothiocyanate solution in 5 ml anhydrous HPLC grade CH<sub>2</sub>Cl<sub>2</sub> in a drop wise fashion. The reaction mixture was allowed to stir at room temperature for 24 hrs. During this time; the formation of product was monitored by TLC (CH<sub>2</sub>Cl<sub>2</sub>/MeOH/NH<sub>4</sub>OH 89:10:1). After the completion of the reaction, the solvent was removed *in vacuo* and the crude product was dissolved in 10 ml of hexane. This solution was vacuum filtered through a plug of silica gel followed by washing of the plug with small quantities of the eluent (CH<sub>2</sub>Cl<sub>2</sub>/MeOH/NH<sub>4</sub>OH 89:10:1). The solvent was removed *in vacuo* and the solid so obtained was filtered and washed with small quantities of hexane and DCM. The filter cake was then dried at 80°C for 30 min to afford the final pure product in good yields. Please refer to Chapter 3 for detailed NMR data for compounds A1S-A5O.

## 2.2 Antiplasmodial activity determination

### 2.2.1 Preparation of erythrocytes and culture medium

Type O+ or A+ blood was collected in blood bags (SO Fenwal® AFR0193 blood bag, 70 mL anticoagulant, Adcock Ingram) and left overnight at 4°C to separate. The serum and white blood cells above the erythrocytes were aspirated off and discarded, using a vacuum pump system (Integra Vacusafe, Labotec). This was followed by re-suspension in phosphate buffered saline (1x PBS; 10 mM Na<sub>2</sub>HPO<sub>4</sub>, 1.4 mM KH<sub>2</sub>PO<sub>4</sub>, 137 mM NaCl and 2.7 mM KCl, pH 7.2) and centrifugation at 3500xg (C-28A, Boeco) for 10 min. This was repeated until all visible serum and white blood cells were removed. Erythrocytes were stored as a 50% haematocrit solution with incomplete RPMI 1640 culture medium (Sigma) (23.81 mM sodium bicarbonate (Sigma), 0.024 mg/ml gentamycin (HyClone Laboratories Inc.), 25 mM HEPES (Sigma), 0.2% glucose (Sigma), 0.2 mM hypoxanthine (Sigma) and 5 g/l Albumax II (GIBCO™ Invitrogen Corporation) at 4°C until use [115]. HEPES is a buffer maintaining the culture at pH 7.5 in combination with a carbon dioxide-

bicarbonate (CO<sub>2</sub>-HCO<sub>3</sub>) buffer system consisting of the sodium bicarbonate and CO<sub>2</sub>. Albumax II is used as a source of essential lipids and proteins; it is used in place of human serum to prevent contaminating immunoglobulins from entering the culture. Gentamycin is used as an antibiotic to prevent bacterial contamination. Hypoxanthine is required for parasite nucleotide synthesis [116]. Glucose maintains the osmolarity of the solution and is a carbon source required for metabolism [117].

### **2.2.2 *In vitro* culturing of *P. falciparum* parasites**

*P. falciparum* (3D7) infected erythrocytes stored in cryotubes, were removed from liquid nitrogen storage and thawed at 37°C for 5 min. Thawed parasites were transferred to a 50 ml falcon tube and 0.2 ml of sterile 12% (w/v) NaCl was added drop wise to gradually increase the osmolarity of the solution. The solution was re-suspended and allowed to incubate at room temperature for 5 min. Followed by the addition of 1.8 ml of 1.6% (w/v) NaCl and re-suspension. The solution was then centrifuged (C-28A, Boeco) at 3500xg for 5 min and the supernatant aspirated using a vacuum pump system (Integra Vacusafe, Labotec). Erythrocytes (50% haematocrit) was added to the pellet of infected erythrocytes and pre-warmed culture medium heated in a water bath at 37°C was added to a total volume of 20 ml to obtain a 5% haematocrit culture. The mixture was then transferred to a 75 ml culture flask (Greiner bio-one) and gassed for approximately 30 sec with a low-oxygen gas mixture (90% nitrogen, 5% oxygen and 5% carbon dioxide (Afrox)). The culture flask was sealed and placed in a shaking incubator (Ratek, Orbital Mixer Incubator) at 37°C and rotated at 58 rpm, to decrease the prevalence of multiple infections [115, 118]. Routine culturing was performed daily by replacing spent media, gassing and maintaining parasitaemia at 3-5%. Parasitaemia was monitored by means of Giemsa stained thin microscope slides as follows: approximately 0.5 ml of culture suspension was pelleted by centrifugation (Combi-spin FVL-2400N, Boeco) for 30 sec. A drop of the pellet was then placed on a microscope slide and spread across the slide using another clean slide. The slide was dried and fixed in methanol (Merck, Germany) followed by staining in a 10% Giemsa solution (Merck, Germany) for 3-5 min. Excess stain was removed by rinsing under running water and the slide was then dried. A 100x oil immersion lens light microscope was used to determine parasitaemia by counting the total number of erythrocytes and infected erythrocytes present in the microscope field for at least 10 fields. Parasitaemia was then calculated by dividing the number of infected erythrocytes by the total number of erythrocytes counted and multiplying by 100.



### 2.2.3 Sorbitol synchronisation

The *P. falciparum* parasite cultures were synchronised every second day to be >95% ring-stage by means of sorbitol synchronisation. Metabolically active trophozoite stage cells are permeable to sorbitol and can be selectively lysed when incubated with iso-osmolar sorbitol solutions [119, 120]. Parasite cultures were transferred to 50 ml falcon tubes centrifuged at 3500xg for 5 min, the supernatant was removed and discarded. To the pellet was added 10x the pellet volume of 5% (w/v) D-sorbitol pre-heated to 37°C in a water bath and the pellet re-suspended. The solution was then incubated at 37°C for 15 min followed by centrifugation as above. The supernatant was removed and discarded and 10x the pellet volume phosphate buffered saline (1x PBS; 10 mM Na<sub>2</sub>HPO<sub>4</sub>, 1.4 mM KH<sub>2</sub>PO<sub>4</sub>, 137 mM NaCl and 2.7 mM KCl, pH 7.2) was added and the pellet re-suspended followed by centrifugation and supernatant discarding as above. This was repeated three times to ensure sorbitol removal [121].

### 2.2.4 Dose-response analyses for inhibition of parasite proliferation

The Malaria SYBR Green I based fluorescence assay was used to determine the inhibition of parasite proliferation [106]. The assay utilises the intercalation of a fluorescent DNA stain (SYBR Green I) into dsDNA molecules. By measuring the fluorescence of the dye following excitation a quantitative measure of DNA can be obtained, allowing a direct correlation between DNA levels and parasite proliferation [122]. Synchronised cultures of ring-stage *P. falciparum* (>95% ring-stage) were treated with the polyamine analogues, dissolved in DMSO and diluted to specific concentrations in complete RPMI 1640 culture medium. Chloroquine sulphate was used as a positive drug control (0.5 µM in complete RPMI 1640 culture medium) and was compared to untreated parasite as a 100% viable parasite control. Parasitaemia was determined as previously discussed and sorbitol synchronisation was carried out. A parasite suspension (2% haematocrit and 1% parasitaemia) was prepared and treated with the selected concentrations of compounds in 96-well plates. The plates were incubated in a modular gas chamber and gassed with a low-oxygen gas mixture (90% nitrogen, 5% oxygen and 5% carbon dioxide (Afrox); the gas chamber was incubated at 37°C for 96 hrs in a stationary incubator (HERAcell 150i, Thermo Scientific). The plates were removed and 100 µl of each well was re-suspended, transferred to another 96-well plate containing 100 µl SYBR Green I lysis buffer (0.2 µl/ml 10 000xSYBR Green I (Invitrogen, Inc.), 20 mM Tris, pH 7.5; 5 mM EDTA; 0.008% (w/v) saponin; 0.08% (v/v) Triton X-100) in each well.

The plate was incubated at 37°C in the dark for 1 hrs followed by fluorescence measurement using a GloMax®-Multi microplate fluorometer (Promega) at an excitation of 490 nm and emission of 540 nm, integration time 1000 ms. The data after subtraction of background (chloroquine control) were expressed as percentage values of the untreated control to determine parasite proliferation. Data were analysed for at least three independent biological controls, each performed in technical triplicates, and plotted using Graphpad Prism 5.0 software.

## **2.3 Cheminformatic analysis of Polyamino(bis)ureas and Polyamino(bis)thioureas**

### **2.3.1 Determination of drug-likeness**

The physiochemical properties, ADMET descriptors and Quantitative Estimate of Drug-likeness (QED) were determined. All the descriptors were calculated using Discovery Studio (Accelrys Software Inc., V4.0). The compound structures were first drawn in ChemSketch (Accelrys Software Inc., V 12.01) and saved as .mol files. These structure files were then loaded into Discovery Studio and force field simulations were applied (CHARMm). An energy minimization cascade was subsequently performed (CHARMm) using an energy tolerance of 0.001 Kcal/mol. Finally, the ADMET descriptors were predicted using the small-molecule protocols the following was predicted; intestinal absorption, aqueous solubility, blood brain barrier penetration, plasma protein binding, cytochrome P450 2D6 inhibition, and hepatotoxicity.

Further physiochemical properties were determined for each structure using the small-molecule protocols predicting namely; the molecular weight, lipophilicity (AlogP), hydrogen bond donors, hydrogen bond acceptors, rotatable bonds aromatic rings, violations of Lipinski's rules and the QED. The QED is a probability based metric that is based on the underlying distributions of favourable physiochemical drug properties. It captures the drug-likeness of a drug numerically rather than as a rule based metric. Allowing it to quantify drug-likeness while tolerating unfavourable physiochemical properties.

### **2.3.2 Structure-activity relationship analysis**

The analysis of structure-activity relationships was performed in Osiris DataWarrior V 4.2.2 (Actelion Pharmaceuticals Ltd) freely available at (<http://www.openmolecules.org/datawarrior/>) [123]. The polyamine analogue data presented here, together with a number of series previously tested were combined into a

database, appendix Table 1 [106, 107]. The removal of compounds with amidine functional groups was performed as the low antiplasmodial activity analogues distorted the analysis. Furthermore, all the  $IC_{50}$  values were log transformed to reduce dimensionality. The compound structures were first drawn in ChemSketch (Accelrys Software Inc., V 12.01) and saved as .mol files, followed by conversion into Smiles notation using Open Babel and uploaded into Datawarrior. The similarity criterion used was the Skeleton Spheres descriptor, which considers stereochemistry, counts duplicate fragments and encodes hetero-atom depleted skeletons. It is the most accurate descriptor for calculating similarities of chemical graphs. Visualisation of the chemical space of the analogues was accomplished using dimensionality reducing techniques such as principal component analysis (PCA) and molecular similarity analysis (MSA). Matched molecular pair activity cliff analysis was performed using the Structure-Activity Landscape Index (SALI) metric, calculated for all pairs of similar molecules. It is a measure of how much activity is gained or lost as a result of small changes in structure.

### 2.3.3 Quantitative structure-activity relationship model development

The compound structures were first drawn in ChemSketch (Accelrys Software Inc., V 12.01) and saved as .mol files. These structure files were then loaded into Discovery Studio (Accelrys Software Inc., V4.0) and force field simulations were applied (CHARMm). An energy minimization cascade was subsequently performed (CHARMm) using an energy tolerance of 0.001 Kcal/mol. The entire dataset  $IC_{50}$  values were converted to  $-\log(IC_{50})$  values. The removal of compounds with biguanide internal substitution, amidine internal substitution and alkyl terminal substituents was performed to remove the structural outliers present. The entire dataset of compounds (35), was then split into a 29 compound training set and 5 compound test set using the diverse molecules splitting method. The splitting method used 20 similarity clusters and used a center selection method of maximum dissimilarity using the predefined descriptors: AlogP; molecular weight; number of hydrogen bond donors; number of hydrogen bond acceptors; number of rotatable bonds; number of aromatic rings; number of atoms; number of fragments and molecular polar surface area. These datasets were then uploaded to the online chemical modelling environment (<https://ochem.eu/>) [124]. The multiple model builder application was used and fast stagewise multivariate linear regression (FSMLR) and multiple linear regression analysis (MLRA) amongst others were selected as machine learning methods. The three-dimensional chemical structures were generated by CORINA [125]. Various descriptor packages were selected and descriptor

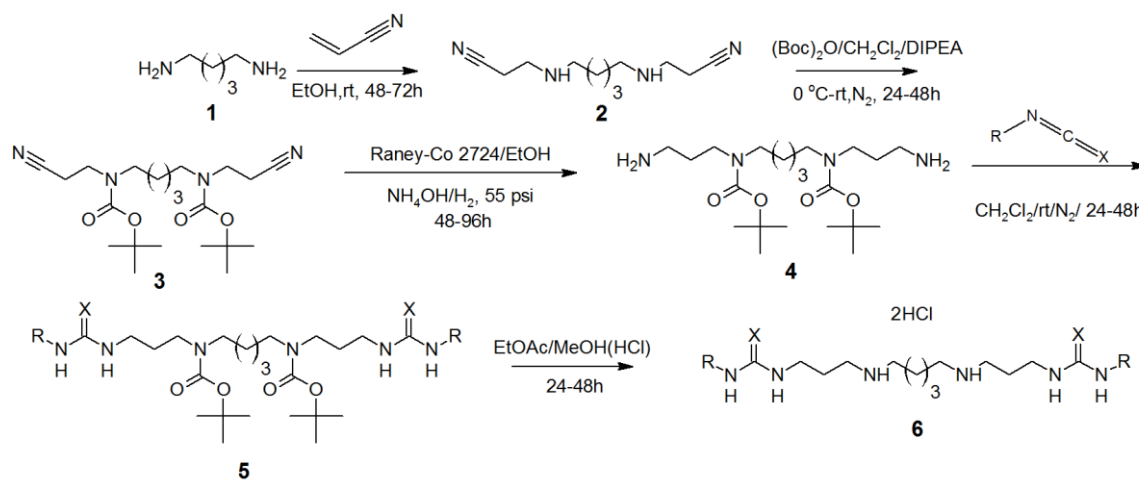
filtering was performed using unsupervised forward selection. Generated models were validated using 5-fold cross validation. The resultant models were then assessed based on the following statistical parameters: Pearson's correlation coefficient ( $R^2$ ); cross-validated  $R^2$  ( $q^2$ ), root mean square error (RMSE) and the mean absolute error (MAE).

## Chapter 3: Results

### 3.1 Synthesis of Polyamino(bis)ureas and Polyamino(bis)thioureas

#### 3.1.1 Synthesis of analogues based on the 3-5-3 backbone

The synthesis of the polyamine analogues based on the 3-5-3 backbone was performed based on the proposed structural modifications. Substitution at the *para*-position of the phenyl rings of the polyamine analogues was accomplished based on a previously published method [126]. As illustrated in Scheme 1, the synthesis of the precursors was carried out by bis-cyanoethylation of cadaverine to obtain the bis-nitrile (**2**) [127]. The bis-nitrile (**2**) was then N-Boc protected to form the intermediate (**3**), which was then subjected to Raney-Nickel reduction to obtain the amine (**4**) [128]. The final precursor was then reacted with the corresponding aryl isocyanate or isothiocyanate to obtain compounds **E1OB-E4OB**. These were then N-Boc deprotected to yield the final compounds **E1OD-E4OD** as hydrochloride salts.



**E1SB** R = 4-chlorophenyl, X = S

**E1OB** R = 4-chlorophenyl, X = O

**E2SB** R = 4-fluorophenyl, X = S

**E2OB** R = 4-fluorophenyl, X = O

**E3SB** R = 4-trifluoromethylphenyl, X = S

**E3OB** R = 4-trifluoromethylphenyl, X = O

**E4OB** R = 4-bromophenyl, X = O

**E1SD** R = 4-chlorophenyl, X = S

**E1OD** R = 4-chlorophenyl, X = O

**E2SD** R = 4-fluorophenyl, X = S

**E2OD** R = 4-fluorophenyl, X = O

**E3SD** R = 4-trifluoromethylphenyl, X = S

**E3OD** R = 4-trifluoromethylphenyl, X = O

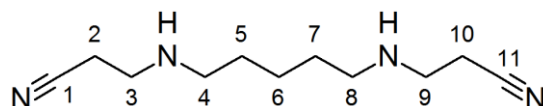
**E4OD** R = 4-bromophenyl, X = O

**Scheme 1: Synthetic scheme of (bis)ureas and (bis)thiourea analogues based on the 3-5-3 backbone.**

The diamine cadaverine (**1**) is bis-cyanoethylated producing the bis-nitrile (**2**). The bis-nitrile is then N-Boc protected to form an intermediate (**3**) which is subjected to Raney-nickel reduction producing the free amine (**4**). The free amine is then reacted with the appropriate isocyanate or isothiocyanate to form the N-Boc protected polyamine analogues (**E1SB-E4OB**). The N-Boc protected polyamine analogues (**E1SB-E4OB**) are then deprotected to form the hydrochloride salts of the polyamine analogues (**E1SD-E4OD**).

### 3.1.1.1 Synthesis and spectral analysis of compounds 2-4

#### 1,13-dinitrile-4,10-diazotridecane (**2**)



The synthesis **1,13-dinitrile-4,10-diazotridecane (2)** was successfully accomplished as shown in Figure 3.1 as the starting material is converted completely to the desired product as in spot P number 1. The product has an increased  $R_f$  value relative to the starting material indicating the bis-cyanoethylation. The presence of impurities present in the starting material was noted in spot S number 2 and 3, furthermore their respective reaction products were noted in spot P number 2 and 3. The product was used as is without further purification as multiple attempts at purification failed, however, upon workup the impurities greatly diminished.

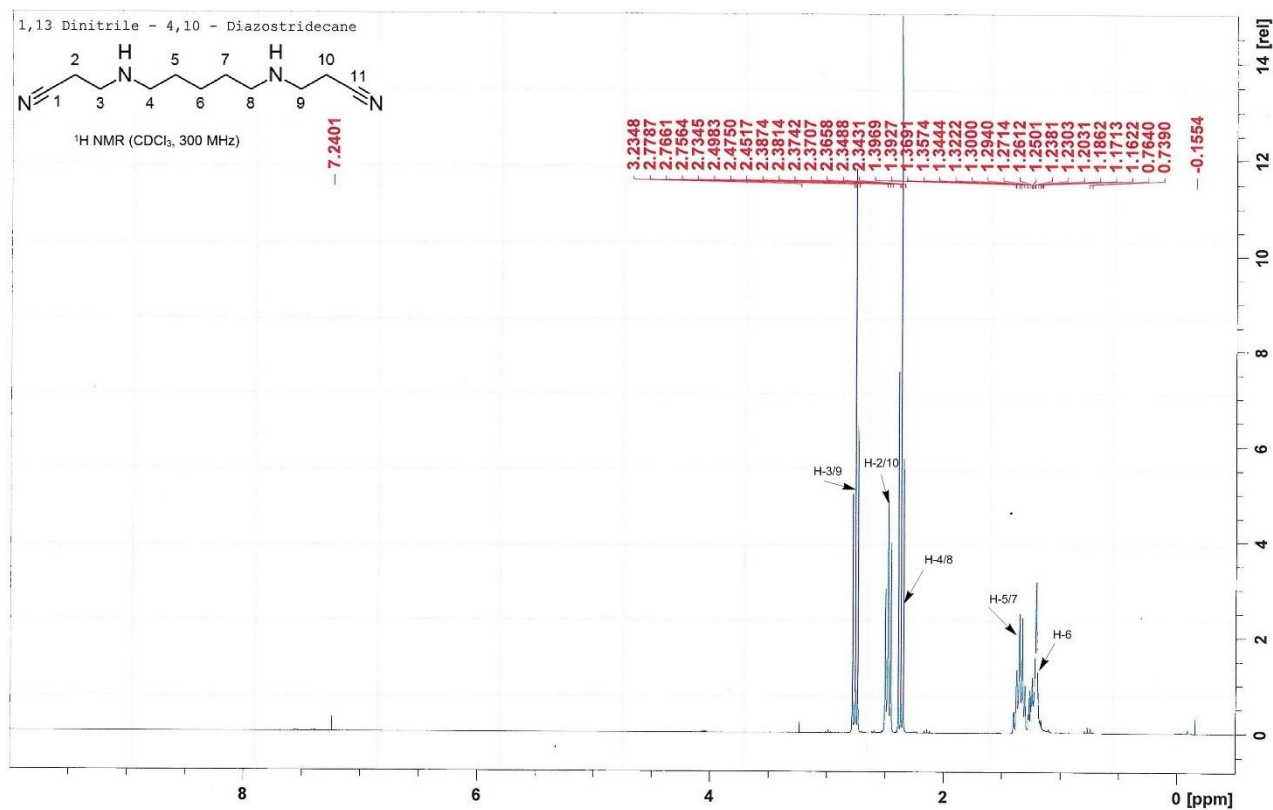


**Figure 3.1: TLC chromatogram of 1,13-dinitrile-4,10-diazotridecane (2)**

The chromatogram obtained for the synthesis of (**2**). S is the *pentane-1,5-diamine (1)*, A is the acrylonitrile and P is the final reaction mixture. The TLC was developed in (40% MeOH in  $\text{CH}_2\text{Cl}_2$ )

The spectral identification of (**2**) was accomplished by  $^1\text{H}$  NMR as shown in Figure 3.2. The presence of all the expected protons in the  $^1\text{H}$  NMR except those of the nitrogen's was seen. The nitrile functionality was confirmed by the peak at 119.25 in the  $^{13}\text{C}$  NMR. The expected splitting pattern obtained for the  $^1\text{H}$  NMR corresponded with the expected

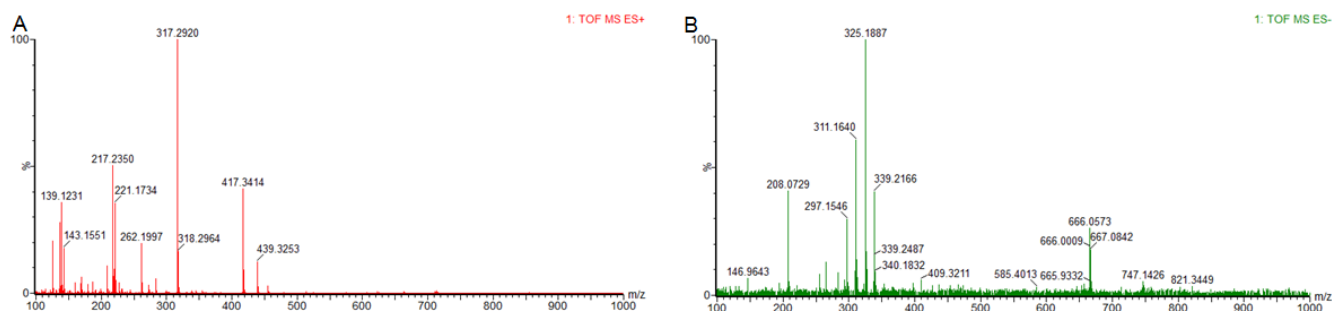
pattern confirming the assigned structure. The presence of a strong band at 2245 in the FT-IR spectrum indicated the presence of a nitrile functional group.



**Figure 3.2:**  $^1\text{H}$  NMR spectrum of **1,13-dinitrile-4,10-diazotridecane (2)**

The  $^1\text{H}$  NMR spectrum obtained for **(2)** in  $\text{CDCl}_3$ . Peak assignment is indicated for the corresponding protons.  $^1\text{H}$  NMR spectrum showing integration is included in Appendix figure 1.

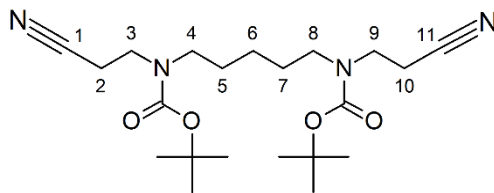
The Mass spectrum obtained for **(2)** as shown in Figure 3.3 corresponded to the expected fragmentation pattern. In Figure 3.3 A, the peak at 417.34 corresponds to the molecular ion adduct  $[2\text{M}+\text{H}]$ . Peak 439.25 corresponds to molecular ion adduct  $[2\text{M}+\text{Na}]$ . In Figure 3.3 B the molecular ion of interest calculated for  $\text{C}_{11}\text{H}_{20}\text{N}_4$  is  $[\text{M}^-] = 208.17$  and 208.07 was found.



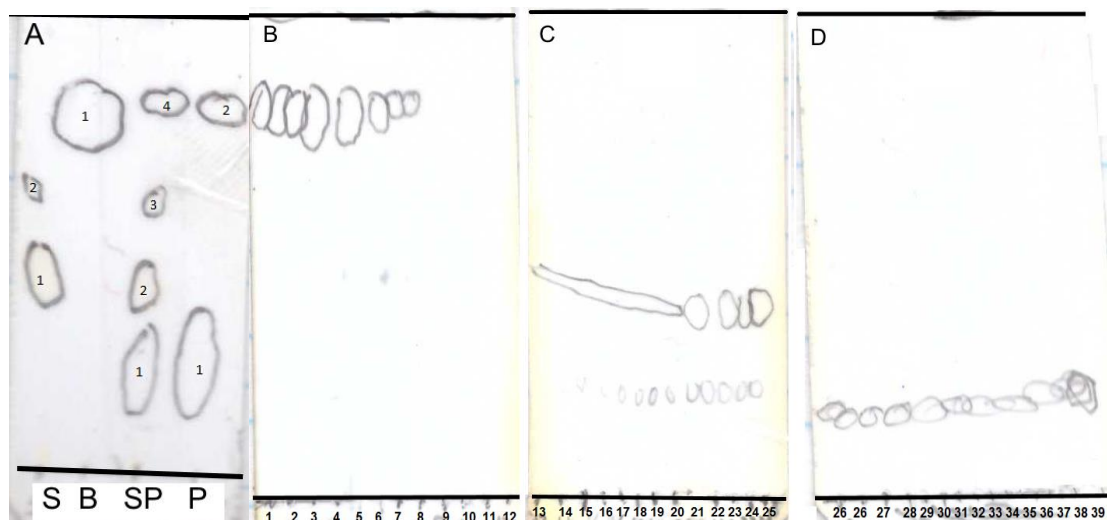
**Figure 3.3:** Mass spectrum of **1,13-Dinitrile-4,10-diazotridecane (2)**

The mass spectrum of **(2)** in A: positive ion mode and B: negative ion mode. MS (EI  $m/z$ ) calculated for  $\text{C}_{11}\text{H}_{20}\text{N}_4$   $[\text{M}^-] = 208.17$ ; found 208.07  $[\text{M}^-]$ .

### 1, 13-dinitrile-4, 10-(di-tert-butylloxycarbonyl)-4, 10-diazotridecane (**3**)



The synthesis of (**3**) was successfully accomplished as shown in Figure 3.4. The starting material was N-Boc protected and consequently the desired product as in spot P number 2 had a greater  $R_f$  value. The workup performed resulted in the removal of the majority of the precursor and DIPEA. Further purification of the reaction mixture was accomplished by silica gel chromatography ( $\text{CH}_2\text{Cl}_2/\text{MeOH}/\text{NH}_4\text{OH}$  89:10:1). Fractions 1-9 were then combined and the solvent was evaporated to yield pure (**3**).



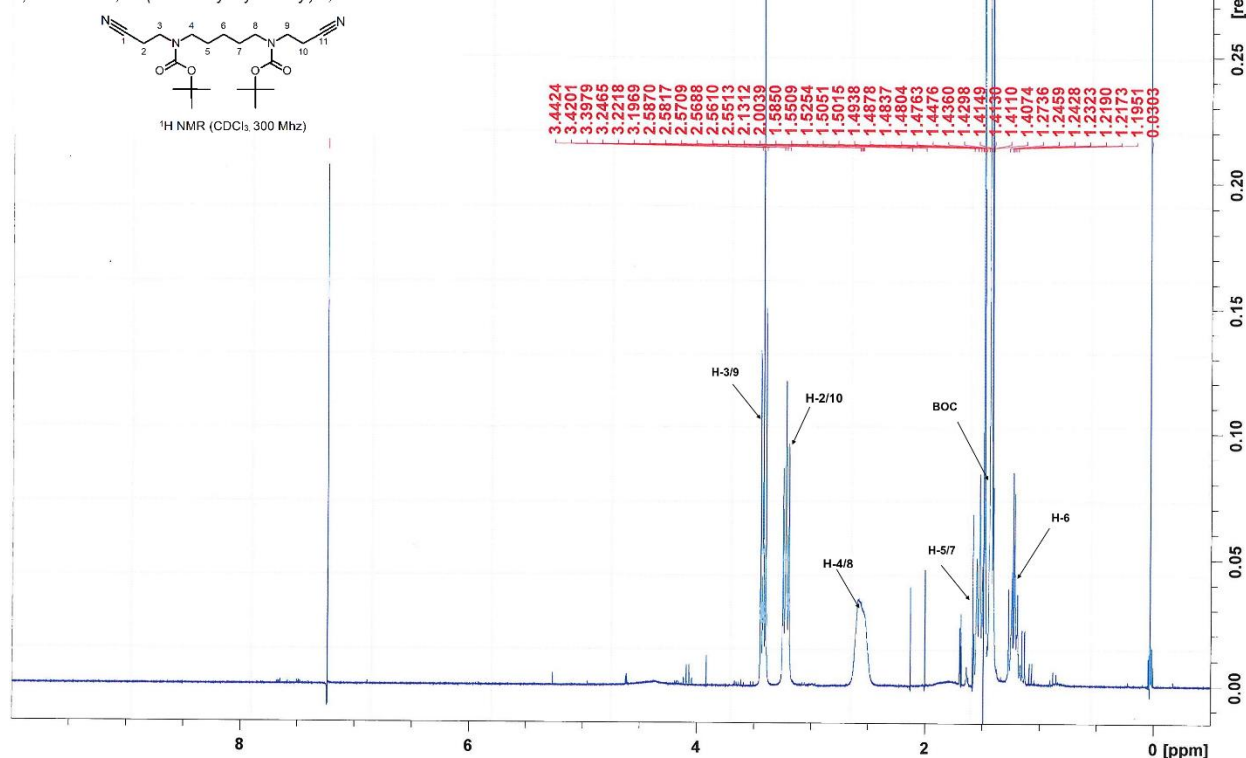
**Figure 3.4: TLC chromatogram of 1, 13-dinitrile-4, 10-(di-tert-butylloxycarbonyl)-4, 10-diazotridecane (**3**) A and column chromatography purification B, C and D**

The chromatogram obtained for the synthesis of (**3**) performed in ( $\text{CH}_2\text{Cl}_2/\text{MeOH}/\text{NH}_4\text{OH}$  89:10:1). S is the starting material, B is the Boc anhydride, SP is the starting material and the final reaction mixture, P is the final reaction mixture. The column chromatography B, C and D was performed with ( $\text{CH}_2\text{Cl}_2/\text{MeOH}/\text{NH}_4\text{OH}$  89:10:1) and fractions 1-9 were combined.

The confirmation of the structure of (**3**) was accomplished by  $^1\text{H}$  NMR spectroscopy as shown in Figure 3.5. The presence of all the expected protons in the  $^1\text{H}$  NMR was seen. The lack of protons associated with the internal amines indicated the N-Boc protection additionally the intense peak at 1.41 ppm with 18 hydrogen's indicated that both nitrogen's were protected. The expected splitting pattern obtained for the  $^1\text{H}$  NMR corresponded with the expected pattern confirming the assigned structure.



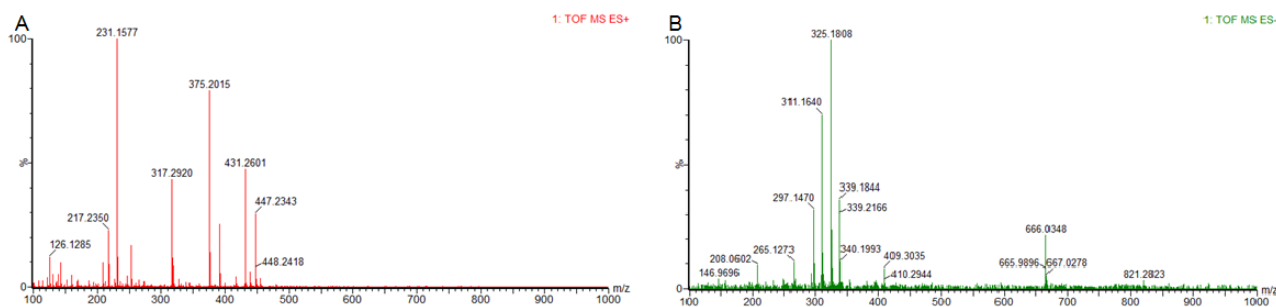
1, 13-dinitrile-4, 10-(di-tert-butylloxycarbonyl)-4, 10-diazotridecane



**Figure 3.5:  $^1\text{H}$  NMR spectrum of 1, 13-dinitrile-4, 10-(di-tert-butylloxycarbonyl)-4, 10-diazotridecane (3)**

The  $^1\text{H}$  NMR spectrum obtained for (3) in  $\text{CDCl}_3$ . Peak assignment is indicated for the corresponding protons.  $^1\text{H}$  NMR spectrum showing integration is included in Appendix figure 2.

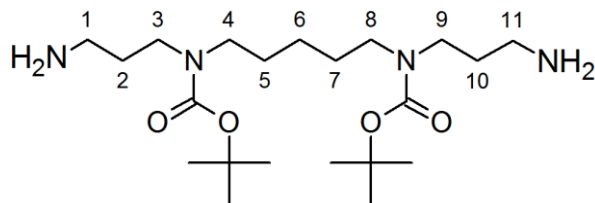
The mass spectrum obtained for (3) as shown in Figure 3.6 corresponded to the expected fragmentation pattern. In Figure 3.6 A, the highest intensity peak 231.16 corresponds to the fragment ion with both Boc groups removed appearing as the sodium adduct  $[\text{M}+\text{Na}]^+$ . Similar to the mass spectrum obtained for (2), while the peaks at 431.26 and 447.23 correspond to the sodium  $[\text{M}+\text{Na}]^+$  and potassium adducts  $[\text{M}+\text{K}]^+$  respectively. In Figure 3.6 B the molecular ion of interest calculated for  $\text{C}_{21}\text{H}_{36}\text{N}_4\text{O}_4$  is  $[\text{M}]^- = 408.27$  and 409.30 is found.



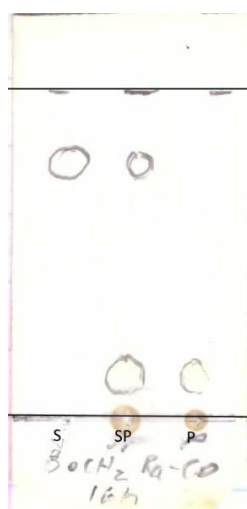
**Figure 3.6: Mass spectrum of 1, 13-dinitrile-4, 10-(di-tert-butylloxycarbonyl)-4, 10-diazotridecane (3).**

The mass spectrum of (3) in A: positive ion mode and B: negative ion mode. MS (EI  $m/z$ ) calculated for  $\text{C}_{21}\text{H}_{36}\text{N}_4\text{O}_4$   $[\text{M}]^- = 408.27$ ; found 409.30  $[\text{M}+\text{H}]^-$ .

**1, 13-diamino-4, 10-di(tert-butyloxycarbonyl)-4, 10-diazatridecane (4)**



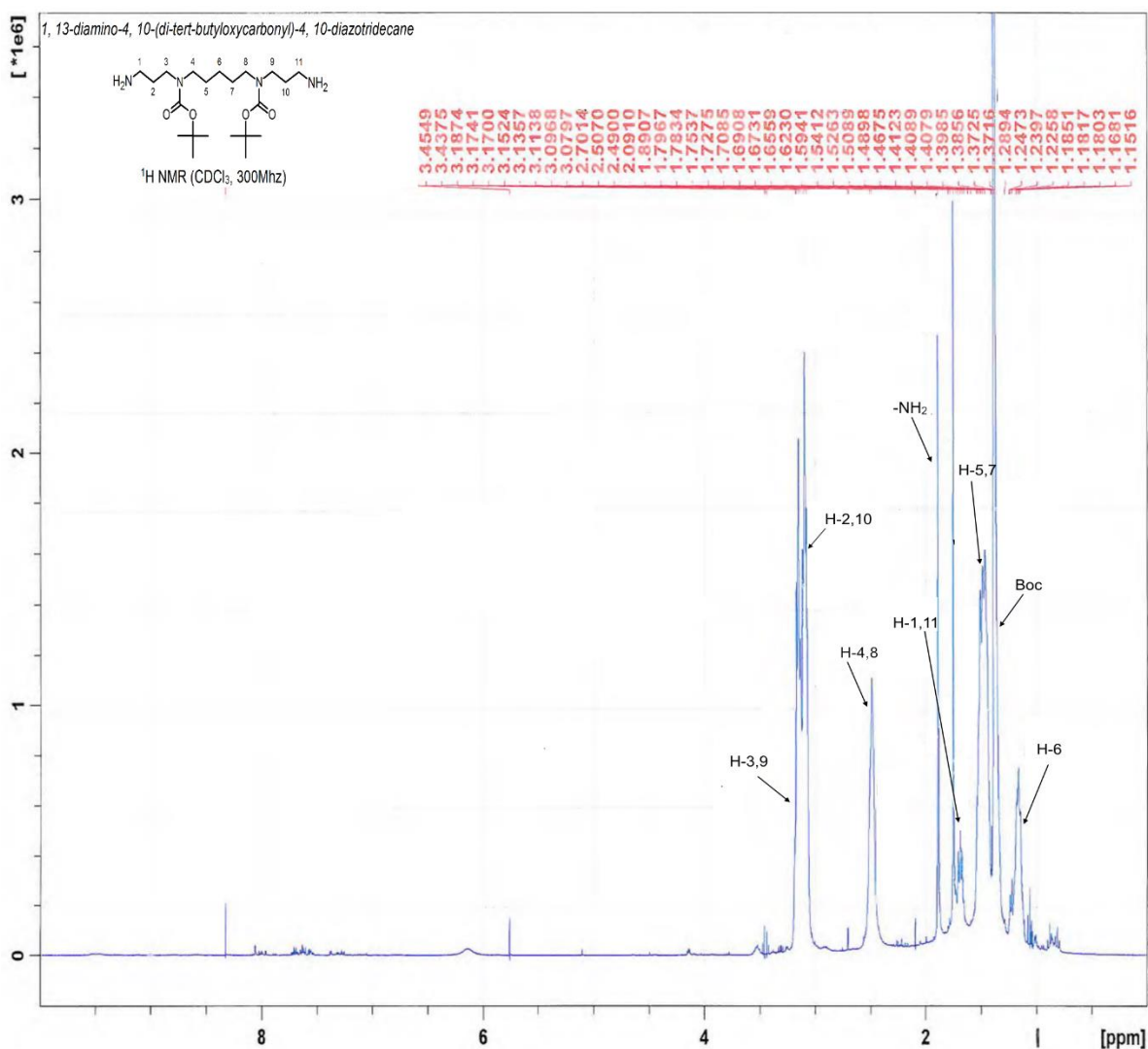
The conversion of (3) to (4) was presumably accomplished as shown in Figure 3.7 as the starting material is completely converted to the product as in spot P number 1. The product has a drastically reduced  $R_f$  value relative to the starting material as expected for the reduction of the nitrile groups to amines. The product was used as is without further purification.



**Figure 3.7: TLC chromatogram of 1, 13-diamino-4, 10-di(tert-butyloxycarbonyl)-4, 10-diazatridecane (4)**

The chromatogram obtained for the synthesis of (4) performed in (CH<sub>2</sub>Cl<sub>2</sub>/MeOH/NH<sub>4</sub>OH 89:10:1). S is the starting material, SP is the starting material and the final reaction mixture, P is the final reaction mixture.

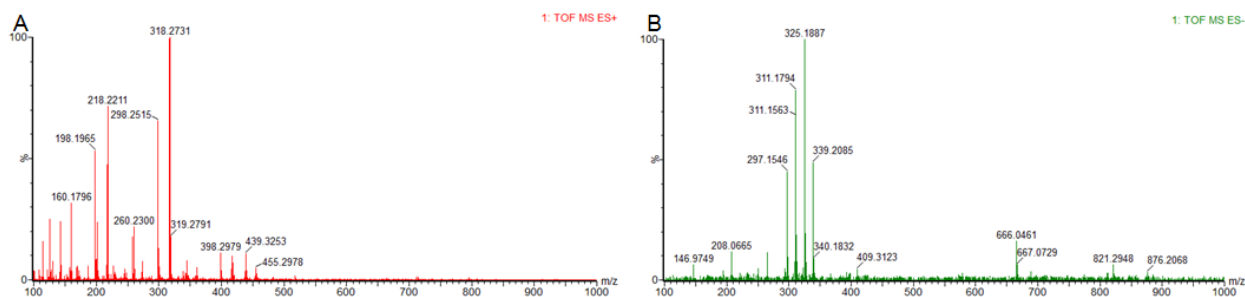
The confirmation of the structure of (4) was accomplished by <sup>1</sup>H NMR spectroscopy as shown in Figure 3.8. The presence of all the expected protons in the <sup>1</sup>H NMR was seen. The appearance of the amine proton peak at 1.89 ppm corresponds to the reduction of the nitrile groups. The shifting of the peaks corresponding to carbon 1 and 11 as seen in both the <sup>1</sup>H NMR and <sup>13</sup>C were indicative of the reduction of the nitrile groups. The expected splitting pattern obtained for the <sup>1</sup>H NMR corresponded with the expected pattern confirming the assigned structure.



**Figure 3.8:** <sup>1</sup>H NMR spectrum of 1, 13-diamino-4, 10-(di-tert-butylloxycarbonyl)-4, 10-diazotridecane (4)

The <sup>1</sup>H NMR spectrum obtained for (4) in CDCl<sub>3</sub>. Peak assignment is indicated for the corresponding protons. <sup>1</sup>H NMR spectrum showing integration is included in Appendix figure 3.

The mass spectrum obtained for (4) as shown in Figure 3.9 corresponded to the expected fragmentation pattern. In Figure 3.9 the peak at 398.29 is formed after the loss of an amine. Peak 298.24 correspond to the loss of one Boc group and one amine. The highest intensity peak 325.18, in Figure 3.9 A corresponds to the loss of a *tert*-butoxide radical and an amine. In Figure 3.9 A, the molecular ion of interest calculated for MS (EI *m/z*) calculated for: C<sub>21</sub>H<sub>44</sub>N<sub>4</sub>O<sub>4</sub> [M+Na]<sup>+</sup> = 439.32; found 439.32 [M+Na]<sup>+</sup>.

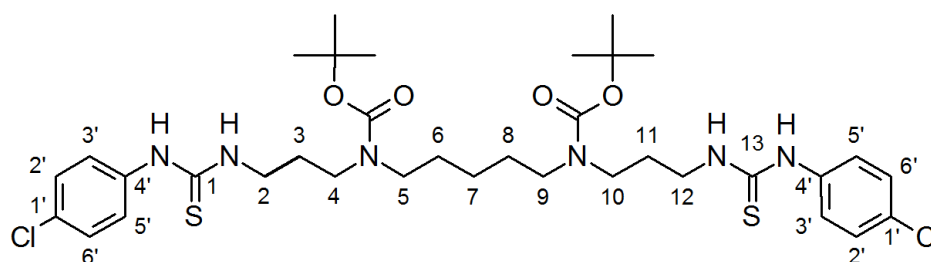


**Figure 3.9: Mass spectrum of 1, 13-diamino-4, 10-(di-tert-butylloxycarbonyl)-4, 10-diazotridecane (4).**

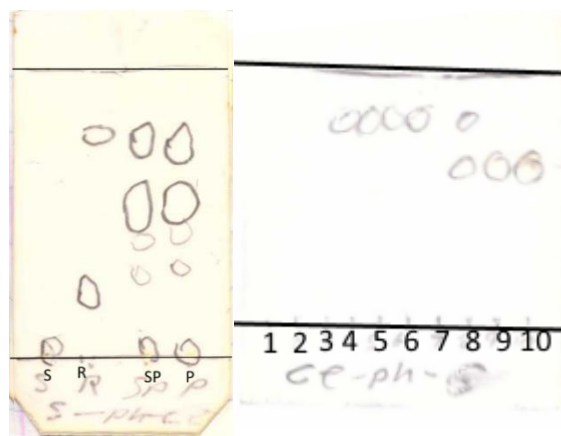
The mass spectrum of (4) in A: positive ion mode and B: negative ion mode. MS (EI  $m/z$ ) calculated for:  $C_{21}H_{44}N_4O_4$   $[M+Na]^+ = 439.32$ ; found 439.32  $[M+Na]^+$ .

### 3.1.1.2 Synthesis and spectral analysis of compounds E1SB-E4OB

#### **1,13-bis-[3-(4-chlorophenyl)thioureido]-4,10-di(tert-butylloxycarbonyl)-4,10-diazotridecane (E1SB)**



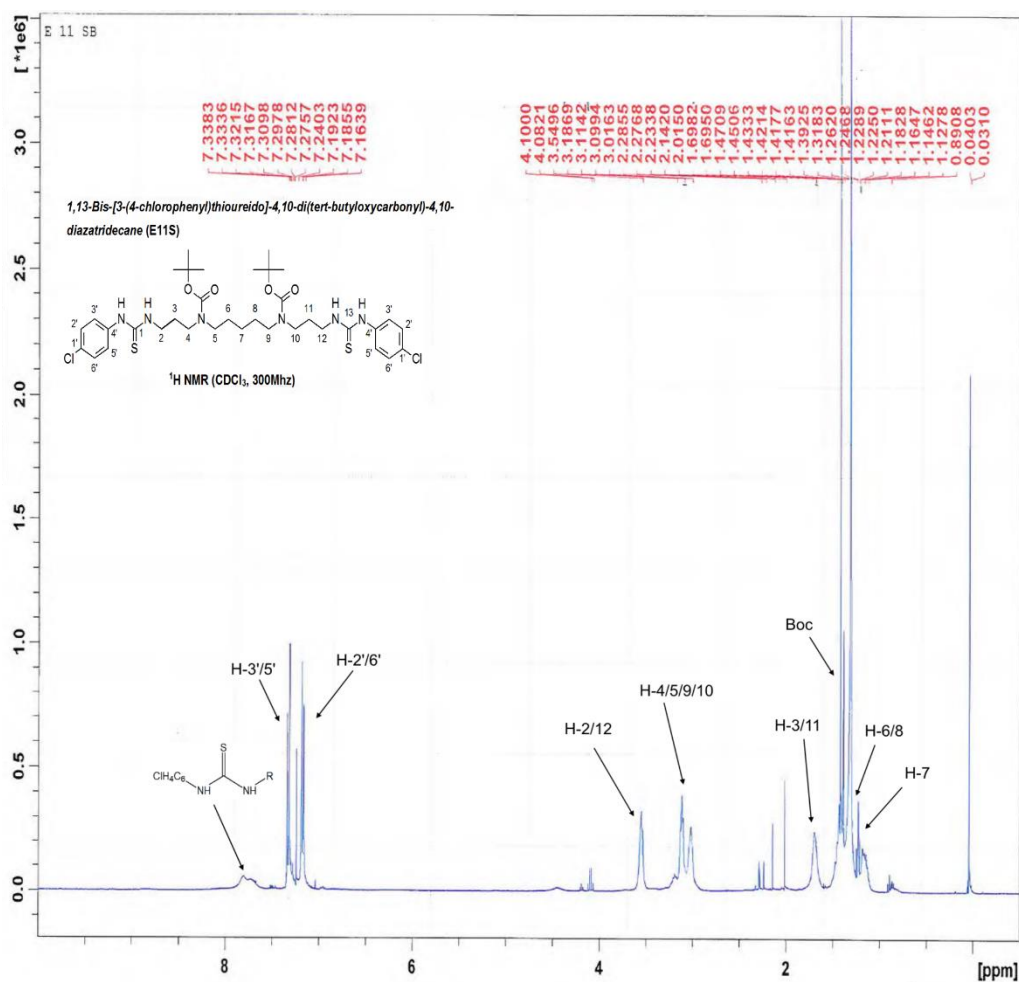
The synthesis of **E1SB** was successful as shown in Figure 3.10 as the starting material **4** was converted to the desired product. The product has a drastically increased  $R_f$  value relative to the starting material, due to the attachment of the terminal group to the amine resulting in increased hydrophobicity. The product mixture obtained was purified on silica gel, the fractions containing the product were combined and the solvent was removed.



**Figure 3.10: TLC chromatogram of 1,13-bis-[3-(4-chlorophenyl)thioureido]-4,10-di(tert-butylloxycarbonyl)-4,10-diazatridecane (E1SB) and column chromatography purification.**

The chromatogram obtained for the synthesis (E1SB) performed in (75% EtOAc in hexane). S is the starting material, R is the isothiocyanate, SP is the starting material and the final reaction mixture, P is the final reaction mixture. The column chromatography was performed with (75% EtOAc in hexane), fractions 9 and onwards were combined.

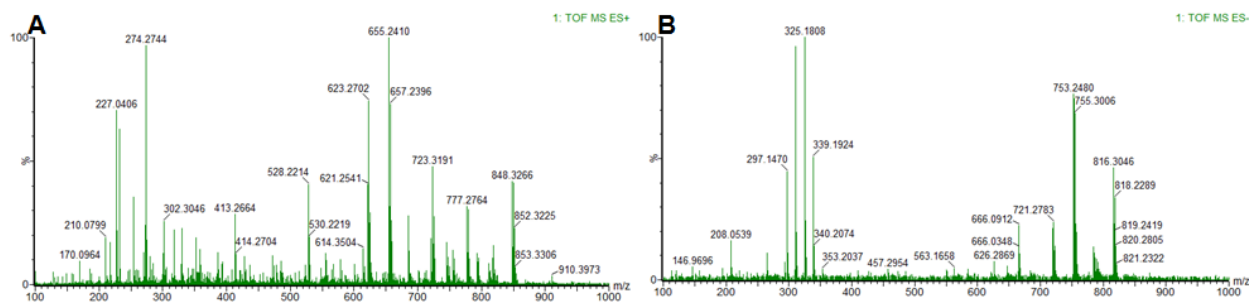
The confirmation of the structure of **E1SB** was accomplished by  $^1\text{H}$  NMR spectroscopy as shown in Figure 3.11. The presence of all the expected protons in the  $^1\text{H}$  NMR was seen. The appearance of the proton peaks at 7.33 ppm and 7.19 ppm corresponds to the addition of aromatic groups. Additionally, carbon peaks corresponding to aromatic groups as well as that of the thiourea were seen in the  $^{13}\text{C}$  NMR spectrum. The IR spectrum obtained also indicated the disappearance of the primary amine peaks indicating that the obtained product corresponded to the predicted structure. The expected splitting pattern obtained for the  $^1\text{H}$  NMR corresponded with the expected pattern confirming the assigned structure.



**Figure 3.11: <sup>1</sup>H NMR spectrum of 1,13-bis-[3-(4-chlorophenyl)thioureido]-4,10-di(tert-butyloxycarbonyl)-4,10-diazatridecane (E1SB)**

The <sup>1</sup>H NMR spectrum obtained for (E1SB) in CDCl<sub>3</sub>. Peak assignment is indicated for the corresponding protons. <sup>1</sup>H NMR spectrum showing integration is included in Appendix figure 4.

The Mass spectrum obtained as shown in Figure 3.12 corresponded to the expected fragmentation pattern. In Figure 3.12 the peak at 655 represents a fragment that is formed after the loss of a *tert*-butoxide radical. The peak seen at 623 could be indicative of the loss of a sulphur radical. Peak 528.22 corresponds to cleavage at one of the Boc-protected amines resulting in a fragment at peak 227.04. The presence of three peaks in Figure 3.12 B, in the molecular ion region separated by 2 m/z units and in the ratio of 9:6:1 is indicative of presence of two chlorine atoms as result of the isotope effect. In Figure 3.12 A, the molecular ion of interest calculated for C<sub>35</sub>H<sub>52</sub>Cl<sub>2</sub>N<sub>6</sub>O<sub>4</sub>S<sub>2</sub> [M-] = 754.29; found 755.30 [M+H]<sup>+</sup> also a sodium adduct was found at 777.26 [M+Na]<sup>+</sup>.

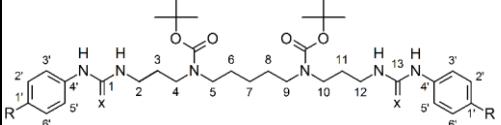


**Figure 3.12: Mass spectrum of 1,13-bis-[3-(4-chlorophenyl)thioureido]-4,10-di(tert-butylloxycarbonyl)-4,10-diazatridecane (E1SB)**

The mass spectrum of (E1SB) in A: positive ion mode and B: negative ion mode. MS (EI m/z) calculated for  $C_{35}H_{52}Cl_2N_6O_4S_2$   $[M^-] = 754.29$ ; found  $755.30$   $[M+H]^+$ .

A summary of the characterisation data of compounds E1SB-E4OB is tabulated below.

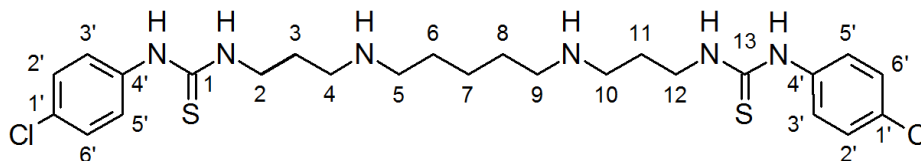
**Table 3.1: Analogue synthesis summary of compounds E1SB-E4OB.**

Analogue Name	X	R	Yield (%) <sup>a</sup>	R <sub>f</sub> <sup>b</sup>	 <sup>1</sup> H NMR <sup>c</sup>	[M <sup>+</sup> ] Pred. <sup>d</sup>	[M <sup>+</sup> ] Act. <sup>e</sup>
E1SB	S	Cl	57	0.52	7.82 (bs, 2 H, NH), 7.33 (m, 4H, H-3', H-5'), 7.19 (m, 4H, H-2', H-6'), 4.08 (bs, 4H, H-2, H-12), 3.10 (m, 8H, H-4, H-5, H-9, H-10), 1.69 (m, 4H, H-3, H-11), 1.43 (m, 18H, Boc), 1.22 (m, 6H, H-6, H-8, H-7)	754.29	755.30
E1OB	O	Cl	45	0.28	7.25 (m, 4H, H-3', H-5'), 7.16 (m, 4H, H-2', H-6'), 4.08 (bs, 4H, H-2, H-12), 3.16 (m, 8H, H-4, H-5, H-9, H-10), 1.65 (m, 4H, H-3, H-11), 1.39 (m, 18H, Boc), 1.22 (m, 6H, H-6, H-8, H-7)	745.32 [M+Na]	745.31 [M+Na]
E2SB	S	F	69	0.65	7.65 (bs, 2 H, NH), 7.36 (m, 4H, H-3', H-5'), 7.17 (m, 4H, H-2', H-6'), 3.41 (bs, 4H, H-2, H-12), 3.11 (m, 8H, H-4, H-5, H-9, H-10), 1.46 (m, 4H, H-3, H-11), 1.35 (m, 18H, Boc), 1.18 (m, 6H, H-6, H-8, H-7)	745.33 [M+Na]	745.33 [M+Na]
E2OB	O	F	70	0.68	8.55 (bs, 2 H, NH), 7.37 (m, 4H, H-3', H-5'), 7.02 (m, 4H, H-2', H-6'), 3.31 (bs, 4H, H-2, H-12), 3.05 (m, 8H, H-4, H-5, H-9, H-10), 1.52 (m, 4H, H-3, H-11), 1.36 (m, 18H, Boc), 1.16 (m, 6H, H-6, H-8, H-7)	713.38 [M+Na]	713.37 [M+Na].
E3SB	S	CF <sub>3</sub>	76	0.63	8.12 (bs, 2 H, NH), 7.96 (m, 4H, H-3', H-5'), 7.37 (m, 4H, H-2', H-6'), 3.57 (bs, 4H, H-2, H-12), 3.07 (m, 8H, H-4, H-5, H-9, H-10), 1.70 (m, 4H, H-3, H-11), 1.45 (m, 18H, Boc), 1.16 (m, 6H, H-6, H-8, H-7)	822.34	822.31
E3OB	O	CF <sub>3</sub>	76	0.33	7.48 (m, 4H, H-3', H-5'), 7.28 (m, 4H, H-2', H-6'), 5.31 (bs, 4H, H-2, H-12), 3.13 (m, 8H, H-4, H-5, H-9, H-10), 1.69 (m, 4H, H-3, H-11), 1.45 (m, 18H, Boc), 1.25 (m, 6H, H-6, H-8, H-7)	790.39	789.36
E4OB	O	Br	51	0.28	7.31 (m, 4H, H-3', H-5'), 7.23 (m, 4H, H-2', H-6'), 3.17 (bs, 4H, H-2, H-12), 3.08 (m, 8H, H-4, H-5, H-9, H-10), 1.63 (m, 4H, H-3, H-11), 1.41 (m, 18H, Boc), 1.20 (m, 6H, H-6, H-8, H-7)	812.23	811.21

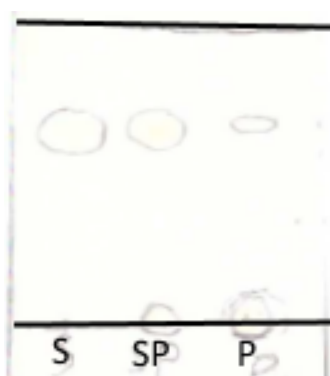
a) Percentage yield of theoretical yield, d) the obtained retention factor for TLC's eluted with (75% EtOAc in hexane), c) <sup>1</sup>H assignments for each analogue, e) Predicted molecular ion based on structure, d) Molecular ion found.

### 3.1.1.3 Synthesis and spectral analysis of compounds E1SD-E4OD

#### 1, 13-bis-[3-(4-chlorophenyl)thioureido]-4,10-diazatridecane dihydrochloride (E1SD)



The de-protection of **E1SB** was presumed to be successful as shown in Figure 3.13 as product spot showed a major decrease in its  $R_f$  value. This was attributed to free amines, which would increase the hydrophilicity of the product versus the starting material.

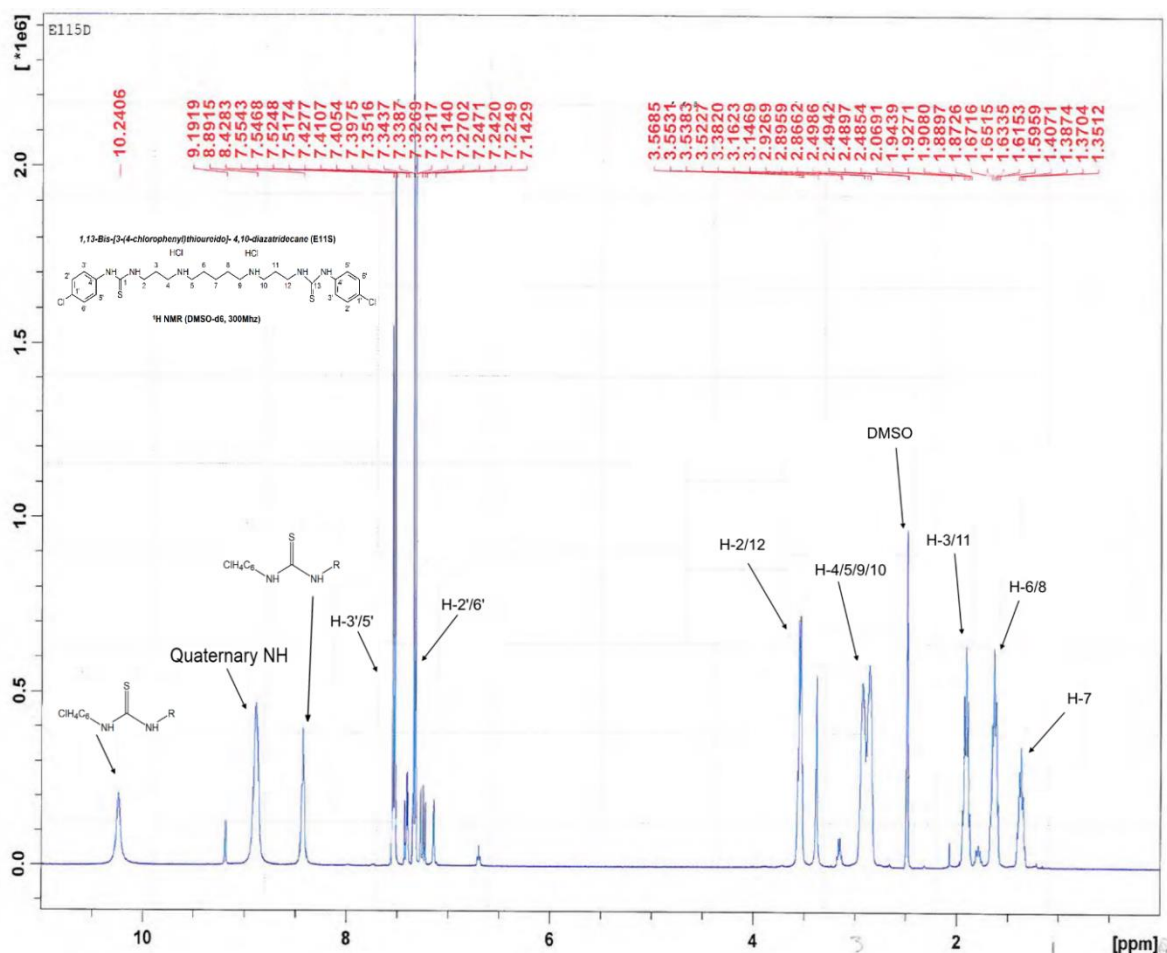


**Figure 3.13:** TLC chromatogram of 1,13-bis-[3-(4-chlorophenyl)thioureido]- 4,10-diazatridecane (**E1SD**).

The chromatogram obtained for the synthesis (**E1SD**) performed in (75% EtOAc in hexane). S is the starting material, SP is the starting material and the final reaction mixture, P is the final reaction mixture.

The confirmation of the structure of **E1SD** was accomplished by  $^1\text{H}$  NMR spectroscopy as shown in Figure 3.14. The presence of all the expected protons in the  $^1\text{H}$  NMR was confirmed. The disappearance of the 18 proton peaks at 1.43 ppm confirms the removal of the *tert*-butoxide protecting groups. Additionally, carbon peaks corresponding to the protecting groups were also absent from the  $^{13}\text{C}$  NMR spectrum. The expected splitting pattern obtained for the  $^1\text{H}$  NMR corresponded with the expected pattern confirming the assigned structure.

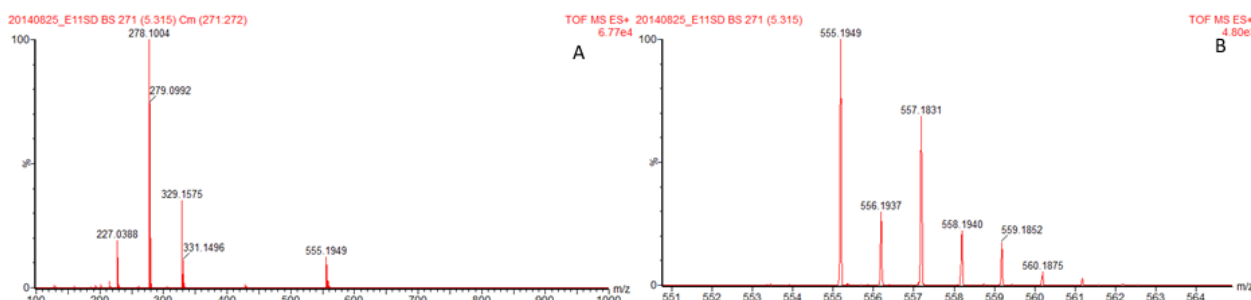




**Figure 3.14:**  $^1\text{H}$  NMR spectrum of *1,13-bis-[3-(4-chlorophenyl)thioureido]-4,10-diazatridecane (E1SD)*

The  $^1\text{H}$  NMR spectrum obtained for **E1SD** in DMSO- $d_6$ . Peak assignment is indicated for the corresponding protons.  $^1\text{H}$  NMR spectrum showing integration is included in Appendix figure 5.

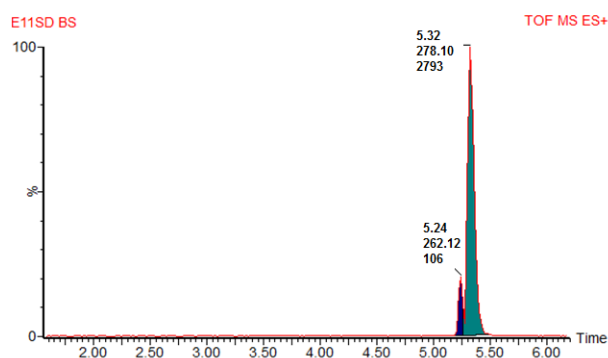
The mass spectrum obtained as shown in Figure 3.15 corresponded to the expected fragmentation pattern. In Figure 3.15, the peak at 555.19 matches the expected molecular ion. The peak seen at 278.10 is the doubly charged molecular ion. In Figure 3.15 B, the molecular ion of interest is at 555.19.



**Figure 3.15:** Mass spectrum of *1,13-bis-[3-(4-chlorophenyl)thioureido]-4,10-diazatridecane (E1SD)*

The mass spectrum of **E1SD** in A: positive ion mode at high electro spray voltage and B: positive ion mode at low electro spray voltage. MS (EI  $m/z$ ) calculated for  $\text{C}_{25}\text{H}_{36}\text{Cl}_2\text{N}_6\text{S}_2$   $[\text{M}^+] = 554.18$ ; found 555.19  $[\text{M}+\text{H}]$ .

The purity analysis of the final compounds was accomplished by UPLC-MS as shown in Figure 3.16, to confirm purity above 95%. Initially all the compounds were tested to confirm that a similar detector response was seen for each. Compounds were then separated using UPLC and detected using MS. Each peak in the UPLC chromatograms was integrated to obtain the area under the curve. The area under the curve of the compound of interest was then used to calculate a percentage of peak area, in relation to the total area of all the peaks. This was used as an unbiased determination of the percentage purity of the compounds.

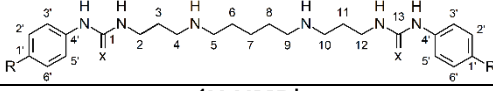


**Figure 3.16: UPLC purity determination chromatogram of 1,13-bis-[3-(4-chlorophenyl)thioureido]-4,10-diazatridecane (E1SD)**

The UPLC chromatogram of **E1SD** next to each peak in descending order is listed the retention time of the compound, the  $M/Z$  of the compound and the area under the curve. The chromatogram indicates a purity of 96% based on the area under the curve of the compound at retention time of 5.32 min.

A summary of the characterisation data of compounds **E1SD-E4OD** is tabulated below.

**Table 3.2: Analogue synthesis summary of compounds E1SD-E4OD.**

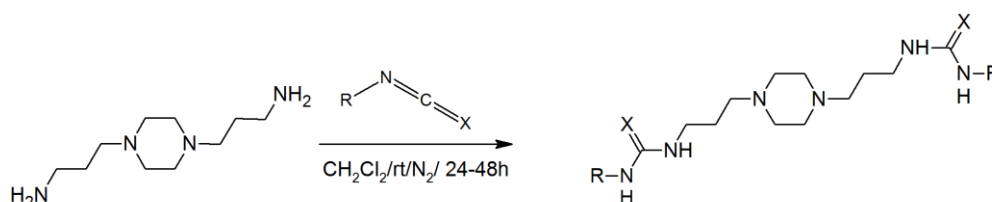
Analogue Name	X	R	Yield (%) <sup>a</sup>			$[M^+]$ Pred. <sup>c</sup>	$[M^+]$ Act. <sup>d</sup>	Purity (%) <sup>e</sup>
				<sup>1</sup> H NMR <sup>b</sup>				
<b>E1SD</b>	S	Cl	57	10.24 (bs, 2 H, thiourea-NH), 9.19 (bs, 4 H, Quaternary NH), 8.42 (bs, 2H, thiourea-NH), 7.52 (m, 4H, H-3',H-5'), 7.32 (m, 4H, H-2',H-6'), 3.55 (m, 4H, H-2, H-12), 2.89 (m,8H, H-4, H-5, H-9, H-10), 1.90 (m, 4H, H-3, H-11), 1.63 (m, 4H, H-6, H-8),1.38 (m, 2H, H-7)		554.18	555.19	96
<b>E1OD</b>	O	Cl	72	9.20 (bs, 2 H, urea-NH), 8.85 (bs, 4 H, Quaternary NH), 7.42 (m, 4H, H-3',H-5'), 7.24 (m, 4H, H-2',H-6'), 6.68 (bs, 2 H, urea-NH), 3.15 (m, 4H, H-2, H-12), 2.87 (m,8H, H-4, H-5, H-9, H-10), 1.82 (m, 4H, H-3, H-11), 1.59 (m, 4H, H-6, H-8),1.26 (m, 2H, H-7)		522.23	523.23	96.7
<b>E2SD</b>	S	F	67	10.05 (bs, 2 H, thiourea-NH), 8.92 (bs, 4 H, Quaternary NH), 8.28 (bs, 2H, thiourea-NH), 7.44 (m, 4H, H-3',H-5'), 7.12 (m, 4H, H-2',H-6'), 3.54 (m, 4H, H-2, H-12), 2.65 (m,8H, H-4, H-5, H-9, H-10), 1.90 (m, 4H, H-3, H-11), 1.65 (m, 4H, H-6, H-8),1.26 (m, 2H, H-7)		522.25	523.24	96.9
<b>E2OD</b>	O	F	64	9.02 (bs, 2 H, urea-NH), 8.88 (bs, 4 H, Quaternary NH), 7.38 (m, 4H, H-3',H-5'), 7.03 (m, 4H, H-2',H-6'), 6.61 (bs, 2 H, urea-NH), 3.16 (m, 4H, H-2, H-12), 2.86 (m,8H, H-4, H-5, H-9, H-10), 1.78 (m, 4H, H-3, H-11), 1.63 (m, 4H, H-6, H-8),1.37 (m, 2H, H-7)		490.29	491.29	100

<b>E3SD</b>	S	CF <sub>3</sub>	35	10.57 (bs, 2 H, thiourea-NH), 8.85 (bs, 4 H, Quaternary NH), 8.66 (bs, 2H, thiourea-NH), 7.78 (m, 4H, H-3',H-5'), 7.62 (m, 4H, H-2',H-6'), 3.56 (m, 4H, H-2, H-12), 2.49 (m,8H, H-4, H-5, H-9, H-10), 1.90 (m, 4H, H-3, H-11), 1.63 (m, 4H, H-6, H-8),1.37 (m, 2H, H-7)	622.23	623.24	97.8
<b>E3OD</b>	O	CF <sub>3</sub>	34	9.52 (bs, 2 H, urea-NH), 8.86 (bs, 4 H, Quaternary NH), 7.60 (m, 4H, H-3',H-5'), 7.52 (m, 4H, H-2',H-6'), 6.84 (bs, 2 H, urea-NH), 3.16 (m, 4H, H-2, H-12), 2.49 (m,8H, H-4, H-5, H-9, H-10), 1.80 (m, 4H, H-3, H-11), 1.63 (m, 4H, H-6, H-8),1.37 (m, 2H, H-7)	590.28	591.29	100
<b>E4OD</b>	O	Br	62	9.18 (bs, 2 H, thiourea-NH), 8.85 (bs, 4 H, Quaternary NH), 7.36 (m, 8H, H-3',H-5', H-2',H-6'), 6.69 (bs, 2 H, urea-NH), 3.15 (m, 4H, H-2, H-12), 3.87 (m,8H, H-4, H-5, H-9, H-10), 1.78 (m, 4H, H-3, H-11), 1.62 (m, 4H, H-6, H-8),1.36 (m, 2H, H-7)	610.13	611.13	100

Percentage yield of theoretical yield, b) <sup>1</sup>H assignments for each analogue, c) Predicted molecular ion based on structure, d) Molecular ion found, e) The calculated percentage purity based on UPLC-MS. The area under the curve of the compound of interest was used to calculate a percentage of peak area, in relation to the total area of all the peaks.

### 3.1.2 Synthesis of analogues based on the 3-piperazinyl-3 backbone

Modification of the polyamine backbone to reduce the number of rotatable bonds was accomplished by inserting a piperazine backbone. The final precursor **1,4-bis(3-aminopropyl)piperazine** was commercially available and was subsequently reacted with the corresponding aryl isocyanate or isothiocyanate to obtain compounds **A10-A50**. It should be noted that compounds **A10**, **A1S** and **A20** were synthesised by Dr. Andrew Andayi, consequently not all characterisation data is included.



**A1S** R = 4-chlorophenyl, X = S

**A10** R = 4-chlorophenyl, X = O

**A20** R = phenyl, X = O

**A3S** R = 4-fluorophenyl, X = S

**A3O** R = 4-fluorophenyl, X = O

**A4S** R = 4-trifluoromethylphenyl, X = S

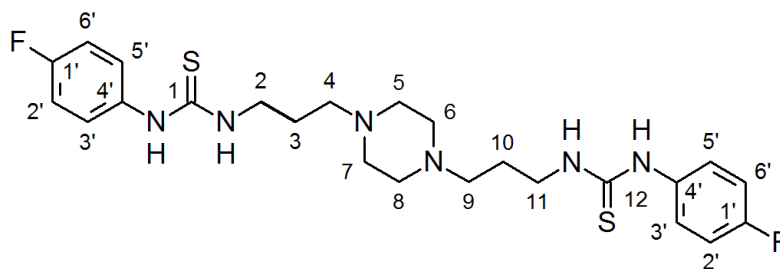
**A4O** R = 4-trifluoromethylphenyl, X = O

**A5O** R = 4-bromophenyl, X = O

#### Scheme 2: Synthetic scheme of (bis)ureas and (bis)thiourea analogues based on the 3-piperazinyl-3 backbone.

The precursor **1,4-bis(3-aminopropyl)piperazine** is reacted with the appropriate isocyanate or isothiocyanate to form the polyamine analogues (**A1S-A50**).

### 1,4-bis-3-[3-(4-fluorophenyl)thioureido]propyl-piperazine (A3S)



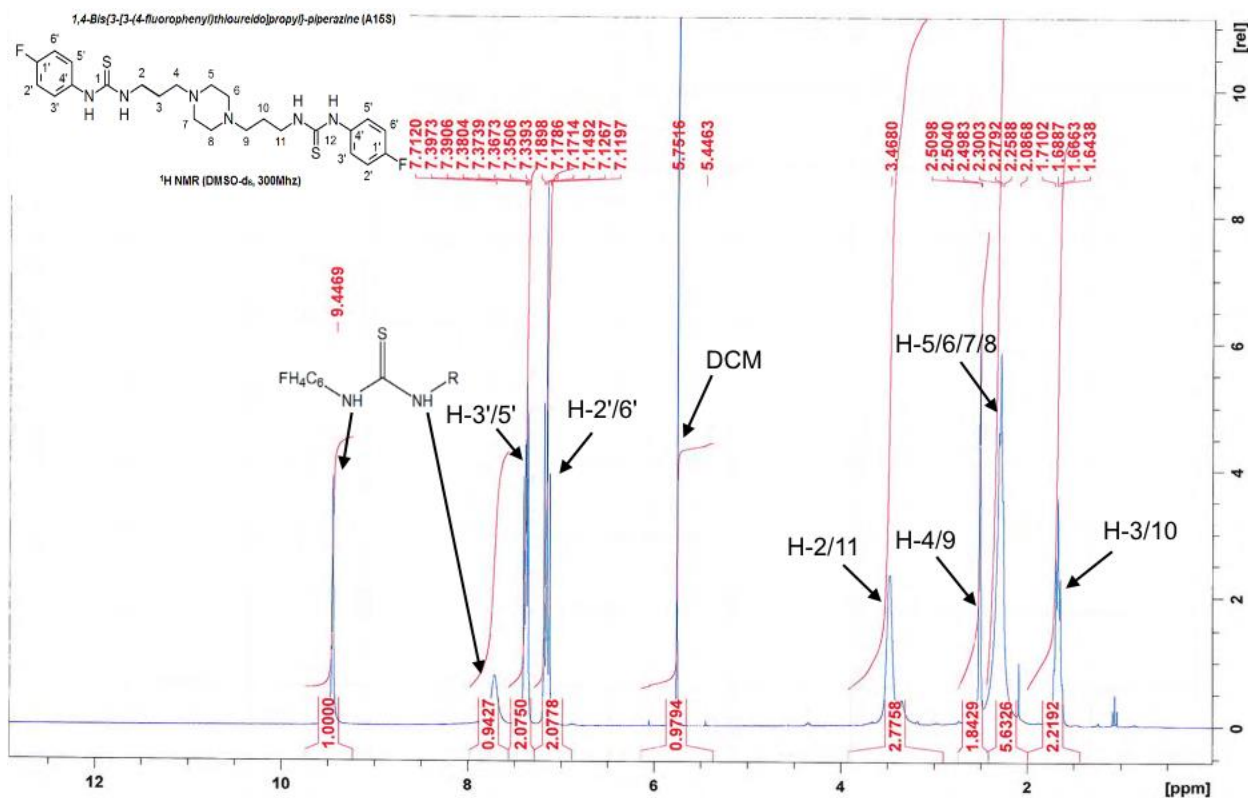
The synthesis of **A3S** was assumed to be successfully accomplished as depicted in Figure 3.17 as the product spot showed a major increase in its  $R_f$  value relative to that of the starting material. This phenomenon was recognised to be due to the addition of the isothiocyanate which lead to an increase in hydrophobicity.



**Figure 3.17:** TLC chromatogram of 1,4-bis{3-[3-(4-fluorophenyl)thioureido]propyl}-piperazine (**A3S**).

The chromatogram obtained for the synthesis (**A3S**) performed in (CH<sub>2</sub>Cl<sub>2</sub>/MeOH/NH<sub>4</sub>OH 89:10:1). S is the starting material, SP is the starting material and the final reaction mixture, P is the final reaction mixture.

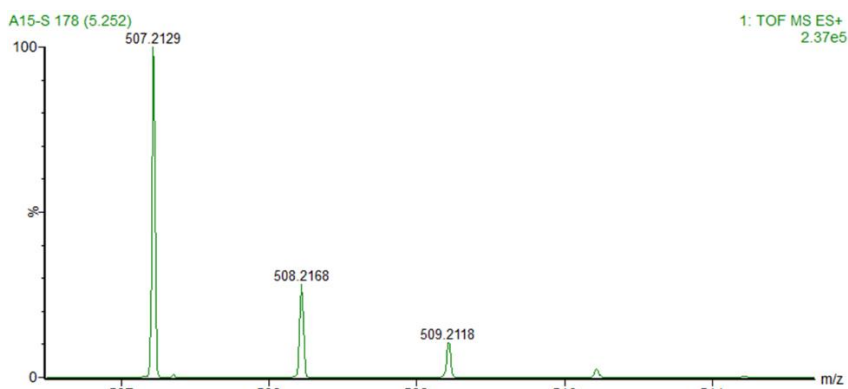
The confirmation of the structure of **A3S** was accomplished by <sup>1</sup>H NMR spectroscopy as shown in Figure 3.18. The presence of all the expected protons in the <sup>1</sup>H NMR was confirmed as indicated in the figure. The major distinguishing characteristic seen was that of the aromatic protons occurring at 7.40 ppm and 7.14 ppm.



**Figure 3.18:** <sup>1</sup>H NMR spectrum of **1,4-bis{3-[3-(4-fluorophenyl)thioureido]propyl}piperazine (A3S)**.

The <sup>1</sup>H NMR spectrum obtained for **A3S** in CDCl<sub>3</sub>. Peak assignment is indicated for the corresponding protons in addition to peak integration.

The Mass spectrum obtained as shown in Figure 3.19 corresponded to the expected molecular ion. The purity analysis of the final compounds was accomplished by UPLC-MS total ion current to confirm purity above 95%. Initially all the compounds were tested to confirm that a similar detector response was seen for each. Compounds were then separated using UPLC and detected using MS. Each peak in the UPLC chromatograms was integrated to obtain the area under the curve. The area under the curve of the compound of interest was then used to calculate a percentage of peak area, in relation to the total area of all the peaks. This was used as an unbiased determination of the percentage purity of the compounds.

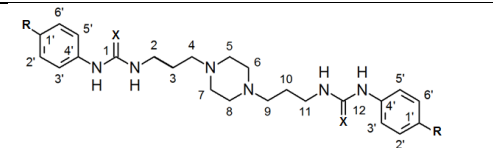


**Figure 3.19: Mass spectrum of 1,4-bis{3-[3-(4-fluorophenyl)thioureido]propyl}-piperazine (A3S)**

The mass spectrum of **A3S** in positive ion mode. MS (EI  $m/z$ ) calculated for  $C_{24}H_{32}F_2N_6S_2$   $[M^+] = 506.21$ ; found 507.21 $[M+H]$ .

A summary of the characterisation data of compounds **A1S-A5O** is tabulated below.

**Table 3.3: Analogue synthesis summary of compounds A1S-A5O.**

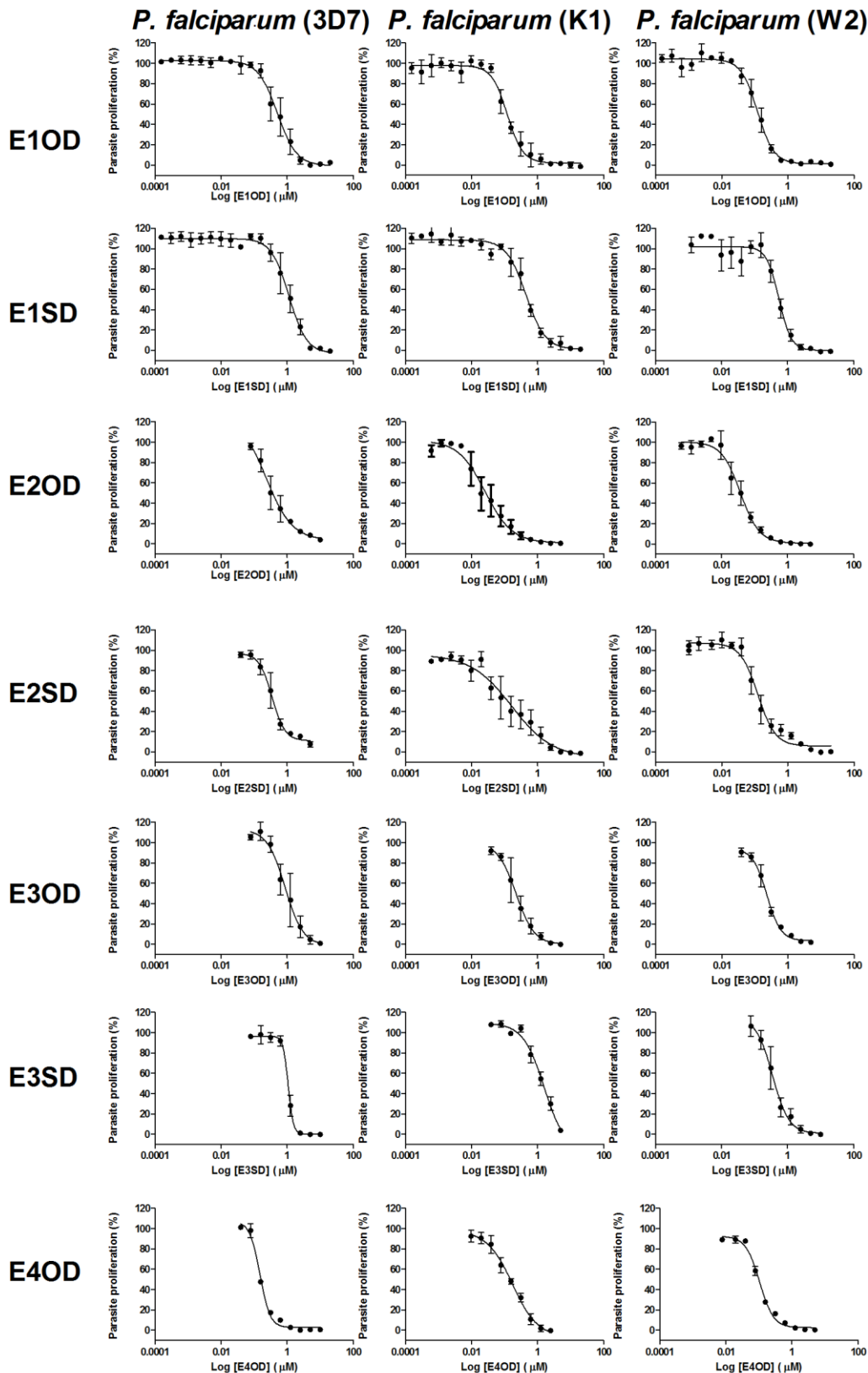
Analogue Name	X	R	Yield (%) <sup>a</sup>		$[M^+]$ Pred. <sup>c</sup>	$[M^+]$ Act. <sup>d</sup>	Purity (%) <sup>e</sup>
				<sup>1</sup> H NMR <sup>b</sup>			
<b>A1S</b>	S	Cl	N/A	9.6 (2H, br.s, urea NH), 7.8 (2H, bs., urea NH), 7.4 (4H, d, H-3', 5'), 7.3 (4H, d, H-2', 6'), 3.4 (4H, m, H-2, 11), 2.2 (12H, m, H-, 4, 5, 6, 7, 8,9), 1.7 (4H, m, H-3, 10)	538.15	539.15	96
<b>A1O</b>	O	Cl	N/A	8.6(2H, br.s, urea NH), 7.4 (4H,m, H-3', 5'), 7.2 (4H, m, H-2', 6'), 6.1 (2H,m, urea NH), 3.1 (4H, m, H-2, 11), 2.4 (12H, , H-4, 5, 6, 7, 8,9), 1.6 (4H, m, H-3, 10)	506.19	507.19	100
<b>A2O</b>	O	H	N/A	8.5 (2H, br.s, NH), 7.4 (4H,m, H-3', 5'), 7.2 (4H, m, H-2', 6'), 6.8 (2H,m, urea NH), 6.3 (2H,m, urea NH), 3.1 (4H, m, H-2, 11), 2.4 (12H, m, H-4, 5, 6, 7, 8,9), 1.6 (4H, m, H-3, 10)	438.56	439.56	96.5
<b>A3S</b>	S	F	70	9.44 (bs, 2H, thiourea NH), 7.71 (bs, 2H, thiourea NH), 7.36 (m, 4H, H-3', 5'), 7.15 (m, 4H, H-2', 6'), 3.46 (m, 4H, H-2, 11), 2.50 (bs, 4H, H-4, 9), 2.30 (m, 8H, H-5, 6, 7, 8), 1.66 (m, 4H, H-3, 10).	506.21	507.21	98.1
<b>A3O</b>	O	F	80	8.41(bs, 2H, urea NH), 7.36 (m, 4H, H-3', 5'), 7.03 (m, 4H, H-2', 6'), 6.08 (bs, 2H, urea NH), 3.05 (m, 4H, H-2, 11), 2.49 (bs, 4H, H-4, 9), 2.28 (m, 8H, H-5, 6, 7, 8), 1.55 (m, 4H, H-3, 10).	474.26	475.25	98.9
<b>A4S</b>	S	CF <sub>3</sub>	76	8.57 (bs, 2H, thiourea NH), 7.35 (m, 8H, H-3', 5', H-2', 6'), 6.16 (bs, 2H, thiourea NH), 3.07 (m, 4H, H-2, 11), 2.48 (m, 4H, H-4, 9), 2.27 (m, 8H, H-5, 6, 7, 8), 1.55 (m, 4H, H-3, 10).	606.20	607.21	96.1
<b>A4O</b>	O	CF <sub>3</sub>	87	8.86 (bs, 2H, urea NH), 7.56 (m, 8H, H-3', 5', H-2', 6'), 6.28 (bs, 2H, urea NH), 3.10 (m, 4H, H-2, 11), 2.48 (m, 4H, H-4, 9), 2.27 (m, 8H, H-5, 6, 7, 8), 1.56 (m, 4H, H-3, 10).	574.24	575.24	96.3
<b>A5O</b>	O	Br	32	9.87 (bs, 2H, urea NH), 8.12 (bs, 2H, urea NH), 7.65 (m, 8H, H-3', 5', H-2', 6'), 3.50 (m, 4H, H-2, 11), 2.50 (m, 4H, H-4, 9), 2.32 (m, 8H, H-5, 6, 7, 8), 1.28 (m, 4H, H-3, 10).	594.10	595.10	98.8

a) Percentage yield of theoretical yield, b)  $^1\text{H}$  assignments for each analogue, c) Predicted molecular ion based on structure, d) Molecular ion found, e) The calculated percentage purity based on UPLC-MS. The area under the curve of the compound of interest was used to calculate a percentage of peak area, in relation to the total area of all the peaks.

### 3.2 Antiplasmodial activity determination

#### 3.2.1 Antiplasmodial activity determination of analogues based on the 3-5-3 backbone

To determine the effect of halogenation of the original 3-5-3 parent compound (compound 12 from Verlinden, *et al* [107], on the *in vitro* proliferation of *P. falciparum* parasites, dose-response analysis was performed with the Malaria SYBR Green I based fluorescence assay [106]. The halogenated polyamine analogues (**E10D-E40D**) were tested against various drug sensitive and resistant strains of *P. falciparum* including 3D7 as chloroquine sensitive strain; K1 as chloroquine, pyrimethamine and sulfadoxine resistant strain and W2, a chloroquine resistant strain. The recorded fluorescence values were used to create dose-response curves as depicted in Figure 3.20.



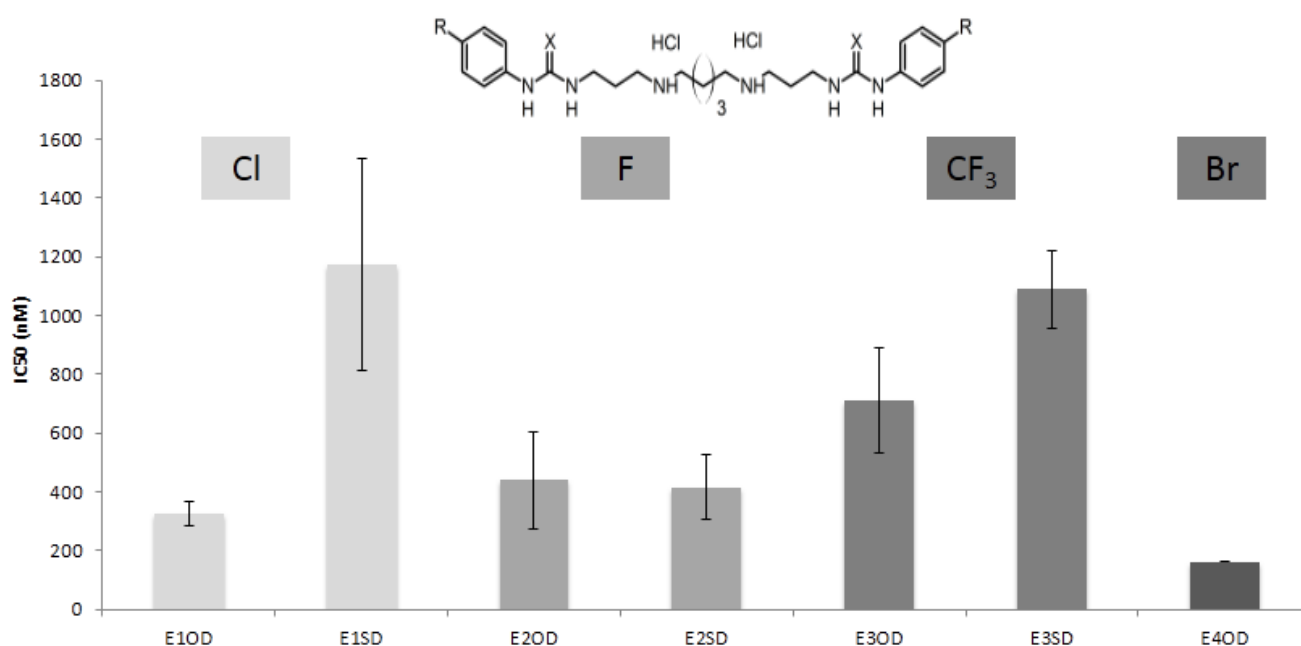
**Figure 3.20: Dose-response curve of *P. falciparum* parasites after treatment with the 3-5-3 polyamine analogues.**

Illustrating the parasite proliferation percentage of growth relative to control (%) of various *P. falciparum* strains (3D7, K1 and W2) measured using SYBR Green I fluorescence as proxy for parasite proliferation over 96 h. Values are the means of 3 independent experiments each performed in triplicate with error bars showing  $\pm$  SEM. Where not shown, error bars fall within the marker.



The results obtained for the antiplasmodial activity of the 3-5-3 polyamine analogues indicated that compound **E4OD** had the best antiplasmodial activity for all the strains tested at 98-162 nM. Interestingly, the urea fluorinated compound **E2OD** show markedly better activity against the resistant strains versus **E4OD**. The bromination in compound **E4OD** therefore resulted in an improved activity over that of the parent compound **12** [107] with an antiplasmodial  $IC_{50}$  of 246 nM. The other compounds tested were shown to have varying antiplasmodial activities, however, the thiourea-substituted compounds were less effective at inhibiting *in vitro* parasite proliferation, the only exception to this was noticed in the fluorinated compounds (Table 3.4).

The compounds inhibitory effects versus the resistant strains indicated that the compounds were generally more effective versus the resistant strains. The only exception noted for the latter generalisation was for compound **E3SD**. This trend can be further seen in the calculated resistance indexes (RI) values. RI values are calculated by dividing the  $IC_{50}$  value obtained in the resistant-strain by the  $IC_{50}$  value obtained in the sensitive-strain. RI values less than 1 indicate that the compound is more active in the resistant-strain than in the sensitive-strain, while values larger than 1 indicate the opposite. These values ranged from 0.1 to 1.2 (Table 3.4), in comparison to the RI (W2/3D7) of chloroquine (value of 7.78) [107], the difference in the values show that these polyamine analogues do not have similar resistance activities to the chloroquine-sensitive 3D7 or chloroquine-resistant W2 parasite strains, consequently it will not follow the same resistance pathway or have similar MOA's. This is equally applicable to the K1 strain, a chloroquine, pyrimethamine and sulfadoxine resistant-strain. Thiourea substitution had more of a dramatic influence on the activity of the compounds than the specific halogenation as well, with no significant difference ( $P=0.633$ ,  $P>0.05$ ,  $n=3$ ) observed between chlorination or fluorination. The latter could be due to the large degree of uncertainty in the chlorinated compounds measured  $IC_{50}$ . Chlorination modification, also had no significant difference ( $P=0.174$ ,  $P>0.05$ ,  $n=3$ ) dependent on the thiourea or urea substitution, however, this could also be due to the large degree of uncertainty. Trifluoromethylation did in totality not improve activity versus the other halogen substituted compounds.



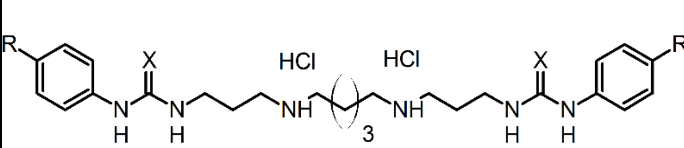
**Figure 3.21: *P. falciparum* (3D7) parasites after treatment with the 3-5-3 polyamine analogues.**

IC<sub>50</sub> (nM) of compounds obtained against *P. falciparum* (3D7) measured using SYBR Green I fluorescence as proxy for parasite proliferation over 96 h. Values are the means of 3 independent experiments each performed in triplicate with error bars showing  $\pm$  SEM. Where not shown, error bars fall within the marker. Halogenation and internal substitution was compared with a non-paired t-test and significant differences determined (\* =  $P < 0.05$ , \*\* =  $P < 0.01$ ).

The corresponding IC<sub>50</sub> values obtained for the compounds on each strain were used to calculate resistance indexes (RI) as summarised in Table 3.4. This provides an indication of the cross-resistance of compounds against various genetic backgrounds of resistant forms of the parasite.

**Table 3.4: Antiplasmodial activities of the 3-5-3 backbone polyamine analogues.**

*In vitro* *P. falciparum* proliferation was measured using SYBR Green I fluorescence Assay.

Analogue Name	X	R				RI <sup>b</sup> (W2/ 3D7)	RI <sup>b</sup> (K1/ 3D7)
			<i>P. falciparum</i> IC <sub>50</sub> (nM) <sup>a</sup>				
			3D7	K1	W2		
E1OD	O	Cl	326.4 $\pm$ 39.8	169.0 $\pm$ 76.4	131.3 $\pm$ 40.8	0.4	0.5
E1SD	S	Cl	1175.2 $\pm$ 369.7	434.4 $\pm$ 128.4	524.2 $\pm$ 123.1	0.4	0.4
E2OD	O	F	439.0 $\pm$ 162.8	33.7 $\pm$ 13.0	36.1 $\pm$ 14.3	0.1	0.1
E2SD	S	F	416.8 $\pm$ 111.3	165.1 $\pm$ 83.5	178.3 $\pm$ 71.5	0.4	0.4

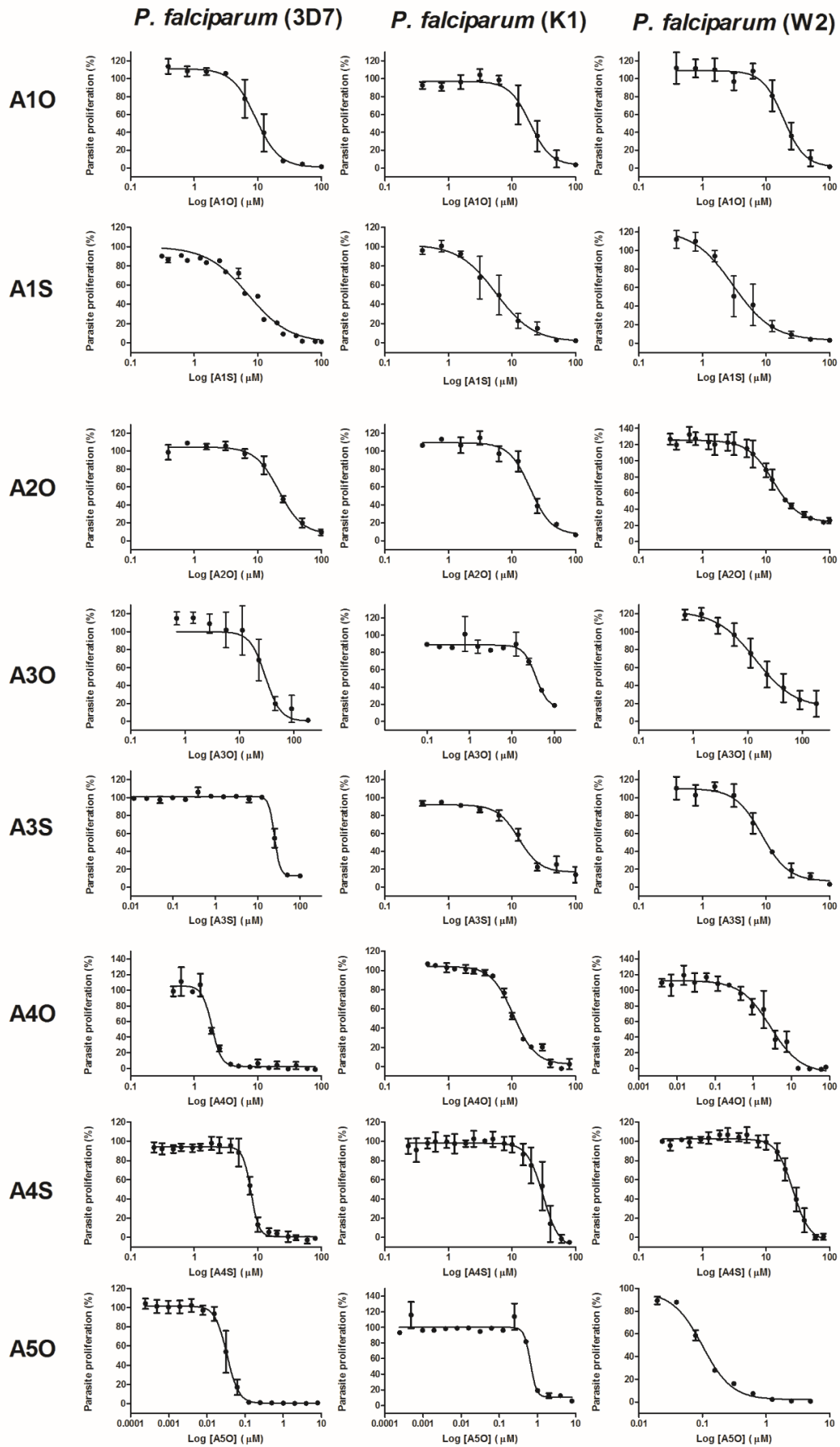
E3OD	O	CF <sub>3</sub>	710.2±179.2	252.9±71.6	222.5±37.1	0.3	0.4
E3SD	S	CF <sub>3</sub>	1088.2±133.4	1276.4±387.2	467.8±143.4	0.4	1.2
E4OD	O	Br	162.6±0.3	141.3±37.3	98.2±6.4	0.6	0.9

a) Values are the means ± SEM of 3 independent experiment performed in triplicate. b) Resistance index (RI), defined as the ratio of the IC<sub>50</sub> values of the resistant to sensitive strains, W2/3D7 and K1/3D7

The compounds generally showed better antiplasmodial activity against the resistant strains. This mimicked the parent compound and indicates that the compounds have a very low risk of cross-resistance developing.

### 3.2.2 Antiplasmodial activity determination of analogues based on the 3-piperazinyl-3 backbone

To determine the effect of rigidity on the original 3-5-3 parent compound (compound **12** from [107]) novel analogues possessing a piperazine backbone were tested on the *in vitro* proliferation of *P. falciparum* parasites, dose-response analysis was performed with a fluorescence-based assay. The halogenated polyamine analogues (**A10-A50**) were tested against various drug-sensitive and resistant-strains of *P. falciparum* including 3D7 as chloroquine-sensitive strain; K1, a chloroquine, pyrimethamine and sulfadoxine resistant strain and W2, a chloroquine-resistant strain. The recorded fluorescence values were used to create dose-response curves as depicted in Figure 3.22.



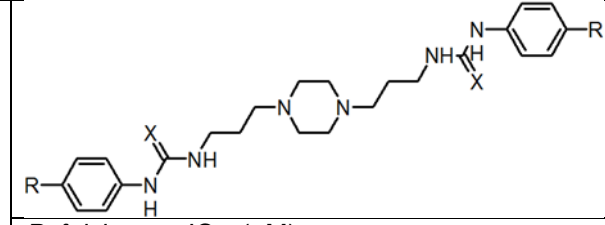
**Figure 3.22 as on page 57: Dose-response curve of *P. falciparum* parasites after treatment with the 3-piperazinyl-3 polyamine analogues.**

Illustrating the parasite proliferation percentage of growth relative to control (%) of various *P. falciparum* strains (3D7, K1 and W2) measured using SYBR Green I fluorescence as proxy for parasite proliferation over 96 h. Values are the means of at least 2 independent experiments each performed in triplicate with error bars showing  $\pm$  SEM. Where not shown, error bars fall within the marker.

The antiplasmodial activity of the 3-piperazinyl-3 polyamine analogues indicated that compound **A5O** had the best antiplasmodial activity for all the strains tested at 98-162 nM. This bromination in compound **A5O** therefore resulted in improved activity of the parent compound **A2O**.

**Table 3.5: Antiplasmodial activities of the 3-piperazinyl-3 backbone polyamine analogues.**

*In vitro* *P. falciparum* proliferation was measured using SYBR Green I fluorescence Assay.

Analogue Name	X	R				RI <sup>b</sup> (W2/3D7)	RI <sup>b</sup> (K1/3D7)
			<i>P. falciparum</i> IC <sub>50</sub> (μM) <sup>a</sup>				
			3D7	K1	W2		
A1O	O	Cl	10±3	22±7	21±5	2.1	2.2
A1S	S	Cl	7.06 <sup>#</sup>	6.454±2.33	2.01±0.016	0.28	0.91
A2O	O	H	24.65±1.66	22.97±2.65	12.41±1.25	0.5	0.9
A3O	O	F	28.95±6.76	36.13±4.89	38.05±21.2	1.3	1.2
A3S	S	F	24.25±2.02	12.36±3.71	8.27±3.55	0.3	0.5
A4O	O	CF <sub>3</sub>	1.90±0.04	10.15±1.69	2.94±1.16	1.5	5.3
A4S	S	CF <sub>3</sub>	7.62±0.36	29.51±2.54	27.94±4.84	3.7	3.9
A5O*	O	Br	0.036±0.016	0.658±0.004	0.101±0.095	2.8	18.2

a) Values are the of at least means  $\pm$  SEM of at least 2 independent experiments performed in triplicate. \*  $\pm$  SEM of 3 independent experiments performed in triplicate, <sup>#</sup> only 1 independent experiment performed b) Resistance index (RI), defined as the ratio of the IC<sub>50</sub> values of the resistant to sensitive strains, W2/3D7 and K1/3D7

The results obtained for the antiplasmodial activity of the 3-piperazinyl-3 polyamine analogues indicated that compound **A5O** had the best antiplasmodial activity for all the strains tested at 36-658 nM, however, overt resistance was seen in the W2 strain. The other compounds showed considerably higher IC<sub>50</sub> values in comparison being in the μM range. Compounds **A4O** and **A4S** showed the second lowest IC<sub>50</sub> values and indicated the previously seen favourability of urea substitution. The chlorine-substituted analogues also had lower IC<sub>50</sub> values versus the un-substituted phenyl **A2O** and the fluorine substituted analogues indicating that bulkier halogens increase activity. In contrast to the

previous series that showed that decreased halogen bulkiness is favourable. The compounds generally showed reduced antiplasmodial activity against the resistant strains, indicating cross-resistance or a shared resistance pathway to these compounds.

### 3.3 Cheminformatic analysis of Polyamino(bis)ureas and Polyamino(bis)thioureas polyamine analogues

#### 3.3.1 Determination of drug-likeness

All newly synthesised halogenated polyamine analogues (**E1SD-E4OD** and **A1S-A5O**) were subsequently evaluated computationally for drug-likeness to assess if they possess desirable orally bioavailable drug properties. Various ADMET descriptors were predicted in addition to evaluating the compounds based on Lipinski's rule of 5 and predicting the compounds' quantitative estimation of drug-likeness (QED).

In Table 3.6, the ADMET predictions of the E-series of compounds are presented.

**Table 3.6: ADMET prediction of 3-5-3 polyamine analogues.**

*In silico* physiochemical predictors were obtained using the Discovery Studio Modelling Environment program.

Descriptor	Analogue Name							
	12	E1SD	E1OD	E2SD	E2OD	E3SD	E3OD	E4OD
<b>Human Intestinal Absorption (HIA)<sup>a</sup></b>	0	0	0	0	0	1	1	1
<b>Aqueous Solubility</b>	-1.24	-4.79	-3.21	-3.98	-2.41	-6.42	-4.85	-3.36
<b>Aqueous Solubility level<sup>b</sup></b>	4	2	3	3	3	1	2	3
<b>Blood Brain Barrier (BBB)</b>	N/A	N/A	N/A	0.026	N/A	N/A	N/A	N/A
<b>BBB level<sup>c</sup></b>	4	4	4	2	4	4	4	4
<b>Cytochrome P450 2D6 (CYP2D6)</b>	-4.42	2.76	-2.17	3.29	-2.66	5.29	-0.48	-4.556
<b>CYP2D6 prediction</b>	FALSE	TRUE	FALSE	TRUE	FALSE	TRUE	FALSE	FALSE
<b>Hepatotoxicity</b>	-0.485	-2.2	1.06	0.079	3.27	-6.79	-3.35	1.62
<b>Hepatotoxicity prediction</b>	TRUE	TRUE	TRUE	TRUE	TRUE	FALSE	TRUE	TRUE
<b>Plasma Protein Binding (PPB)</b>	1.809	2.5	5.06	2.22	3.74	1.94	4.34	0.64
<b>PPB Prediction</b>	TRUE	TRUE	TRUE	TRUE	TRUE	TRUE	TRUE	TRUE

0 = Good absorption, 1 = Moderate absorption, 2 = Low absorption, 3 = Very low absorption.

<sup>b</sup>**Drug-likeness:** 0 = Extremely low, 1 = No, very low, but possible, 2 = Yes, low, 3 = Yes, good, 4 = Yes, optimal, 5 = No, too soluble.

<sup>c</sup>**Blood brain penetration:** 0 = very high penetrant (Brain-Blood ratio greater than 5:1), 1 = High (Brain-Blood ratio between 1:1 and 5:1), 2 = (Medium Brain-Blood ratio between 0.3:1 to 1:1), 3 = Low (Brain-Blood ratio less than 0.3:1), 4 = Undefined (Outside 99% confidence ellipse)

The predicted ADMET descriptors for the 3-5-3 series of halogenated polyamines analogues (Table 3.6) indicated that the compounds should show good to moderate intestinal absorption. While they are predicted to possess low to good aqueous solubility, compound **12**'s aqueous solubility could not be predicted. The majority of the compounds had undefined blood brain penetration and minimal or non-existent cytochrome P450 inhibition. The majority of the compounds were predicted to be hepato-toxic, however, to a low degree. All the compounds were predicted to possess high plasma protein binding.

The compounds adherence to Lipinski's rule of 5 (Table 3.7), indicated that the 3-5-3 polyamine analogues all violated at least 1 of the rules. This was partially attributed to the addition of high molecular weight halogens and in particular, trifluoromethylation and bromination increased the size of the compound above the required 500 kDa; the remaining compounds were also quite large but not explicitly so from the parent compound (compound **12**, MW 454.61). Thiourea substitution again led to the highest numbers of violations of Lipinski's rules (3, mostly associated with AlogP, RotB and MW). Lastly, all the compounds had QED values that were all much less than 1 indicating unfavourable drug-likeness, similar to the parent compound, compound **12**. However, the parent compound still possessed the best QED score overall.

**Table 3.7: Drug-likeness prediction of 3-5-3 polyamine analogues.**

*In silico* physiochemical predictors were obtained using the Discovery Studio Modelling Environment program

Analogue Name	MW <sup>a</sup>	ALOGP <sup>b</sup>	HBD <sup>c</sup>	HBA <sup>d</sup>	ROTB <sup>e</sup>	AROM <sup>f</sup>	Lipinski's Violations <sup>g</sup>	QED <sup>h</sup>
12	454.61	2.14	6	4	16	2	1	0.2337
E1SD	555.63	6.601	6	4	20	2	3	0.10257
E1OD	523.498	3.469	6	4	16	2	2	0.20274
E2SD	522.72	5.683	6	4	20	2	3	0.12459
E2OD	490.589	2.551	6	4	16	2	1	0.21754
E3SD	622.735	7.156	6	4	22	2	3	0.06135
E3OD	590.604	4.024	6	4	18	2	1	0.14763
E4OD	612.4	3.637	6	4	16	2	1	0.1743

a) MW – Molecular Weight (g/mole); b) ALOGP – A log P (lipophilicity); c) HBD - Hydrogen Bond Donors; d) HBA – Hydrogen Bond Acceptors; e) ROTB – Rotatable Bonds; f) AROM – Aromatic rings; g) Violations of Lipinski's rules should be ≤1; h) QED – 0 = unfavourable; 1 = favourable.

Similarly, to the analysis of the halogenated 3-5-3 series of polyamine analogues, the 3-piperazinyl-3 polyamine analogues were also evaluated for their ADMET properties and drug-likeness.

**Table 3.8: ADMET prediction of 3-piperazinyl-3 polyamine analogues.**

*In silico* physiochemical predictors were obtained using the Discovery Studio Modelling Environment program.

Descriptor	Analogue Name								
	12	A1S	A1O	A2O	A3S	A3O	A4S	A4O	A5O
<b>Human Intestinal Absorption (HIA)<sup>a</sup></b>	0	0	0	0	0	0	1	0	0
<b>Aqueous Solubility</b>	-1.24	-6.11	-3.72	-2.02	-5.31	-2.92	-7.95	-4.88	-3.87
<b>Aqueous Solubility level<sup>b</sup></b>	4	1	3	3	2	3	1	2	3
<b>Blood Brain Barrier (BBB)</b>	N/A	0.583	-0.611	-1.021	0.3	-0.894	0.755	-0.439	N/A
<b>BBB level<sup>c</sup></b>	4	1	3	3	1	3	0	2	4
<b>Cytochrome P450 2D6 (CYP2D6) prediction</b>	-4.42	0.9001	-2.420	-4.677	4.548	-2.911	6.556	0.0482	-4.809
	FALSE	TRUE	FALSE	FALSE	TRUE	FALSE	TRUE	FALSE	FALSE
<b>Hepatotoxicity</b>	-0.485	-2.810	-1.105	-2.754	-4.12	1.004	-10.70	-5.568	-0.847
<b>Hepatotoxicity prediction</b>	TRUE	TRUE	TRUE	TRUE	TRUE	TRUE	FALSE	FALSE	TRUE
<b>Plasma Protein Binding (PPB)</b>	1.809	3.484	8.056	4.555	7.937	6.742	7.313	7.086	3.637
<b>PPB Prediction</b>	TRUE	TRUE	TRUE	TRUE	TRUE	TRUE	TRUE	TRUE	TRUE

0 = Good absorption, 1 = Moderate absorption, 2 = Low absorption, 3 = Very low absorption.

<sup>b</sup>**Drug-likeness:** 0 = Extremely low, 1 = No, very low, but possible, 2 = Yes, low, 3 = Yes, good, 4 = Yes, optimal, 5 = No, too soluble.

<sup>c</sup>**Blood brain penetration:** 0 = very high penetrant (Brain-Blood ratio greater than 5:1), 1 = High (Brain-Blood ratio between 1:1 and 5:1), 2 = (Medium Brain-Blood ratio between 0.3:1 to 1:1), 3 = Low (Brain-Blood ratio less than 0.3:1), 4 = Undefined (Outside 99% confidence ellipse)

The assessed ADMET descriptors for the 3-piperazinyl-3 series of halogenated polyamines analogues (Table 3.8) indicated that the compounds show good to moderate intestinal absorption. The aqueous solubility of the compounds was predicted as being low especially in comparison to the parent compound **12**. The predicted blood brain penetration was low overall. Cytochrome P450 inhibition was predicted to be minimal or non-existent. While the majority were predicted to be positive for hepatotoxicity, all the compounds were predicted to have high plasma protein binding predictions.

The drug-likeness properties calculated for the 3-piperazinyl-3 polyamine analogues showed that these analogues are generally predicted to be more favourable than the E series. Particularly, only one compound (**A4S**) was particularly large in comparison to the other compounds in this series. In totality, two compounds did not have any Lipinski



violations. However, similarly to what was observed for the halogenated E-series of compounds, thiourea substitution and trifluoromethylation resulted in the highest number of violations e.g. compounds **A1S** and **A4S** violating MW, ALogP and RotB. Lipinski's rules were violated at least once in the majority of cases except for compounds **A3O** and **A2O**. Similarly, to the E-series, QED values calculated were all much less than 1 indicating unfavourable drug-likeness properties.

**Table 3.9: Drug-likeness prediction of 3-piperazinyl-3 polyamine analogues**

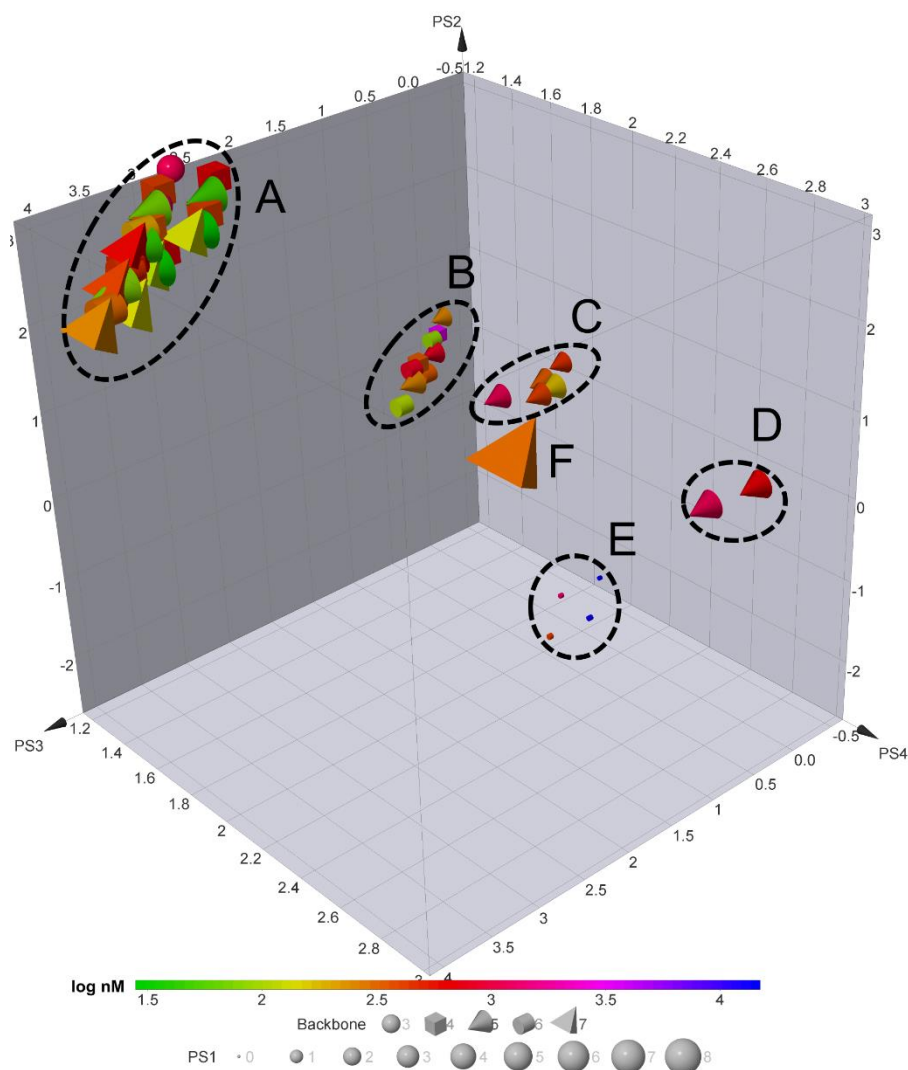
*In silico* physiochemical predictors were obtained using the Discovery Studio Modelling Environment program.

Analogue Name	MW <sup>a</sup>	ALOGP <sup>b</sup>	HBD <sup>c</sup>	HBA <sup>d</sup>	ROTB <sup>e</sup>	AROM <sup>f</sup>	Lipinski's Violations <sup>g</sup>	QED <sup>h</sup>
12	454.61	2.14	6	4	16	2	1	0.2337
A1S	541.603	5.621	6	4	12	2	3	0.11804
A1O	507.456	3.26	4	4	10	2	1	0.39775
A2O	438.566	1.932	4	4	10	2	0	0.4565
A3S	508.694	4.704	6	4	12	2	2	0.14058
A3O	474.547	2.343	4	4	10	2	0	0.42577
A4S	608.709	6.177	6	4	14	2	3	0.06609
A4O	574.562	3.816	4	4	12	2	1	0.29059
A5O	596.358	3.428	4	4	10	2	1	0.33886

a) MW – Molecular Weight (g/mole); b) ALOGP – A log P (lipophilicity); c) HBD - Hydrogen Bond Donors; d) HBA – Hydrogen Bond Acceptors; e) ROTB – Rotatable Bonds; f) AROM – Aromatic rings; g) Violations of Lipinski's rules should be  $\leq 1$ ; h) QED – 0 = unfavourable; 1 = favourable.

### 3.3.2 Structure-activity relationship analysis of Polyamino(bis)ureas and Polyamino(bis)thioureas

The polyamine analogue data presented here, together with a number of series previously tested [106, 107], were combined into a database (Appendix, Table 1). Visualisation of the chemical space of the analogues was subsequently performed to determine the distribution of the analogues based on their chemical similarity, and to determine if clusters with similar chemical backgrounds could be correlated to the observed *in vitro* activity against *P. falciparum* parasites. To accomplish this, various dimensionality-reducing techniques such as PCA and MSA were used. Furthermore, matched molecular pair (MMP) analysis was performed on the compounds to determine the specific structural modifications associated with an increase in antiplasmodial activity.

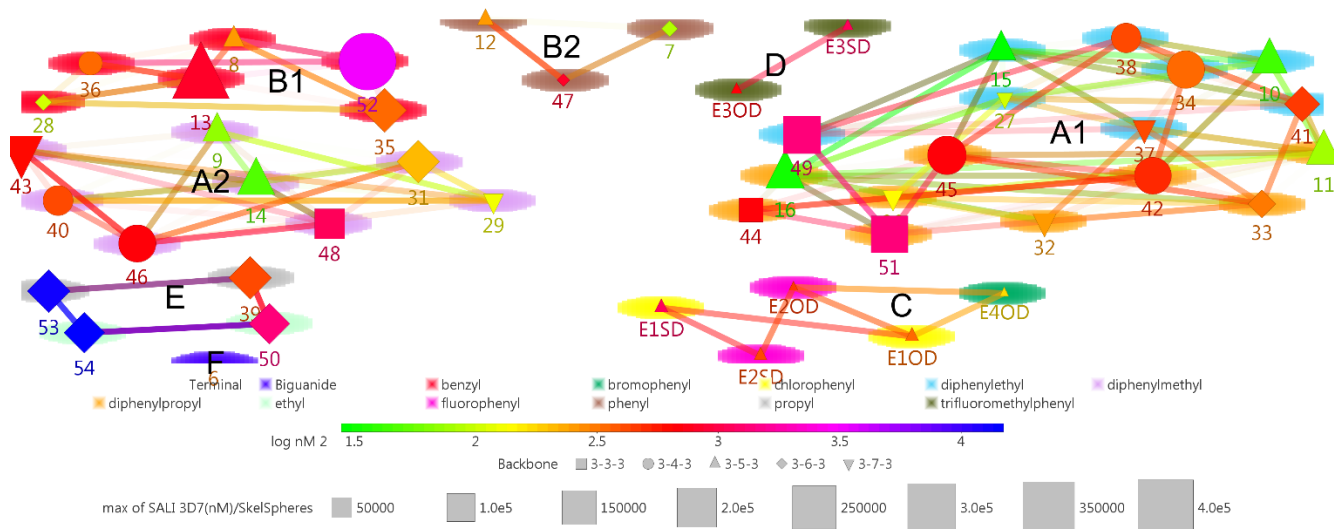


**Figure 3.23: Principle component analysis of the polyamine analogues chemical space using Chem-GPS.**

The visualisation was obtained by principal component analysis of the coordinates generated with Chem-GPS. Data points are coloured by their log IC<sub>50</sub> (log nM) values in a continuous scale. The shape of the marker indicates the backbone of the data point. Dimensions: PS1-size (represented by size of the markers), PS2-aromaticity, PS3-lipophilicity and PS4-flexibility. Clusters are represented as follows, A: (bis)diphenyl analogues, B: (bis)phenyl analogues, C: halogenated (bis)phenyl analogues, D: trifluorinated (bis)phenyl analogues, E: (bis)alkyl analogues, F: Analogue 6.

Figure 3.23 indicates the resultant 3-D PCA analysis of the dataset. The visualisation of the chemical space indicated that the polyamine analogues are structurally clustered according to their terminal groups, 6 distinct clusters occupying the chemical space emerged. Namely; A: (bis)diphenyl analogues, B: (bis)phenyl analogues, C: halogenated (bis)phenyl analogues, D: trifluorinated (bis)phenyl analogues, E: (bis)alkyl analogues and F: Analogue 6. The clusters shown in Figure 3.23 indicate that the highly lipophilic compounds with low flexibility (cluster A) have the greatest antiplasmodial activity in comparison to the other clusters. The clusters containing diarene terminal groups (cluster A) showed greater separation as compared to the clusters of arene terminal analogues

(cluster B). Large variations in antiplasmodial activity were observed between clusters irrespective of terminal substitutions indicating a large amount of chemical diversity in terms of effective activity. Throughout the clusters, the 3-5-3 backbone analogues were seen to have the greatest antiplasmodial activity.

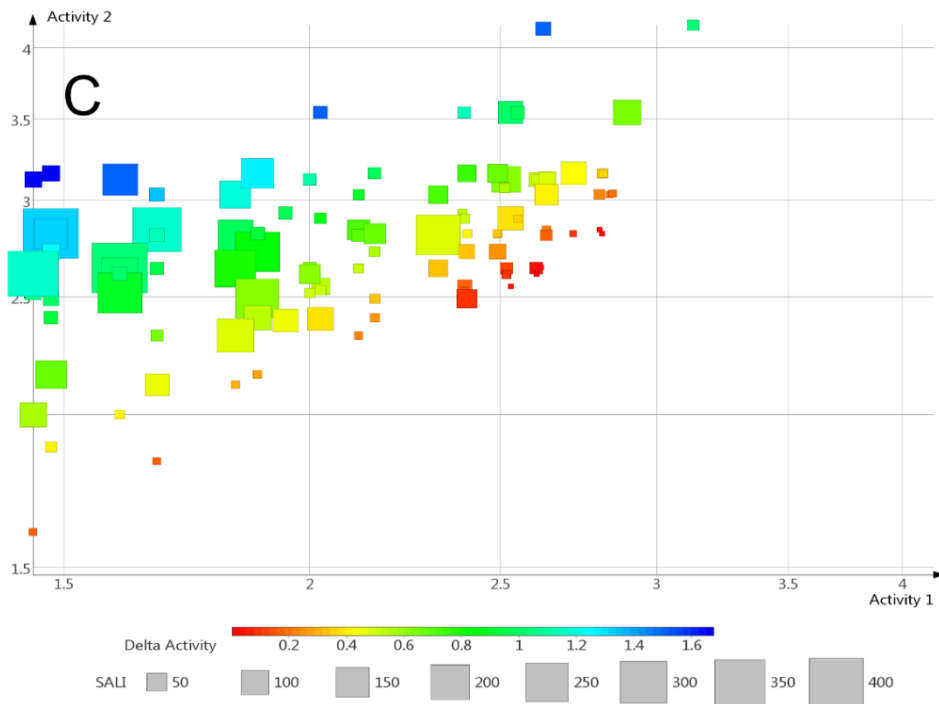
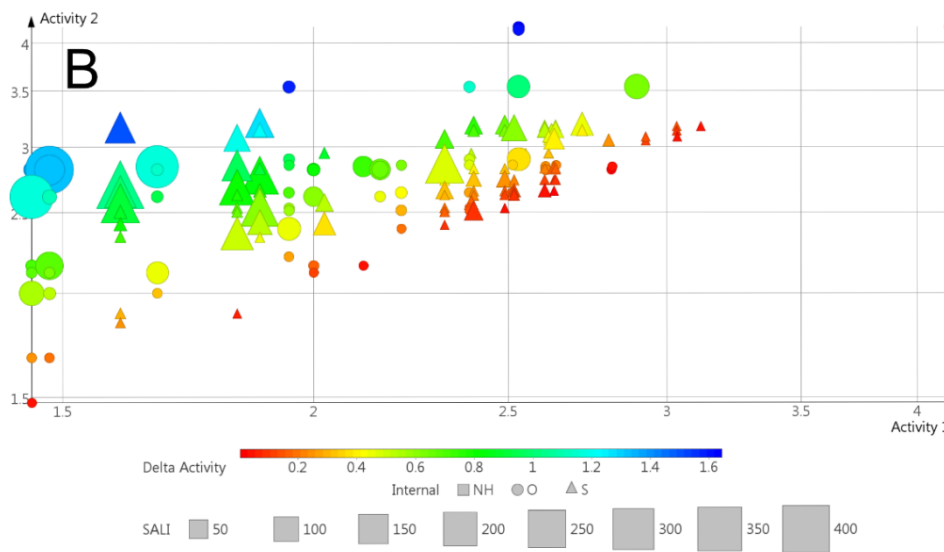
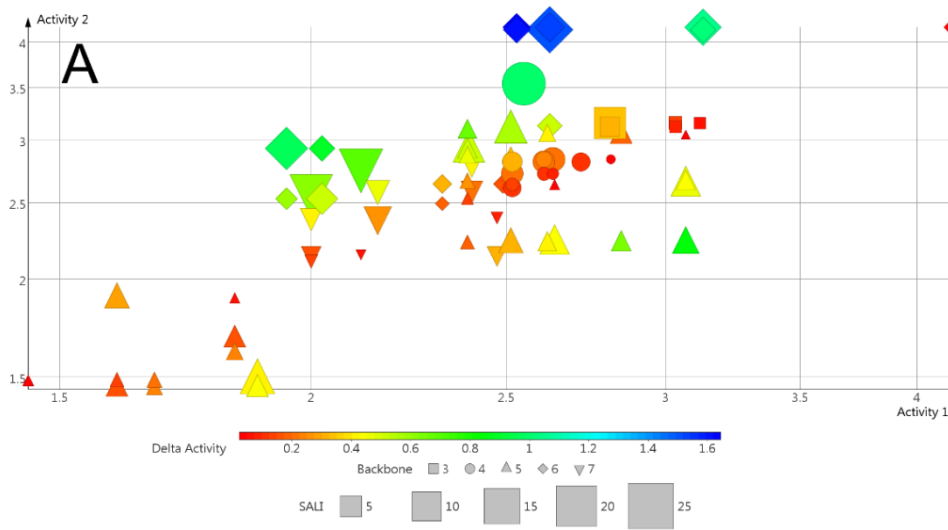


**Figure 3.24: Molecular similarity analysis of the chemical space of the polyamine analogues. Self-organizing map depicting structural-activity landscape.**

The molecular similarity analysis of the similarity matrices was computed with Skelspheres at a 95% similarity cut off. Data points are coloured by the log IC<sub>50</sub> (log nM) values in a continuous scale. The shape of the marker indicates the backbone of the data point. The background colour indicates the terminal group substitution. Connecting lines between points indicate >95% similarity. The marker size indicates SALI values. Clusters are represented as follows, A1: (bis)diphenyl analogues with propyl and ethyl linkers, A2: (bis)diphenyl analogues with methyl linkers, B1: (bis)benzyl analogues, B2: (bis)phenyl analogues, C: halogenated (bis)phenyl analogues, D: trifluorinated (bis)phenyl analogues, E: (bis)alkyl analogues, F: Analogue 6.

Molecular space analysis (Figure 3.24) again indicated that the polyamine analogues are structurally clustered according to their terminal groups showing a very similar separation to the PCA, however, the clusters separated more with greater differentiation between the linkers present in the terminal groups. The MSA showed very similar trends to the PCA. In that the biological activity of these compounds is not ascribable to one cluster of similar compounds and that the SAR of the analogues is discontinuous. This discontinuity is seen in all the clusters as the lines connecting markers indicates greater than 95% structural similarity, however, the marker colour indicates the antiplasmodial activity which changes abruptly in closely related pairs. This indicates that small structural differences are responsible for the gain in antiplasmodial activity, this is defined as an activity cliff. Consequently, the dataset was evaluated with matched molecular pairs in an activity cliff analysis (ACA), to determine the structural requirements for activity. This was performed separating backbone pairs (Figure 3.24 A), internal substituents pairs

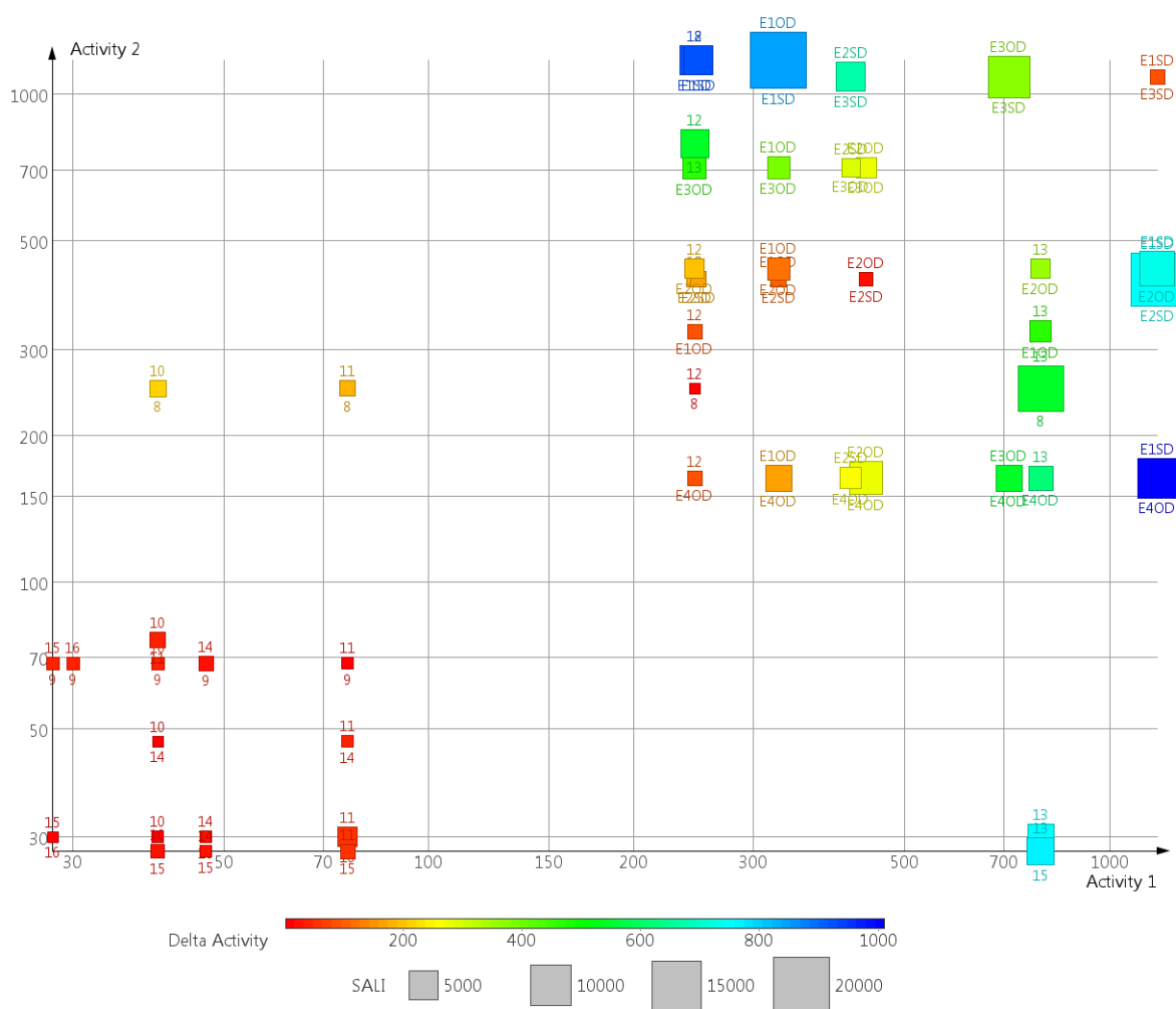
(Figure 3.24B), or terminal groups pairs (Figure 3.24C). Summaries of these MMP's and their corresponding Structure activity landscape index values (SALI) are included in the appendix in Tables 2A, 2B and 2C as non-normalised values (not log transformed), indicating the top 20% of the SALI values. Appendix Figure 1 was also included analysing the neighbour tree of compound 15, this indicated the compounds with 80% similarity by connecting lines, their structural properties and antiplasmodial activities.



**Figure 3.25 as on page 66: Matched molecular pair activity cliff analysis of the polyamine analogues. A) Separated on backbone, B) separated on internal substituents and C) separated on terminal groups.**

Activity cliff analysis was performed by molecular similarity analysis of the similarity matrices computed with Skelspheres at 80% similarity cut off and separated based on their backbone, internal substituents and terminal groups. Each data point indicates a matched molecular pair of  $\geq 80\%$  similarity. Data points are coloured by the difference in the matched molecular pair (MMP)'s log  $IC_{50}$  (log nM) values in a continuous scale. The shape of the marker indicates the; A) backbone of the data point, B) internal substituents. The size of the marker indicates the structure-activity landscape index (SALI) value for each MMP.

The analysis of activity cliffs allows the determination of structural changes resulting in increased antiplasmodial activity. As is seen in (Figure 3.25) numerous markers indicating MMP's occur, especially at the low cut-off value of greater than 80% structural similarity. This was done to capture the entire structure activity landscape and to visualise the greatest structural diversity. The colouring of the markers indicates the difference in each pairs log normalised  $IC_{50}$ , while the size of the markers indicates the SALI values for the MMP. The SALI value is calculated by the absolute difference in biological activity of the two compounds in a MMP divided by one minus their molecular similarity. Consequently, the SALI value gives a relative measure of how much activity is gained or lost as a result of a small modification in structure. The observed abrupt change in activity as a result of slight molecule differences allows activity cliffs to be identified. MMP's which lie near to the line of best fit have low differences in activity and therefore low SALI values, unless they have high similarity. Conversely MMP's removed from the line of best fit have higher SALI values, unless they have low similarity. Figure 3.25 A indicates that the 3-7-3, 3-6-3 and 3-4-3 backbones have large activity cliffs within their pairs whereas the 3-5-3 backbone has many more MMP's but possess lower SALI scores, this implies that the 3-5-3 backbone is the optimal backbone. The MMP's Figure 3.25 B shows that MMP's with the same internal substitution have numerous activity cliffs, but urea analogues possess larger activity cliffs, in comparison to the similarity of Figure 3.25 C it indicates that analogues with the same terminal substitution gain activity with the variability of the internal substitution. Due to the favourable nature of the 3-5-3 backbone the above analysis was repeated using only the analogues possessing this backbone.



**Figure 3.26: Matched molecular pair activity cliff analysis of the 3-5-3 backbone compounds in the data set.**

Activity cliff analysis was performed by molecular similarity analysis of the similarity matrices computed with Skelspheres at 80% similarity cut off. Each data point indicates a matched molecular pair of  $\geq 80\%$  similarity. Data points are coloured by the difference in the MMP's  $IC_{50}$  (nM) values in a continuous scale. The size of the marker indicates the structure-activity landscape index (SALI) value for each MMP. The numbering above of each MMP indicates the first molecule in the MMP followed by the second molecule in the MMP just below.

The distinction between the lower SALI value 3-5-3 backbone MMP's with lower changes in activity is of interest as they cluster entirely separately from the other backbones indicating that the 3-5-3 backbone is a prerequisite for good activity. The activity cliff analysis of the 3-5-3 backbone indicated the same general trends observed for the entire dataset in terms of the requirement of urea and diarene terminal groups for increased activity. The MMP's of the current analogues indicated that the greatest gain in activity was for urea substitution and bromination of the *para*-position of the phenyl ring.

### 3.3.3 Quantitative structure-activity relationship model development

The development of a predictive QSAR equation was undertaken to complement the SAR-based analysis and to allow further insight into the structural requirements for the polyamine analogues activity. The use of regression analysis on various physiochemical descriptors generated for the compounds contained in the database (Appendix, Table 1), was performed to predict antiplasmodial activity. This was accomplished by making use of the online chemical modelling environment, OChem (<https://ochem.eu/>) [124].

**Table 3.10: Training set models summary.**

The best performing models obtained during the regression analysis using OChem and their statistical performance.

Descriptor package	Number of compounds	Equation	R <sup>2</sup>	q <sup>2</sup>	RMSE	MAE
ECFP	29	Y=-2.81-0.635*ECFP4_186 + 0.688*ECFP4_221	0.4 ± 0.1	0.4 ± 0.2	0.42 ± 0.04	0.34 ± 0.04
Adriana	29	Y = 1.87 - 0.0507*2DACorr_LpEN_1 - 5.57*3DACorr_SigChg_6 + 14.5*3DACorr_TotChg_3 + 1.24*3DACorr_TotChg_4 + 3.4*3DACorr_TotChg_5 + 0.0211*3DACorr_LpEN_12 - 0.0697*2DACorr_LpEN_9	0.6 ± 0.1	0.6 ± 0.1	0.33 ± 0.03	0.29 ± 0.03

The QSAR analysis performed on the range of polyamine analogues resulted in numerous models being developed, however, only the best performing models were selected based on their statistical performance. The physiochemical descriptors generated for the compounds were selected with unsupervised forward selection. The statistical performers for both equations indicated that they are within acceptable ranges, however the Adriana descriptor based equation showed greater predictive strength. To confirm this a set of test compounds was used to validate the models predictive power.



**Table 3.11: Test set models summary**

The test set results obtained during the regression analysis using OChem and their statistical performance.

Descriptor	Number of compounds	R <sup>2</sup>	q <sup>2</sup>	RMSE	MAE
ECFP	5	0.6 ± 0.2	0.2 ± 0.2	0.23 ± 0.03	0.21 ± 0.05
Adriana	5	0.5 ± 0.3	0 ± 0	0.5 ± 0.2	0.4 ± 0.1

The determination of two QSAR equations based on various descriptors with reasonable performance indicated that the use of non-linear regression to predict novel polyamine analogue's compound activity is possible, albeit with a low level of statistical significance. The correlation of the polyamine analogues antiplasmodial activity to the molecular descriptor extended connectivity fingerprints (ECFPs) and Adriana descriptors, indicated that the analogues possess common structural features required for activity. ECFPs descriptors are encoded by the ordering of the substituents in the molecular structure. This is further highlighted in the Adriana molecular descriptors which dealt with charge and electronegativity. The construction and validation of these models allows the prediction of antiplasmodial activity of future analogues which are similar to those reported here.

## Chapter 4: Discussion

Malaria is caused by parasites of the genus *Plasmodium*; it is considered to be the world's most devastating parasitic disease. Current chemotherapeutics have shown decreased efficacy as a result of *P. falciparum* developing resistance, emphasising that the sustained control and elimination of malaria requires drugs utilising novel modes of action to combat the emergence of drug resistance [43].

A promising class of novel chemotherapeutics for hyper-proliferative diseases such as cancer and parasitic diseases has emerged in the form of polyamine analogues [46, 78]. The rationale behind polyamine analogue design and synthesis is that they function using multiple mechanisms. The polyamine analogues act functionally either as (1) anti-metabolites that function by depleting intracellular polyamine concentrations, or as (2) polyamine mimetics that function by displacing the natural polyamines from their binding sites, but are not able to substitute in function [87]. In addition, these analogues can act as antagonists interfering with polyamine transport systems that are essential for continued proliferation [88]. Furthermore, polyamine analogues have been shown to act as epigenetic regulators as a result of their LSD1 inhibitory activity in cancer cells [103].

Terminally alkylated polyamine analogues were previously shown to possess significant anti-cancer activity [103, 105] and potent *in vitro* antiplasmodial activity [106]. The lead compound of this generation (compound **30**, a 3-6-3 (bis)urea internal substituent with phenyl terminal groups) exhibited an *in vitro* IC<sub>50</sub> of 88 nM against *P. falciparum* parasites, but had no potency against a murine malaria model. Subsequent fluorination of the aromatic ring with the goal of improving pharmacokinetic properties by enhancing metabolic stability and absorption did not improve *in vivo* antimalarial activity [108]. Due to the activity of the previous generations of polyamine analogues, and the potent activities found against human African trypanosomiasis for the 3-5-3 backbone [101,85], further investigation of the antiplasmodial properties of substituted 3-5-3 backbone polyamine analogues was conducted. They were shown to possess significant activity against *P. falciparum* [107]. Based on the poor *in vivo* efficacy of compound **30**, this project aimed to modify the lead 3-5-3 analogue compound **7** to incorporate structural features that could potentially enhance metabolic stability and increase absorption.

Additionally, this project aimed to determine the antiparasitic structural requirements of the polyamine analogues.

An attractive strategy to improve metabolic stability is to block the metabolically labile sites present in the analogues with a fluorine or a halogen substituent [111], due to hydroxylation in Phase I metabolism that occurs at the *para*-position of the phenyl ring. Therefore, analogues halogenated at the *para*-position of the phenyl ring are expected to be more metabolically stable as the C-X bond is considerably stronger [112]. This strategy has been applied successfully to a large range of previously inactive compounds [113]. The absorption of these analogues can be further enhanced by reducing the basicity of the outer amino groups; this would result in better membrane permeation of the analogue and thus improved bioavailability. The substitution of hydrogen atoms with fluorine in the polyamine backbone was one of the first strategies used to influence the pKa values of neighbouring amino groups [129]. Further modification of the polyamine backbone to reduce the number of rotatable bonds by using a conformationally restrained cyclic ring such as a piperazine could also lead to increased bioavailability. Also, the cyclic ring would drastically decrease the basicity of the amine functionalities. However, the charged nature of the polyamines is a prerequisite for active transport [109].

The synthesis of polyamine analogues can be accomplished using various synthetic methodologies dependant on the required analogues. A fragment-based method was chosen targeting a common intermediate, as it allows the introduction of great chemical diversity as the synthesis of novel thioureas and ureas requires only the corresponding isothiocyanate or isocyanate. The method employed was previously reported [105, 106]. The selective functionalisation of multiple amines in the polyamine backbone and the subsequent purification of the hydrophilic products is challenging [130].

The compounds synthesised for the 3-5-3 polyamine analogues (**E10D-E40D**) was accomplished by means of synthetic pathways that are facile and relatively inexpensive. Elongation of the polyamine backbone can be accomplished by various N-alkylation methods. Michael addition of acrylonitrile was chosen as the subsequent reduction of the nitrile group produces the required aminopropyl moieties. Michael addition reactions with primary amines can lead to side products of mono- and biscyanoalkylated amines. The synthesis of **2** was accomplished in high yields at multigram quantities. The presence of

additional carbons in the  $^{13}\text{C}$  NMR and the IR peak of the nitrile were the most characteristic identifiers. The synthesis of the N-Boc protected bis-nitrile **3** was carried out by N-Boc protection of **2**. It was, however, noted that the N-Boc protection reaction gave low yields (54%) relative to that previously reported. This was attributed to the large quantities of unprotected amine that were used in addition to the rigorous workup conditions employed to remove unprotected amine. The most characteristic identifier being the 18 hydrogen multiplet present in the  $^1\text{H}$  NMR.

Reduction of nitrile groups to amines during polyamine analogue synthesis is generally achieved with either catalytic hydrogenation or with metal hydrides [130]. The catalytic hydrogenation of nitriles often forms mixtures of primary, secondary and tertiary amines [131]. During the catalytic hydrogenation of a nitrile, the imine is formed as an intermediate; this is then hydrogenated to produce the primary amine. The use of catalytic hydrogenation is preferred as it is less vigorous and can tolerate N-Boc protected amines. Whereas metal hydride reductions can be harsh and can result in degradation and most probably the formation of un-isolatable chelation complexes [128]. However, metal hydride reductions are advantageous as secondary and tertiary amines are not formed. Additionally, the reaction and workup procedure are comparatively easier than metal hydride reductions, which involve hazardous and flammable reagents. The reduction of the dinitrile **3** was initially found to be problematic when using Raney-Nickel 2800, resulting in incomplete reductions and multiple side products requiring extended periods of time (>240h). Optimisation of the reaction was carried out by varying the quantities of base and catalyst. The formation of side products was greatly reduced by addition of greater amounts of ammonium hydroxide base due to the suppression of secondary and/or tertiary amines. This is due to the ammonium hydroxide shifting the equilibrium of the transamination toward the imine. Increasing the quantity of catalyst present in the reaction resulted in slightly reduced reaction times, however, a greater quantity of side products was present.

In an attempt to decrease the time of the reduction, a modified Parr-hydrogenator apparatus was constructed that allowed the magnetic stirring of the reaction mixture rather than the classical shaking. This apparatus greatly reduced the reaction times, however, greater quantities of the catalyst were required due to some of the catalyst sticking to the magnetic stirrer bar. The problematic reduction was attributed to inactivation of the Raney-Nickel 2800 catalyst as a result of oxidation and also extended

storage time [132, 133]. Purification using column chromatography on SiO<sub>2</sub> and deactivated Al<sub>2</sub>O<sub>3</sub> resulted in complete decomposition as previously reported [128]. This was most likely due to the hydrophilic nature of the product as well as the acid labile nature of the N-Boc protecting group. To overcome the decomposition a hydrophobic and non-acidic solid phase was used namely Diaion HP-20, a reversed phase resin, using a gradient elution of methanol and water. This allowed effective separation of the product mixture, however, combination of the pure fractions followed by rotary evaporation resulted in degradation of the N-Boc protected diamine. This was attributed to the presence of water and high temperatures which has shown the ability to hydrolyse the N-Boc protecting group [134]. These difficulties experienced during the purification of the N-Boc protected diamine were in agreement with those previously reported [130].

In an attempt to overcome the problematic hydrogenation, a previously reported metal hydride (LiAlH<sub>4</sub>) reduction method was used with modifications to the molar equivalents [135]. The reaction resulted in the formation of the expected product; however, large quantities of precursor were still present and satisfactory purification could not be achieved. This was most likely as a result of polymer formation as reduction of polyfunctional molecules with LiAlH<sub>4</sub> often leads to cross linking. Dinitriles tend to form insoluble precipitates that remove hydride from the solution and thus give poor yields. The incomplete reduction was overcome by making use of a Ni–Cr-promoted Raney-Co (#2724) catalyst; that is more selective in the reduction of nitrile functional groups and possess greater catalytic activity [132, 136]. This resulted in quantitative conversion of multigram quantities of the diamine in greatly reduced periods of time (<96h). Confirmation of the proposed structure was accomplished with IR, MS and NMR. The most characteristic identifiers being the disappearance of the nitrile group's IR peak and the presence of additional protons relative to the reactant.

Synthesis of the N-Boc protected intermediates (**E10B-E40B**) was accomplished by reacting the precursor with isothiocyanate or isocyanate as described in general method A. The reaction was seen to be relatively high yielding with the majority of compounds, however, large losses in yield were seen occasionally and were attributed to losses during column chromatography and workup. Specifically, the low yields seen for both **E3SB** and **E30B** were thought to be as a result of the respective isothiocyanate and isocyanate's lower reactivity as a result of the trifluoromethyl group. The presence of aromatic protons

present in the  $^1\text{H}$  NMR was the most characteristic identifier. Deprotection of the N-Boc protected intermediates **E10B-E40B** was accomplished by means of acid catalysed hydrolysis resulting in the dihydrochloride salts. This reaction was high yielding with the majority of compounds, however, losses in yield were seen occasionally and were attributed to losses during workup. The most likely culprit of this was insufficiently dried washing solvents and the overzealous use of multiple washing steps to ensure high purity. The proposed structures for all the N-Boc deprotected compounds were confirmed with IR, MS and NMR. The absence of the 18 proton multiplet indicating N-Boc protection in the  $^1\text{H}$  NMR was the most characteristic identifier.

Modification of the polyamine backbone to reduce the number of rotatable bonds was accomplished by inserting a piperazine backbone. Initially, the backbone was prepared by bis-cyanoethylation of piperazine followed by catalytic hydrogenation. The catalytic hydrogenation presented similar problems as that experienced for the 3-5-3 backbone, however, they could not be resolved. This could be due its exposure to carbon dioxide in the air to form amine-carbamate salts, secondary amine formation or hydrogenation of the tertiary amines present in the ring. Thus, it was decided to obtain the final precursor **1,4-bis(3-aminopropyl)piperazine** commercially. This was subsequently reacted with the corresponding aryl isocyanate or isothiocyanate to obtain compounds **A10-A50**. The proposed structures for all the 3-piperazinyl-3 compounds were confirmed by IR, MS and NMR. The characteristic identifier for these compounds was the presence of the aromatic protons seen in the  $^1\text{H}$  NMR in comparison to the precursor **1, 4-bis(3-aminopropyl)piperazine**. The successfully synthesised compounds were then assessed for their *in vitro* antiplasmodial activity against a panel of *P. falciparum* strains.

The antiplasmodial activities determined for the E-series as shown in Table 3.4, indicated that the novel series of polyamine analogues have nanomolar  $\text{IC}_{50}$  values against the various strains tested, without any overt cross-resistance observed. This is encouraging, as novel antimalarial drugs should not share the same possibility of development of resistance due to similar resistance mechanisms [137]. The polyamine analogues consisting of 3-piperazinyl-3 backbones were also assessed for their *in vitro* antiplasmodial activity as tabulated in Table 3.5. The *in vitro* antiplasmodial activity determined for the A series of polyamines analogues indicated that this class of analogues have low antiplasmodial activity that falls within the micromolar range.

The antiplasmodial activities obtained for the E-series varied based on the halogen substitution and the presence of either urea or thiourea. This was also true for the A-series analogues. Analogues possessing thiourea's showed reduced activity versus the urea analogues, indicating the importance of the urea functionality for activity. This is in agreement with all the previous generations of compounds where the same general trend was observed [107]. This observation could be as a result of the removal of a hydrogen acceptor group namely the carbonyl of the urea, leading to less hydrogen bonding and reduced potency, assuming that hydrogen bonding is present in the drug target interaction. Additionally, this observation could be attributed to the lower pKa values for the more acidic thiourea terminal nitrogen's versus the urea analogues because sulphur is less electronegative than oxygen. The observed trend does however not always hold true as is tabulated in appendix Table 2A. This indicates that the preference is backbone specific, however, the high SALI values obtained for certain MMP's such as for compounds 7 and 47 indicate its general applicability.

This study confirms that the activity of the polyamine analogues is associated with an increase of the bulkiness of the terminal substituent, as the polyamine analogues (**E10D-E40D**) showed decreased activity versus the diaryl substituents seen in the previous generations. Contradicting this is the fact that the analogue's **E3S** and **E3O** showed low potency. Because the volume of a trifluoromethyl group is comparable in size to an isopropyl group, and it has been suggested that it can exert an effect comparable to a phenyl ring or even a *tert*-butyl group [111]. However, substitution at the *para*-position of the phenyl ring with a trifluoromethyl group could also aid in increasing the metabolic stability of the analogues by blocking oxidation at the *para*-position of the phenyl ring, in addition to deactivating the  $\pi$  system of the benzene ring [114]. The trifluoromethyl group has also been associated with drastic conformational changes, which could impart greater "drug-likeness" and increase the binding affinity of a compound drastically [138].

The influence of halogenation on the compounds activity showed that increasing the size of the halogen substituent correlated to increased activity. In contrast to earlier findings which found that fluorine substitution resulted in greater antiplasmodial activity. The compounds showing the lowest IC<sub>50</sub> values in both the E and A series was **E40D** (162 nM) and **A50** (36 nM) against the drug sensitive 3D7 strain. Both these compounds possess a bromine in the *para*-position of the phenyl ring. In opposition, compound **E20D**

show markedly better activity against the resistant strains K1 and W2, with IC<sub>50</sub>'s of 33.7 nM and 36.1 nM respectively. The activity of these analogues could be due to the larger size of the halogen and its reduced electronegativity. Additionally, recent evidence has emerged that halogens larger than fluorine possess special electronic properties when bound to aryl or electron-withdrawing alkyl groups [139]. This leads to the formation of  $\sigma$ -holes in the C-X moieties allowing attractive interactions towards carbonyl groups and other H-bond acceptors. The halogen bond donor ability increases with polarizability, and decreases with the electronegativity, matching the observed correlation in activity. Recent drug discovery efforts have successfully implemented halogen bonding in a variety of lead optimisation efforts including; nicotinic acetylcholine  $\alpha$ 4 $\beta$ 2 receptor antagonists; HIV reverse transcriptase inhibitors and inhibitors of malarial enoyl acyl carrier protein reductase [140-142].

The antiplasmodial activity determined for **A50** is in contrast to the low antiplasmodial activity determined for the other A series analogue. This surprising result could be due to various factors such as compound decomposition due to the instability of the piperazine backbone as discussed previously, however, the IC<sub>50</sub> did not vary greatly between biological repeats indicating no decomposition. Furthermore, the general trend seen in the antiplasmodial activities for these compounds indicate that halogenation at the *para*-position of the aromatic ring is important for activity, as can be seen when compound **A20's** activity is compared to the halogenated derivatives. The low antiplasmodial activity of these compounds could be explained in terms of the transport of polyamine analogues, as it has been determined that the charged nature of the backbone in linear polyamine analogues is a prerequisite for transport, but terminal substitutions are generally tolerated [121, 143]. Previous, studies on partially related aryl piperazine antiplasmodial compounds found similar activities to those reported here [144]. This could also be due to the difficulty experienced during the dissolution of these compounds in DMSO, as compound precipitation occurred in even partially wet DMSO, this was overcome with drying of the DMSO and vortexing of the analogue solution. The compounds could thus have precipitated during assay setup and dilution which could explain the observed low activity.

Oral bioavailability can be understood as a combination of factors concerning a fraction of the oral dose namely; the fraction of the dose absorbed across the gastro intestinal



wall; the fraction that survives gut metabolism and the fraction that survives liver metabolism [145]. Therefore, oral bioavailability can be described as a combination of absorption and metabolism factors. The determination of the compounds ADMET descriptors was performed computationally by using Accelrys Discovery studio. This included models for intestinal absorption, aqueous solubility, blood brain barrier penetration, plasma protein binding, cytochrome P450 2D6 inhibition and hepatotoxicity. Intestinal absorption is defined as the percentage absorbed. Level 0 indicates good absorption and level 3 has very poor absorption. The assessed ADMET descriptors for the E series of polyamines analogues (Table 3.6) and the A series (Table 3.8). Indicated that the E series compounds showed good absorption for compounds **E1SD**, **E1OD**, **E2SD**, **E2OD** and moderate intestinal absorption for **E3SD**, **E3OD** and **E4OD**. While the A series had overall good absorption except for **A4S** which had moderate intestinal absorption. The naturally occurring polyamines are rapidly and completely absorbed in the duodenum and first portions of the jejunum [146]. It has been shown that putrescine transport occurs by diffusion, due to polyamine flux being neither saturable or temperature dependent [146]. Furthermore, three oligoamines with four carbon backbones have been shown to be orally active in the treatment of diarrhoea [147].

The assessment of aqueous solubility indicated that the E series analogues had low (**E3SD**) to good aqueous solubility. While the A series had low (**A4S**) to good aqueous solubility. Blood brain penetration of the E series analogues was mostly undefined, most likely due to their charged nature. The A series was predicted to have high to low blood brain penetration. The latter property is vital for the effective treatment of cerebral malaria. The E series analogues showed varied results with regards to cytochrome P450 inhibition, compounds **E1SD**, **E2SD** and **E3SD** indicated inhibition. The A series analogues **A1S**, **A3S** and **A4S** were predicted to inhibit cytochrome P450. Correlating to presence of their thiourea moieties in the analogues. The inhibition of cytochrome P450 by a drug candidate can create drug-drug interactions resulting in adverse reactions. All of the polyamine analogues in the E series were predicted to be hepatotoxic except for **E3SD**. While all the A series analogue's except for **A4S** and **A4O** were predicted to be hepatotoxic. All of the analogues were predicted to bind to the plasma proteins although all too a relatively low degree. This could affect the drug's efficacy as only unbound drug can exert a pharmacological effect. The main catabolic pathway of natural polyamine and their acetyl derivatives is by oxidative deamination by the enzyme diamine oxidase, which

is present in substantial amounts in gut mucosa, liver, and kidneys [148]. Numerous amine xenobiotics and polyamine analogues such as MDL 27695 have been shown to be metabolised by polyamine oxidases [97, 143].

Pharmacokinetic properties can be optimised by modifying the physiochemical properties of the analogue such as pKa, electronegativity, lipophilicity, hydrogen bond acceptors and donors to improve the “drug-like” properties of the compound [149]. The phrase “drug-like” describes the concept that certain compound properties are advantageous in their becoming successful drug candidates. The term became synonymous with drug design strategies following the rule of five proposed by Lipinski [150]. The rule of five is indicative of compounds with good oral bioavailability and permeability. The rules state that poor absorption or permeation of drug candidates generally results when there are >5 H-bond donors, >10 H-bond acceptors, the molecular weight is >500 Da and the calculated Log P (CLogP) is >5. Additionally, further rules were later proposed based on their ability to increase compound oral bioavailability in rats. These rules indicated the importance of molecular flexibility, polar surface area and hydrogen bond count as indicators of increased oral bioavailability and stated that rotatable bonds should be <10, the polar surface area should be <140 Å<sup>2</sup> and <12 total hydrogen bonds should be present [151]. These rules are predictive of good ADMET properties (Absorption, Distribution, Metabolism, Excretion and Toxicity); these criteria influence the performance and pharmacological activity of a compound as a drug.

The Cheminformatic analysis of the compounds synthesised in this study allowed prediction of their drug-likeness. These physiochemical properties indicate that the compounds overall show unfavourable drug-like properties. The compounds adherence to Lipinski’s rule of 5 (Table 3.3), indicated that the 3-5-3 polyamine analogues all violated at least 1 of the rules. Whereas the 3-piperazinyl-3 polyamine analogues violated at least one in the majority of cases except for compounds **A30** and **A20**. Although violation of Lipinski’s rules is predictive of low oral bioavailability, 16% of oral drugs violate at least one of the criteria and 6% fail two or more [150]. Additionally, the polyamines are taken up by epithelial cells via a carrier mediated active transport system [152]. These active transport systems have been shown to have wide substrate specificities and uptake of polyamine analogues has previously been shown [143]. The first four rules of Lipinski are considered not to apply to a molecule, if that molecule is recognised by an active transport

system [150]. The use of a more sophisticated determinant of drug-likeness based on the underlying data distribution of drug properties rather than rule based metrics was assessed using the quantitative estimate of drug-likeness (QED). QED values range from zero to one, where 0 is unfavourable and 1 is nearly ideal. QED is advantageous as it ranks a compounds drug-likeness even if they fail the rule of 5 and tolerates generally unfavourable properties when other properties are favourable [153]. The polyamine analogues all had relatively low QED values, between 0.061 and 0.217 for the E series whereas the A series had slightly better QED values of between 0.118 and 0.456. This indicated that these compounds generally possess undesirable drug-likeness in respect to Lipinski's rules and QED prediction, however, overall the A series had greater drug-likeness properties.

Combining previous polyamine analogue data with that reported here allowed for refinement of their structure-activity relationships. This was initially assessed by determining the chemical space of all the analogues previously reported including the newly assessed E series [107]. The chemical space of a group of compounds can be defined as the placement of a compound based on its physiochemical properties in context of the other compounds in the set. The chemical space was navigated with PCA analysis using Chem-GPS [154]. The analogues were placed together based on their physical-chemical properties, including size, aromatic properties, lipophilic properties, polarity, and flexibility as illustrated in Figure 3.23. Analysis of these clusters indicated that the high antiplasmodial activity of these compounds cannot be ascribed to one cluster in particular, 6 distinct clusters occupying the chemical space emerged, showing a large amount of physical-chemical diversity associated with antiplasmodial activity. This was similarly seen in Figure 3.24 when molecular similarity analysis of the chemical space was performed. The MSA indicates that the use of the descriptor namely the Skelspheres, a similarity based descriptor using chemical graphs, is justified as it separates the analogues and encodes the finer details of the analogues chemical structures. A discontinuous SAR emerged reflecting multiple clusters of compounds which had dramatic differences in activity seen within clusters. Activity cliffs can be described as the marked gain of activity of a compound over a parent compound due to a relatively small structural modification [155]. Consequently, analysis of the activity cliffs was performed using matched molecular pairs and structure activity landscape index. Matched molecular pairs are pairs of compounds possessing a high degree of molecular similarity. As is

illustrated in Figure 3.24 A, B and C, the analysis of the polyamine analogues activity landscape allowed the determination of structural changes resulting in increased antiplasmodial activity. This was summarised in the Appendix Tables 2 A, B and C where the top 20% of the range of SALI values is presented. This was further analysed and indicated general trends in molecular substitution's which are required for increased antiplasmodial activity, which are all in agreement with the preliminary structure activity relationship model [107]. The activity cliffs observed indicate that substitution of thiourea with urea was favourable for increasing antiplasmodial activity. Increasing the terminal groups chain length leads to increased antiplasmodial activity. Decreasing the backbone length is generally favourable until analogues of the 4 carbon backbone are reached, however analogues of either 3-5-3 or 3-6-3 are ideal. Appendix Figure 1 was also included analysing the neighbour tree of compound 15, this indicated the compounds with 80% similarity by connecting lines, their structural properties and antiplasmodial activities. From this the current understanding of the SAR for these compounds was confirmed and relates directly to those presented in Figure 1.14. In addition to these findings the current generation of polyamine analogues seem to suggest that larger halogen substitution is a prerequisite for increased antiplasmodial activity, although further studies are required to confirm this.

The use of QSAR analysis was performed to determine if certain physio-chemical descriptors could be used to predict compound activity for the polyamine analogues. The models developed made use of the chemical modelling environment, OChem (<https://ochem.eu/>) [124]. The models developed were assessed statistically for their predictive power by means of Pearson's correlation coefficient ( $R^2$ ); cross-validated  $R^2$  ( $q^2$ ), root mean square error (RMSE) and the mean absolute error (MAE). The parameters obtained indicated that the activity of the analogues could be predicted with a low level of significance for both models, however, the Adriana descriptor package was seen to have slightly better performance. To confirm the models validity a set of test compounds with known  $IC_{50}$  values were predicted using both models. The resultant statistical parameters indicated that the model using ECFP fragments was considerably better at predicting the antiplasmodial activities of the test compounds. This was however expected due to the large amount of variables present in the Adriana descriptor model. Additionally, the SAR landscape of these compounds contained numerous activity cliffs which would impact the models reliability in predicting antiplasmodial activity.

## Chapter 5: Conclusion

The aim of this study was to synthesise novel polyamine analogues, based on the previous series of analogues optimised with structural modifications, which are expected to overcome the oral bioavailability problems faced by the previous series. The polyamine analogues possessing both the 3-5-3 and 3-piperazine-3 backbone were successfully synthesised and characterised by making use of previously published methods. The determination of these compounds activity against the *in vitro* proliferation of *P. falciparum* revealed that these analogues possessed lower activities in comparison the previous series. However, these analogues showed similar trends versus drug-resistant parasites by possessing similar selectivity. These compounds were shown to possess low drug-likeness using *in silico* prediction models, however, certain compounds showed considerably better drug-likeness *in silico* in comparison to the previous analogue series. The analysis of SAR using various methodologies allowed for the delineation of the structural requirements for good antiplasmodial activity for the polyamine analogues.

## Chapter 6: References

1. Cox, F.E.G., *History of Human Parasitology*. Clinical Microbiology Reviews, 2002. 15(4): p. 595-612.
2. WHO. *World Malaria Report 2015*. 2015 [cited 2015 05 December]; Available from: [http://www.who.int/malaria/publications/world\\_malaria\\_report\\_2015/wmr2015\\_full\\_report.pdf](http://www.who.int/malaria/publications/world_malaria_report_2015/wmr2015_full_report.pdf).
3. Pouvelle, B., et al., *Cytoadhesion of Plasmodium falciparum ring-stage-infected erythrocytes*. Nature medicine, 2000. 6(11): p. 1264-1268.
4. Krotoski, W., et al., *Demonstration of hypnozoites in sporozoite-transmitted Plasmodium vivax infection*. The American Journal of Tropical Medicine and Hygiene, 1982. 31(6): p. 1291-1293.
5. Richter, J., et al., *What is the evidence for the existence of Plasmodium ovale hypnozoites?* Parasitology Research, 2010. 107(6): p. 1285-1290.
6. Ashley, E., et al., *Malaria*. Travel Medicine and Infectious Disease, 2006. 4(3-4): p. 159-173.
7. Cox-Singh, J., et al., *Plasmodium knowlesi malaria in humans is widely distributed and potentially life threatening*. Clinical Infectious Diseases, 2008. 46(2): p. 165-71.
8. White, N., *Plasmodium knowlesi: the fifth human malaria parasite*. Clinical Infectious Diseases, 2008. 46(2): p. 172-173.
9. Bannister, L.H. and I.W. Sherman, *Plasmodium*. Essential for Life Sciences, 2009.
10. El-Shoura, S., *Falciparum malaria in naturally infected human patients: VIII. Fine structure of intraerythrocytic asexual forms before and during chloroquine treatment*. Applied parasitology, 1994. 35(3): p. 207-218.
11. Miller, S.K., et al., *A subset of Plasmodium falciparum SERA genes are expressed and appear to play an important role in the erythrocytic cycle*. Journal of Biological Chemistry, 2002. 277(49): p. 47524-47532.
12. Garcia, C.R., R.P. Markus, and L. Madeira, *Tertian and quartan fevers: temporal regulation in malarial infection*. Journal of biological rhythms, 2001. 16(5): p. 436-443.
13. Bruce, M., et al., *Commitment of the malaria parasite Plasmodium falciparum to sexual and asexual development*. Parasitology, 1990. 100(02): p. 191-200.
14. Dyer, M. and K. Day, *Commitment to gametocytogenesis in Plasmodium falciparum*. Parasitology Today, 2000. 16(3): p. 102-107.
15. Kar, S. and S. Kar, *Control of malaria*. Nature Reviews Drug discovery, 2010. 9(7): p. 511-512.
16. Alonso, P.L., et al., *A research agenda to underpin malaria eradication*. PLoS medicine, 2011. 8(1): p. e1000406.
17. Van Nieuwenhove, S., et al., *Treatment of gambiense sleeping sickness in the Sudan with oral DFMO (DL- $\alpha$ -difluoromethylornithine), an inhibitor of ornithine decarboxylase; first field trial*. Transactions of the Royal Society of Tropical Medicine and Hygiene, 1985. 79(5): p. 692-698.
18. RBM., *RBM: The Global Malaria Action Plan: For a malaria-free world*. 2008, Geneva: Roll Back Malaria Partnership.
19. Enserink, M., *Redrawing Africa's malaria map*. Science, 2010. 328(5980): p. 842-842.
20. Calderón, F., D.M. Wilson, and F.-J. Gamo, *Antimalarial drug discovery: recent progress and future directions*. Prog Med Chem, 2013. 52: p. 97-151.
21. Agnandji, S.T., et al., *First results of phase 3 trial of RTS,S/AS01 malaria vaccine in African children*. New England Journal of Medicine, 2011. 365(20): p. 1863-75.

22. Seder, R.A., *et al.*, *Protection against malaria by intravenous immunization with a nonreplicating sporozoite vaccine*. *Science*, 2013. 341(6152): p. 1359-1365.
23. Biamonte, M.A., J. Wanner, and K.G. Le Roch, *Recent advances in malaria drug discovery*. *Bioorganic & medicinal chemistry letters*, 2013. 23(10): p. 2829-2843.
24. Fitch, C.D., *Ferriprotoporphyrin IX, phospholipids, and the antimalarial actions of quinoline drugs*. *Life sciences*, 2004. 74(16): p. 1957-1972.
25. Fidock, D.A., *et al.*, *Mutations in the P. falciparum digestive vacuole transmembrane protein PfCRT and evidence for their role in chloroquine resistance*. *Molecular cell*, 2000. 6(4): p. 861-871.
26. Gregson, A. and C.V. Plowe, *Mechanisms of resistance of malaria parasites to antifolates*. *Pharmacological reviews*, 2005. 57(1): p. 117-145.
27. Srivastava, I.K., H. Rottenberg, and A.B. Vaidya, *Atovaquone, a broad spectrum antiparasitic drug, collapses mitochondrial membrane potential in a malarial parasite*. *Journal of Biological Chemistry*, 1997. 272(7): p. 3961-3966.
28. Vaidya, A.B. and M.W. Mather, *Atovaquone resistance in malaria parasites*. *Drug Resistance Updates*, 2000. 3(5): p. 283-287.
29. Peterson, D.S., W.K. Milhous, and T.E. Wellems, *Molecular basis of differential resistance to cycloguanil and pyrimethamine in Plasmodium falciparum malaria*. *Proceedings of the National Academy of Sciences*, 1990. 87(8): p. 3018-3022.
30. O'Neill, P.M., V.E. Barton, and S.A. Ward, *The molecular mechanism of action of artemisinin—the debate continues*. *Molecules*, 2010. 15(3): p. 1705-1721.
31. Robert, A., *et al.*, *The antimalarial drug artemisinin alkylates heme in infected mice*. *Proceedings of the National Academy of Sciences of the United States of America*, 2005. 102(38): p. 13676-13680.
32. Ashley, E.A., *et al.*, *Spread of artemisinin resistance in Plasmodium falciparum malaria*. *New England Journal of Medicine*, 2014. 371(5): p. 411-423.
33. White, N.J., *Antimalarial drug resistance*. *The Journal of Clinical Investigation*, 2004. 113(8): p. 1084-1092.
34. Hyde, J.E., *Drug-resistant malaria*. *Trends in Parasitology*, 2005. 21(11): p. 494-498.
35. Denis, M.B., *et al.*, *Surveillance of the efficacy of artesunate and mefloquine combination for the treatment of uncomplicated falciparum malaria in Cambodia*. *Tropical Medicine & International Health*, 2006. 11(9): p. 1360-1366.
36. Jambou, R., *et al.*, *Resistance of Plasmodium falciparum field isolates to in-vitro artemether and point mutations of the SERCA-type PfATPase6*. *The Lancet*, 2005. 366(9501): p. 1960-1963.
37. Winzeler, E.A. and M.J. Manary, *Drug resistance genomics of the antimalarial drug artemisinin*. *Genome biology*, 2014. 15(11): p. 1-12.
38. Sidhu, A.B.S., *et al.*, *Decreasing pfmdr1 copy number in Plasmodium falciparum malaria heightens susceptibility to mefloquine, lumefantrine, halofantrine, quinine, and artemisinin*. *Journal of Infectious Diseases*, 2006. 194(4): p. 528-535.
39. Ariey, F., *et al.*, *A molecular marker of artemisinin-resistant Plasmodium falciparum malaria*. *Nature*, 2014. 505.
40. Ménard, S., *et al.*, *Induction of multidrug tolerance in Plasmodium falciparum by extended artemisinin pressure*. *Emerging Infectious Diseases*, 2015. 21.
41. Dondorp, A.M., *et al.*, *Artemisinin resistance in Plasmodium falciparum malaria*. *New England Journal of Medicine*, 2009. 361(5): p. 455-467.
42. Ashley, E.A., *et al.*, *Spread of artemisinin resistance in Plasmodium falciparum malaria*. *New England Journal of Medicine*, 2014. 371.
43. Burrows, J.N., *et al.*, *Designing the next generation of medicines for malaria control and eradication*. *Malaria journal*, 2013. 12(1): p. 1.

44. Paloque, L., *et al.*, *Plasmodium falciparum: multifaceted resistance to artemisinin*. Malaria Journal, 2016. 15(1): p. 149.
45. Moinard, C., L. Cynober, and J.-P. de Bandt, *Polyamines: metabolism and implications in human diseases*. Clinical Nutrition, 2005. 24(2): p. 184-197.
46. Nowotarski, S.L., P.M. Woster, and R.A. Casero, *Polyamines and cancer: implications for chemotherapy and chemoprevention*. Expert reviews in molecular medicine, 2013. 15: p. e3.
47. Hamana, K. and S. Matsuzaki, *Polyamines as a chemotaxonomic marker in bacterial systematics*. Critical reviews in microbiology, 1992. 18(4): p. 261-283.
48. Wallace, H.M., A.V. Fraser, and A. Hughes, *A perspective of polyamine metabolism*. Biochemical Journal, 2003. 376(Pt 1): p. 1.
49. Bachrach, U., *Naturally Occurring Polyamines: Interaction with Macromolecules*. Current Protein and Peptide Science, 2005. 6(6): p. 559-566.
50. Davis, R.H., *Management of polyamine pools and the regulation of ornithine decarboxylase*. Journal of cellular biochemistry, 1990. 44(4): p. 199-205.
51. Heby, O., S. Roberts, and B. Ullman, *Polyamine biosynthetic enzymes as drug targets in parasitic protozoa*. Biochemical Society Transactions, 2003. 31(2): p. 415-419.
52. Alhonen-Hongisto, L., P. Seppänen, and J. Jänne, *Intracellular putrescine and spermidine deprivation induces increased uptake of the natural polyamines and methylglyoxal bis (guanylylhydrazone)*. Biochemical Journal, 1980. 192(3): p. 941.
53. Senanayake, M.T., *et al.*, *Design of polyamine-based therapeutic agents: new targets and new directions*. Essays in biochemistry, 2009. 46: p. 77.
54. Igarashi, K. and K. Kashiwagi, *Modulation of cellular function by polyamines*. The international journal of biochemistry & cell biology, 2010. 42(1): p. 39-51.
55. Chattopadhyay, M.K., C.W. Tabor, and H. Tabor, *Absolute requirement of spermidine for growth and cell cycle progression of fission yeast (Schizosaccharomyces pombe)*. Proceedings of the National Academy of Sciences, 2002. 99(16): p. 10330-10334.
56. Mandal, S., *et al.*, *Depletion of cellular polyamines, spermidine and spermine, causes a total arrest in translation and growth in mammalian cells*. Proceedings of the National Academy of Sciences, 2013. 110(6): p. 2169-2174.
57. Urdiales, J.L., M.Á. Medina, and F. Sánchez-Jiménez, *Polyamine metabolism revisited*. European Journal of Gastroenterology & Hepatology, 2001. 13(9): p. 1015-1019.
58. Pegg, A.E., *Mammalian polyamine metabolism and function*. International Union of Biochemistry and Molecular Biology life, 2009. 61(9): p. 880-894.
59. Shantz, L., *et al.*, *Regulation of S-adenosylmethionine decarboxylase activity by alterations in the intracellular polyamine content*. Biochemical Journal, 1992. 288(Pt 2): p. 511.
60. Pegg, A.E., *et al.*, *Regulation of mammalian S-adenosylmethionine decarboxylase*. Advances in Enzyme Regulation, 1988. 27: p. 31-39.
61. Teng, R., *et al.*, *Metabolite profiling of the intraerythrocytic malaria parasite Plasmodium falciparum by 1H NMR spectroscopy*. NMR in Biomedicine, 2009. 22(3): p. 292-302.
62. Clark, K., *et al.*, *Functional consequences of perturbing polyamine metabolism in the malaria parasite, Plasmodium falciparum*. Amino Acids, 2010. 38(2): p. 633-644.
63. Müller, S., *et al.*, *In the human malaria parasite Plasmodium falciparum, polyamines are synthesized by a bifunctional ornithine decarboxylase, S-*



- adenosylmethionine decarboxylase*. Journal of Biological Chemistry, 2000. 275(11): p. 8097-8102.
64. Haider, N., et al., *The spermidine synthase of the malaria parasite Plasmodium falciparum. Molecular and biochemical characterisation of the polyamine synthesis enzyme*. Molecular and Biochemical Parasitology, 2005. 142(2): p. 224-236.
65. Seiler, N., *Catabolism of polyamines*. Amino acids, 2004. 26(3): p. 217-233.
66. Birkholtz, L.M., et al., *Polyamine homeostasis as a drug target in pathogenic protozoa: peculiarities and possibilities*. Biochemistry Journal., 2011. 438: p. 229–244.
67. Wrenger, C., et al., *The Plasmodium falciparum bifunctional ornithine decarboxylase, S-adenosyl-L-methionine decarboxylase, enables a well balanced polyamine synthesis without domain-domain interaction*. Journal of Biological Chemistry, 2001. 276(32): p. 29651-29656.
68. Müller, I.B., et al., *Assessing the polyamine metabolism of Plasmodium falciparum as chemotherapeutic target*. Molecular and Biochemical Parasitology, 2008. 160(1): p. 1-7.
69. Meyskens, F.L. and E.W. Gerner, *Development of difluoromethylornithine (DFMO) as a chemoprevention agent*. Clinical Cancer Research, 1999. 5(5): p. 945-951.
70. Assaraf, Y., et al., *Cytostatic effect of DL- $\alpha$ -difluoromethylornithine against Plasmodium falciparum and its reversal by diamines and spermidine*. Parasitology research, 1987. 73(4): p. 313-318.
71. Reguera, R.M., B.L. Tekwani, and R. Balaña-Fouce, *Polyamine transport in parasites: A potential target for new antiparasitic drug development*. Comparative Biochemistry and Physiology Part C: Toxicology & Pharmacology, 2005. 140(2): p. 151-164.
72. Assaraf, Y., et al., *Polyamine levels and the activity of their biosynthetic enzymes in human erythrocytes infected with the malarial parasite, Plasmodium falciparum*. Biochemical Journal, 1984. 222(3): p. 815.
73. Fukumoto, G.H. and C.V. Byus, *A kinetic characterization of putrescine and spermidine uptake and export in human erythrocytes*. Biochimica et Biophysica Acta (BBA)-Biomembranes, 1996. 1282(1): p. 48-56.
74. Kirk, K., *Membrane transport in the malaria-infected erythrocyte*. Physiological Reviews, 2001. 81(2): p. 495-537.
75. Martin, R.E., H. Ginsburg, and K. Kirk, *Membrane transport proteins of the malaria parasite*. Molecular microbiology, 2009. 74(3): p. 519-528.
76. Singh, S., et al., *Characterization of Simian Malarial Parasite (Plasmodium knowlesi)-induced Putrescine Transport in Rhesus Monkey Erythrocytes a novel putrescine conjugate arrests in vitro growth of simian malarial parasite (plasmodium knowlesi) and cures multidrug resistant murine malaria (plasmodium yoelii) infection in vivo*. Journal of Biological Chemistry, 1997. 272(21): p. 13506-13511.
77. Niemand, J., et al., *Polyamine uptake by the intraerythrocytic malaria parasite, Plasmodium falciparum*. International Journal for Parasitology, 2012. 42(10): p. 921-929.
78. Birkholtz, L., et al., *Polyamine homeostasis as a drug target in pathogenic protozoa: peculiarities and possibilities*. Biochemical Journal, 2011. 438(2): p. 229-244.
79. Weeks, C., et al., *alpha-Difluoromethylornithine, an irreversible inhibitor of ornithine decarboxylase, inhibits tumor promoter-induced polyamine accumulation and carcinogenesis in mouse skin*. Proceedings of the National Academy of Sciences, 1982. 79(19): p. 6028-6032.

80. Gupta, R.D., et al., *3-Aminoxy-1-aminopropane and derivatives have an antiproliferative effect on cultured Plasmodium falciparum by decreasing intracellular polyamine concentrations*. Antimicrobial agents and chemotherapy, 2005. 49(7): p. 2857-2864.
81. Nass, M.M., *Analysis of methylglyoxal bis (guanylhydrazone)-induced alterations of hamster tumor mitochondria by correlated studies of selective rhodamine binding, ultrastructural damage, DNA replication, and reversibility*. Cancer research, 1984. 44(6): p. 2677-2688.
82. Byers, T., et al., *Effects of chronic 5'-[(Z)-4-amino-2-butenyl] methylamino)-5'-deoxy-adenosine (AbeAdo) treatment on polyamine and eIF-5A metabolism in AbeAdo-sensitive and-resistant L1210 murine leukaemia cells*. Biochemistry Journal, 1993. 290: p. 115-121.
83. Barker, R.H., et al., *Novel S-adenosylmethionine decarboxylase inhibitors for the treatment of human African trypanosomiasis*. Antimicrobial agents and chemotherapy, 2009. 53(5): p. 2052-2058.
84. le Roux, D., et al., *Novel S-adenosyl-L-methionine decarboxylase inhibitors as potent antiproliferative agents against intraerythrocytic Plasmodium falciparum parasites*. International Journal for Parasitology: Drugs and Drug Resistance, 2014. 4(1): p. 28-36.
85. Bitonti, A.J., P.P. McCann, and A. Sjoerdsma, *Plasmodium falciparum and Plasmodium berghei: Effects of ornithine decarboxylase inhibitors on erythrocytic schizogony*. Experimental parasitology, 1987. 64(2): p. 237-243.
86. Porter, C.W. and R.J. Bergeron, *Regulation of polyamine biosynthetic activity by spermidine and spermine analogs—a novel antiproliferative strategy*, in *Progress in Polyamine Research*. 1988, Springer. p. 677-690.
87. Pegg, A.E. and R.A. Casero Jr, *Current status of the polyamine research field*, in *Polyamines*. 2011, Springer. p. 3-35.
88. Samal, K., et al., *AMXT - 1501, a novel polyamine transport inhibitor, synergizes with DFMO in inhibiting neuroblastoma cell proliferation by targeting both ornithine decarboxylase and polyamine transport*. International Journal of Cancer, 2013.
89. Wolff, A.C., et al., *A Phase II study of the polyamine analog N1, N11-diethylnorspermine (DENSpm) daily for five days every 21 days in patients with previously treated metastatic breast cancer*. Clinical cancer research, 2003. 9(16): p. 5922-5928.
90. Basu, H.S., et al., *Interaction of a polyamine analogue, 1, 19-bis-(ethylamino)-5, 10, 15-triazanonadecane (BE-4-4-4), with DNA and effect on growth, survival, and polyamine levels in seven human brain tumor cell lines*. Cancer research, 1993. 53(17): p. 3948-3955.
91. Casero, R.A.a. and P.M. Woster, *Terminally Alkylated Polyamine Analogues as Chemotherapeutic Agents*. Journal of Medicinal Chemistry, 2001. 44(1): p. 1-26.
92. Casero, R.A.a. and P.M. Woster, *Recent advances in the development of polyamine analogues as antitumor agents*. Journal of Medicinal Chemistry, 2010. 52(15): p. 4551-4573.
93. Casero, R.A. and P.M. Woster, *Terminally alkylated polyamine analogues as chemotherapeutic agents*. Journal of Medicinal Chemistry, 2001. 44(1): p. 1-26.
94. Saab, N.H., et al., *Synthesis and evaluation of unsymmetrically substituted polyamine analogs as modulators of human spermidine/spermine-N1-acetyltransferase (SSAT) and as potential antitumor agents*. Journal of medicinal chemistry, 1993. 36(20): p. 2998-3004.

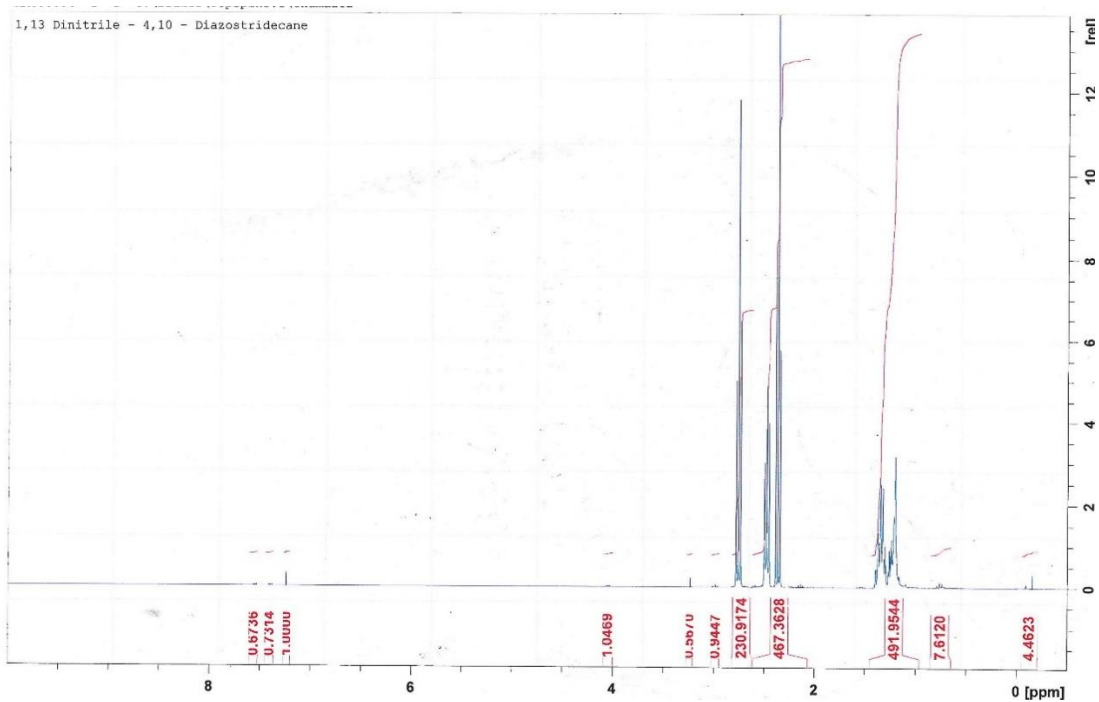
95. Baumann, R., *et al.*, *Suppression of both antimony-susceptible and antimony-resistant Leishmania donovani by a bis (benzyl) polyamine analog*. Antimicrobial agents and chemotherapy, 1990. 34(5): p. 722-727.
96. Bitonti, A.J., *et al.*, *bis (benzyl) polyamine analogs inhibit the growth of chloroquine-resistant human malaria parasites (Plasmodium falciparum) in vitro and in combination with alpha-difluoromethylornithine cure murine malaria*. Proceedings of the National Academy of Sciences, 1989. 86(2): p. 651-655.
97. Bitonti, A., *et al.*, *bis (benzyl) polyamine analogs as novel substrates for polyamine oxidase*. Journal of Biological Chemistry, 1990. 265(1): p. 382-388.
98. Zou, Y., *et al.*, *Novel alkylpolyamine analogues that possess both antitrypanosomal and antimicrosporidial activity*. Bioorganic & medicinal chemistry letters, 2001. 11(12): p. 1613-1617.
99. Ndjonka, D., *et al.*, *The activator-binding site of Onchocerca volvulus S-adenosylmethionine decarboxylase, a potential drug target*. Biological chemistry, 2003. 384(8): p. 1195-1201.
100. Bacchi, C.J., *Chemotherapy of human African trypanosomiasis*. Interdisciplinary perspectives on infectious diseases, 2009. 2009.
101. Bi, X., *et al.*, *Novel alkylpolyaminoguanidines and alkylpolyaminobiguanides with potent antitrypanosomal activity*. Bioorganic & medicinal chemistry letters, 2006. 16(12): p. 3229-3232.
102. Boncher, T., *et al.*, *Polyamine-based analogues as biochemical probes and potential therapeutics*. Biochemical Society Transactions, 2007. 35(2): p. 356-363.
103. Huang, Y., *et al.*, *Inhibition of lysine-specific demethylase 1 by polyamine analogues results in reexpression of aberrantly silenced genes*. Proceedings of the National Academy of Sciences, 2007. 104(19): p. 8023-8028.
104. Zhu, Q., *et al.*, *Polyamine analogs modulate gene expression by inhibiting lysine-specific demethylase 1 (LSD1) and altering chromatin structure in human breast cancer cells*. Amino acids, 2012. 42(2-3): p. 887-898.
105. Sharma, S.K., *et al.*, *(Bis) urea and (bis) thiourea inhibitors of lysine-specific demethylase 1 as epigenetic modulators*. Journal of medicinal chemistry, 2010. 53(14): p. 5197-5212.
106. Verlinden, B.K., *et al.*, *Discovery of novel alkylated (bis) urea and (bis) thiourea polyamine analogues with potent antimalarial activities*. Journal of medicinal chemistry, 2011. 54(19): p. 6624-6633.
107. Verlinden, B.K., *et al.*, *Interrogating alkyl and arylalkylpolyamino (bis) urea and (bis) thiourea isosteres as potent antimalarial chemotypes against multiple lifecycle forms of Plasmodium falciparum parasites*. Bioorganic & medicinal chemistry, 2015.
108. Barnard, B., *Inhibition of lysine-specific demethylase 1 as an antimalarial target by polyamine analogues*, in *Department of Biochemistry*. 2015, University of Pretoria,.
109. Bergeron, R.J., *et al.*, *The role of charge in polyamine analog recognition*. Journal of medicinal chemistry, 1995. 38(13): p. 2278-2285.
110. Kerns, E.H. and D. Li, *Drug-like properties: concepts, structure design and methods*. 2008: Elsevier-Academic Press San Diego CA.
111. Park, B.K., N.R. Kitteringham, and P.M. O'Neill, *Metabolism of fluorine-containing drugs*. Annual Review of Pharmacology and Toxicology, 2001. 41(1): p. 443-470.
112. Uneyama, K., T. Katagiri, and H. Amii,  *$\alpha$ -Trifluoromethylated carbanion synthons*. Accounts of chemical research, 2008. 41(7): p. 817-829.
113. O'Hagan, D., *Fluorine in health care: Organofluorine containing blockbuster drugs*. Journal of Fluorine Chemistry, 2010. 131(11): p. 1071-1081.

114. Cnubben, N.H., *et al.*, *Molecular orbital-based quantitative structure-activity relationship for the cytochrome P450-catalyzed 4-hydroxylation of halogenated anilines*. *Chemical research in toxicology*, 1994. 7(5): p. 590-598.
115. Trager, W. and J.B. Jensen, *Human malaria parasites in continuous culture*. *Science*, 1976. 193(4254): p. 673-675.
116. Chulay, J.D., J.D. Haynes, and C.L. Diggs, *Plasmodium falciparum: Assessment of in vitro growth by [<sup>3</sup>H] hypoxanthine incorporation*. *Experimental parasitology*, 1983. 55(1): p. 138-146.
117. LeRoux, M., V. Lakshmanan, and J.P. Daily, *Plasmodium falciparum biology: analysis of in vitro versus in vivo growth conditions*. *Trends in Parasitology*, 2009. 25(10): p. 474-481.
118. Allen, R.J. and K. Kirk, *Plasmodium falciparum culture: The benefits of shaking*. *Molecular and Biochemical Parasitology*, 2010. 169(1): p. 63-65.
119. Lambros, C. and J.P. Vanderberg, *Synchronization of Plasmodium falciparum erythrocytic stages in culture*. *The Journal of parasitology*, 1979: p. 418-420.
120. Kutner, S., *et al.*, *Characterization of permeation pathways in the plasma membrane of human erythrocytes infected with early stages of Plasmodium falciparum: association with parasite development*. *Journal of cellular physiology*, 1985. 125(3): p. 521-527.
121. Niemand, J., *et al.*, *Anthracene-polyamine conjugates inhibit in vitro proliferation of intraerythrocytic Plasmodium falciparum parasites*. *Antimicrobial agents and chemotherapy*, 2013. 57(6): p. 2874-2877.
122. Smilkstein, M., *et al.*, *Simple and inexpensive fluorescence-based technique for high-throughput antimalarial drug screening*. *Antimicrobial agents and chemotherapy*, 2004. 48(5): p. 1803-1806.
123. Sander, T., *et al.*, *DataWarrior: An Open-Source Program For Chemistry Aware Data Visualization And Analysis*. *Journal of chemical information and modeling*, 2015. 55(2): p. 460-473.
124. Sushko, I., *et al.*, *Online chemical modeling environment (OCHEM): web platform for data storage, model development and publishing of chemical information*. *Journal of computer-aided molecular design*, 2011. 25(6): p. 533-554.
125. Sadowski, J., J. Gasteiger, and G. Klebe, *Comparison of automatic three-dimensional model builders using 639 X-ray structures*. *Journal of chemical information and computer sciences*, 1994. 34(4): p. 1000-1008.
126. Bellevue, F.H., *et al.*, *Structural comparison of alkylpolyamine analogues with potent in vitro antitumor or antiparasitic activity*. *Bioorganic & medicinal chemistry letters*, 1996. 6(22): p. 2765-2770.
127. Edwards, M.L., *et al.*, *Antimalarial polyamine analogs*. *Journal of medicinal chemistry*, 1991. 34(2): p. 569-574.
128. Klenke, B. and I.H. Gilbert, *Nitrile reduction in the presence of Boc-protected amino groups by catalytic hydrogenation over Palladium-activated Raney-Nickel*. *The Journal of organic chemistry*, 2001. 66(7): p. 2480-2483.
129. Weisell, J., *et al.*, *Synthesis and biological characterization of novel charge-deficient spermine analogues*. *Journal of medicinal chemistry*, 2010. 53(15): p. 5738-5748.
130. Karigiannis, G. and D. Papaioannou, *Structure, biological activity and synthesis of polyamine analogues and conjugates*. *European Journal of Organic Chemistry*, 2000. 2000(10): p. 1841-1863.
131. Salvatore, R.N., C.H. Yoon, and K.W. Jung, *Synthesis of secondary amines*. *Tetrahedron*, 2001. 57(37): p. 7785-7811.

132. Banwell, M.G., *et al.*, *RANEY® cobalt—an underutilised reagent for the selective cleavage of C–X and N–O bonds*. *Organic & biomolecular chemistry*, 2014. 12(38): p. 7433-7444.
133. Ertl, G., H. Knözinger, and J. Weitkamp, *Preparation of solid catalysts*. 2008: John Wiley & Sons.
134. Wang, J., Y.-L. Liang, and J. Qu, *Boiling water-catalyzed neutral and selective N-Boc deprotection*. *Chemical communications*, 2009(34): p. 5144-5146.
135. Oshima, T., T. Moriya, and Y. Terui, *Identification, chemical synthesis, and biological functions of unusual polyamines produced by extreme thermophiles*. *Polyamines: Methods and Protocols*, 2011: p. 81-111.
136. Chojceki, A., *et al.*, *Tailoring Raney-catalysts for the selective hydrogenation of butyronitrile to n-butylamine*. *Journal of Catalysis*, 2007. 245(1): p. 237-248.
137. Olliaro, P., *Drug Resistance Hampers Our Capacity to Roll Back Malaria*. *Clinical Infectious Diseases*, 2005. 41(Supplement 4): p. S247-S257.
138. Böhm, H.J., *et al.*, *Fluorine in medicinal chemistry*. *ChemBioChem*, 2004. 5(5): p. 637-643.
139. Wilcken, R., *et al.*, *Principles and applications of halogen bonding in medicinal chemistry and chemical biology*. *Journal of medicinal chemistry*, 2013. 56(4): p. 1363-1388.
140. Rohde, L.A.H., *et al.*, *Intersubunit Bridge Formation Governs Agonist Efficacy at Nicotinic Acetylcholine  $\alpha 4\beta 2$  Receptors unique role of halogen bonding revealed*. *Journal of Biological Chemistry*, 2012. 287(6): p. 4248-4259.
141. Benjahad, A., *et al.*, *3-Iodo-4-phenoxy pyridinones (IOPY's), a new family of highly potent non-nucleoside inhibitors of HIV-1 reverse transcriptase*. *Bioorganic & medicinal chemistry letters*, 2003. 13(24): p. 4309-4312.
142. Freundlich, J.S., *et al.*, *Synthesis, biological activity, and X-ray crystal structural analysis of diaryl ether inhibitors of malarial enoyl acyl carrier protein reductase. Part 1: 4' -substituted triclosan derivatives*. *Bioorganic & medicinal chemistry letters*, 2005. 15(23): p. 5247-5252.
143. Wang, C., *et al.*, *Defining the molecular requirements for the selective delivery of polyamine conjugates into cells containing active polyamine transporters*. *Journal of Medicinal Chemistry*, 2003. 46(24): p. 5129-5138.
144. Ibezim, E., *et al.*, *QSAR on aryl-piperazine derivatives with activity on malaria*. *Chemometrics and Intelligent Laboratory Systems*, 2012. 110(1): p. 81-88.
145. Korfmacher, W.A., *Advances in the integration of drug metabolism into the lead optimization paradigm*. *Mini reviews in medicinal chemistry*, 2009. 9(6): p. 703-716.
146. Milovic, V., *Polyamines in the gut lumen: bioavailability and biodistribution*. *European journal of gastroenterology & hepatology*, 2001. 13(9): p. 1021-1025.
147. Bergeron, R.J., J. Wiegand, and T.L. Fannin, *Control of irritable bowel syndrome with polyamine analogs: a structure–activity study*. *Digestive diseases and sciences*, 2001. 46(12): p. 2615-2623.
148. Larqué, E., M. Sabater-Molina, and S. Zamora, *Biological significance of dietary polyamines*. *Nutrition*, 2007. 23(1): p. 87-95.
149. Van De Waterbeemd, H., *et al.*, *Property-based design: optimization of drug absorption and pharmacokinetics*. *Journal of Medicinal Chemistry*, 2001. 44(9): p. 1313-1333.
150. Lipinski, C.A., *et al.*, *Experimental and computational approaches to estimate solubility and permeability in drug discovery and development settings*. *Advanced Drug Delivery Reviews*, 1997. 23: p. 3-25.

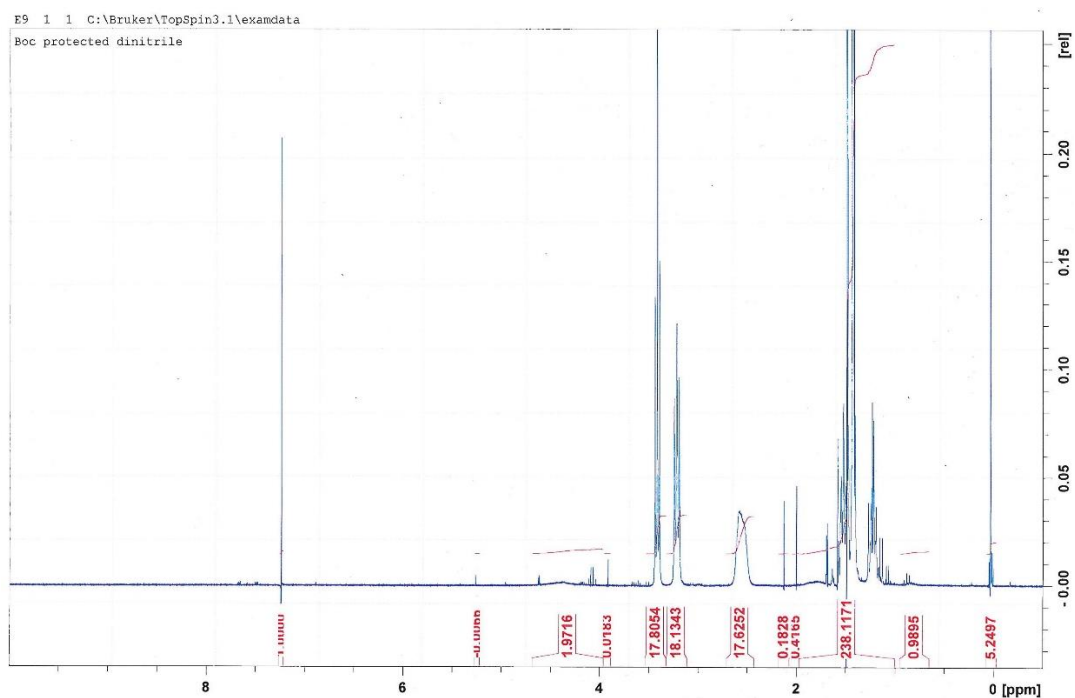
151. Veber, D.F., *et al.*, *Molecular properties that influence the oral bioavailability of drug candidates*. Journal of Medicinal Chemistry, 2002. 45: p. 2615-2623.
152. Seiler, N. and F. Raul, *Polyamines and the intestinal tract*. Critical reviews in clinical laboratory sciences, 2007. 44(4): p. 365-411.
153. Bickerton, G.R., *et al.*, *Quantifying the chemical beauty of drugs*. Nature chemistry, 2012. 4(2): p. 90-98.
154. Larsson, J., *et al.*, *ChemGPS-NP: tuned for navigation in biologically relevant chemical space*. Journal of natural products, 2007. 70(5): p. 789-794.
155. Guha, R. and J.H. Van Drie, *Structure-activity landscape index: identifying and quantifying activity cliffs*. Journal of chemical information and modeling, 2008. 48(3): p. 646-658.

## Appendix:



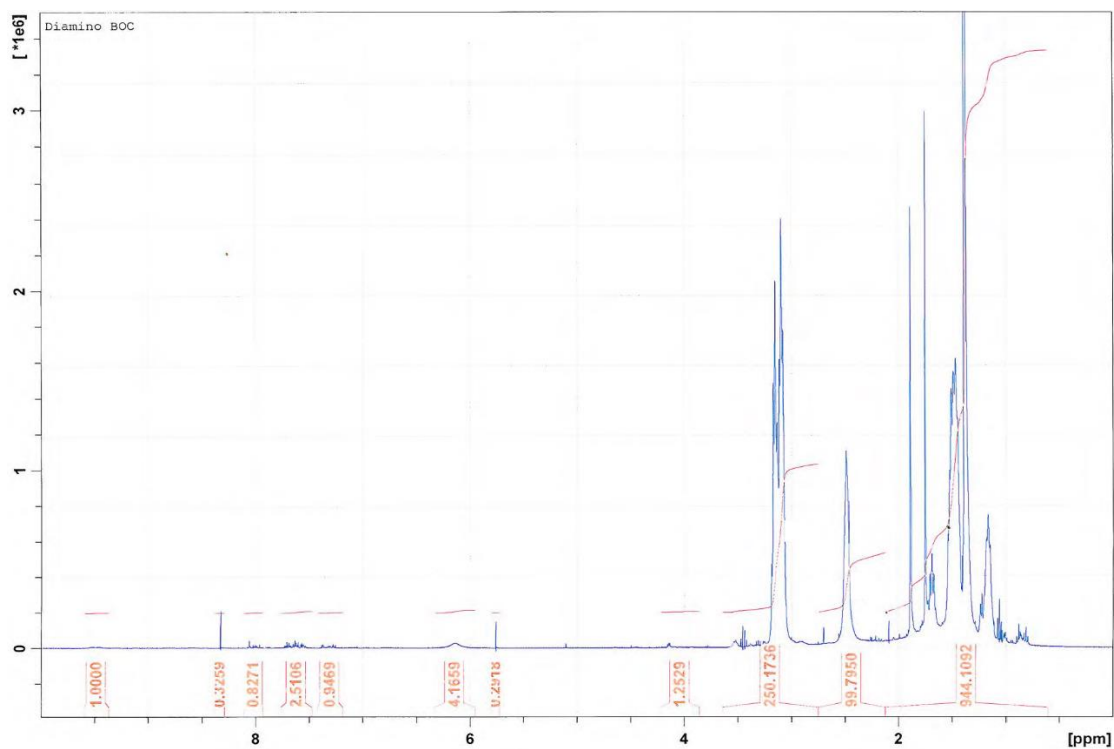
**Appendix figure 1:  $^1\text{H}$  NMR spectrum of 1,13-dinitrile-4,10-diazotridecane (2) showing integration.**

The  $^1\text{H}$  NMR spectrum obtained for (2) in  $\text{CDCl}_3$ .

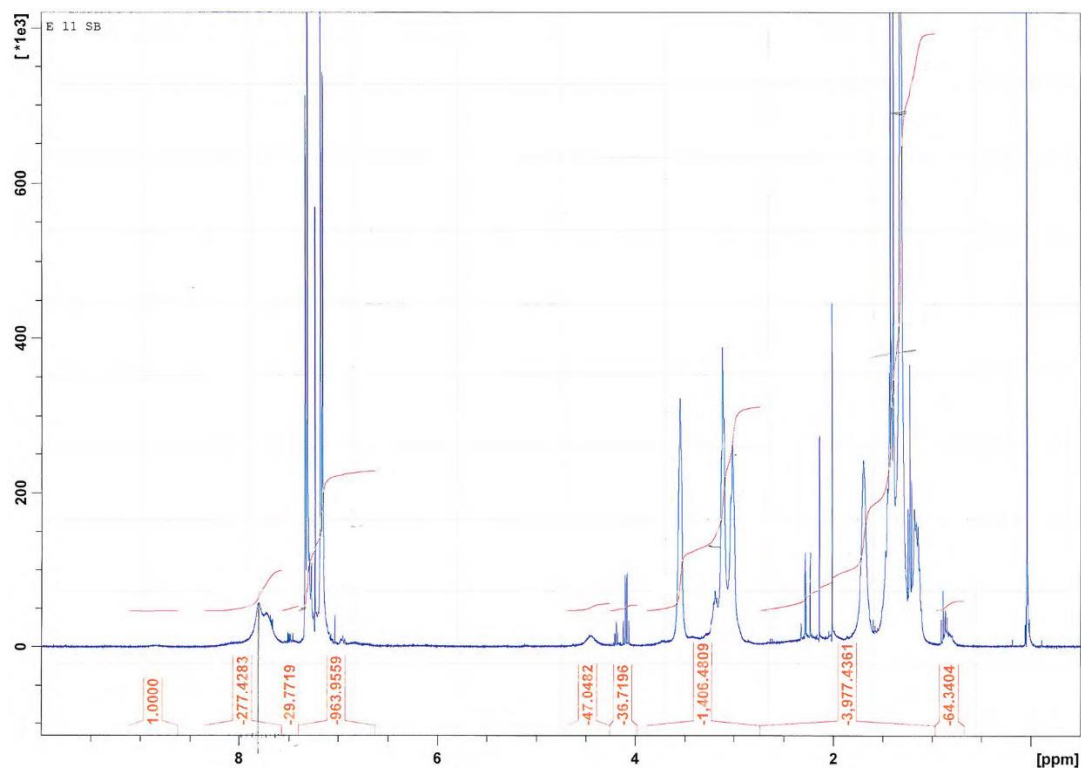


**Appendix figure 2:  $^1\text{H}$  NMR spectrum of 1,13-dinitrile-4,10-(di-tert-butylloxycarbonyl)-4,10-diazotridecane (3) showing integration.**

The  $^1\text{H}$  NMR spectrum obtained for (3) in  $\text{CDCl}_3$ .

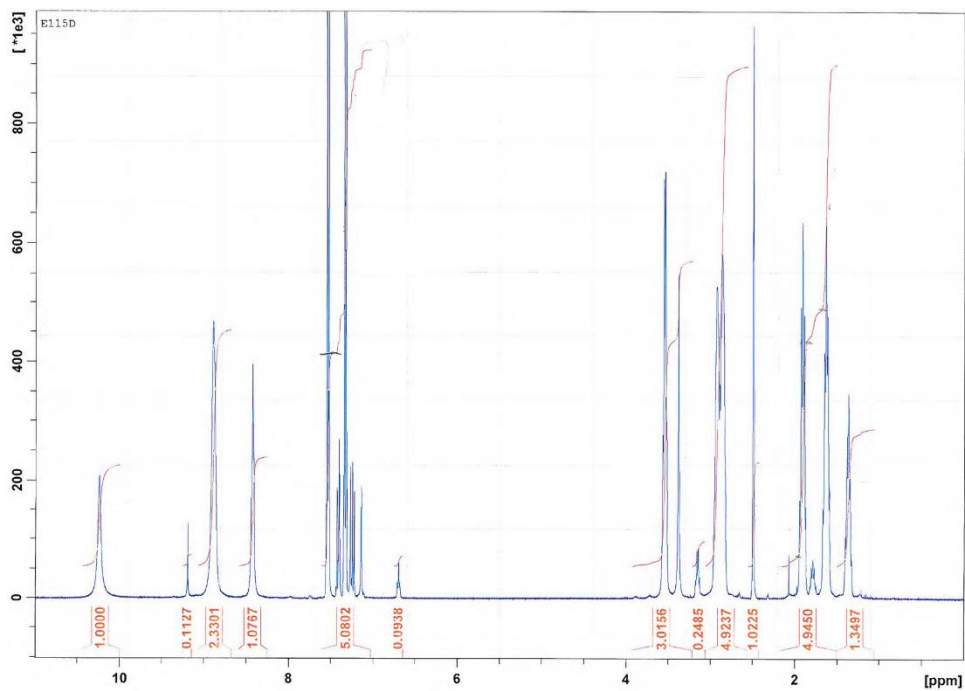


**Appendix figure 3: <sup>1</sup>H NMR spectrum of 1, 13-diamino-4, 10-(di-tert-butylloxycarbonyl)-4, 10-diazotridecane (4) showing integration.**  
The <sup>1</sup>H NMR spectrum obtained for (4) in CDCl<sub>3</sub>.



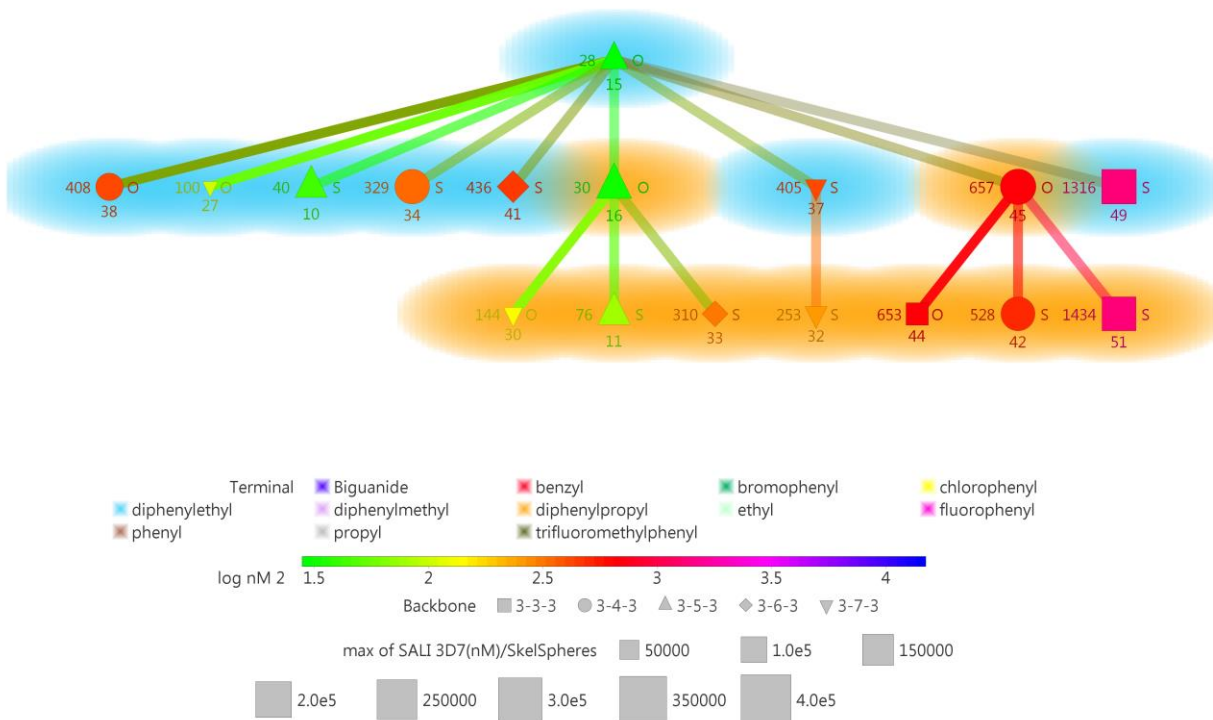
**Appendix figure 4: <sup>1</sup>H NMR spectrum of 1,13-bis-[3-(4-chlorophenyl)thioureido]-4,10-di(tert-butylloxycarbonyl)-4,10-diazotridecane (E1SB) showing integration.**  
The <sup>1</sup>H NMR spectrum obtained for (E1SB) in CDCl<sub>3</sub>.





**Appendix figure 5: <sup>1</sup>H NMR spectrum of 1,13-bis-[3-(4-chlorophenyl)thioureido]- 4,10-diazatridecane (E1SD) showing integration.**  
The <sup>1</sup>H NMR spectrum obtained for E1SD in DMSO-d<sub>6</sub>.




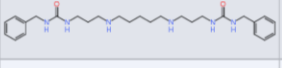

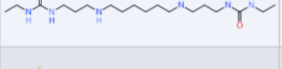
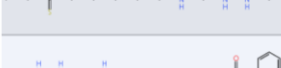
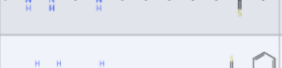
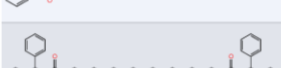
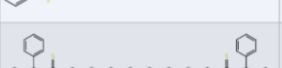



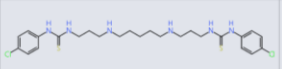



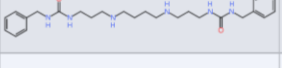


















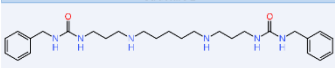
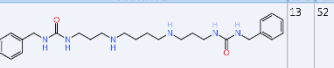

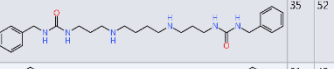


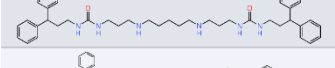



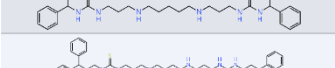





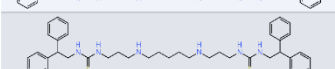

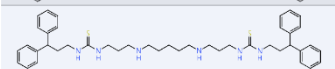
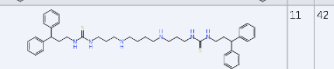


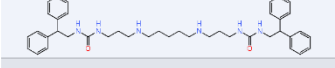



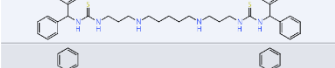

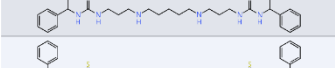
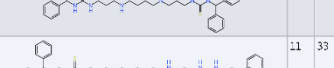
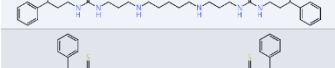
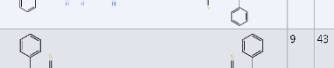
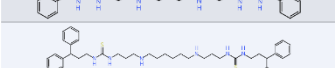

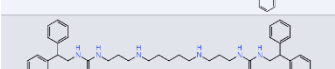


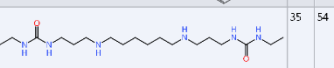
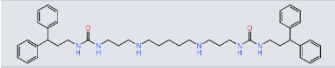


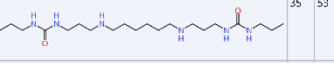




**Appendix figure 6: Neighbour tree analysis of compound 15 at 80% similarity.**

The neighbour tree analysis indicates connects analogues' possessing 80% similarity, showing terminal substitutions' with background colour, Log IC<sub>50</sub> (Log nM) with the colour of the marker, backbone identities are indicated by the marker shape.

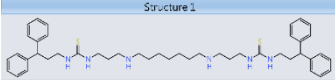
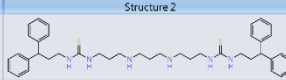


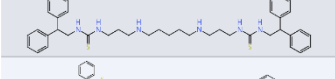

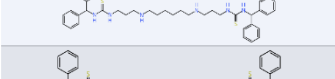

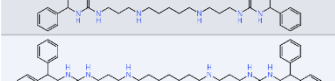
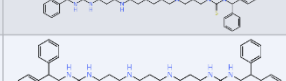





**Appendix Table 2A: Top 20% SALI summary MMP analysis of polyamine analogues separated on backbone.**

Structure 1	Structure 2	ID1	ID2	Similarity	Activity 1	Activity 2	Delta Acti...	SALI	Backbone
		27	37	0.97211	100	405	305	10935	7
		8	13	0.95764	249	793	544	12842	5
		53	54	0.93058	14084	15000	916	13195	6
		39	50	0.93058	425	1353	928	13367	6
		7	47	0.95595	88	846	758	17206	6
		29	43	0.97081	131	641	510	17470	7
		E11S	E15S	0.95764	1175	417	758	17894	5
		E11O	E11S	0.95764	326	1175	849	20042	5
		44	51	0.97081	653	1434	781	26753	3
		36	52	0.95595	355	3475	3120	70822	4
		35	53	0.80911	339	14084	13745	72006	6
		35	54	0.81758	339	15000	14661	80372	6
		50	53	0.86285	1353	14084	12731	92825	6
		39	54	0.85572	425	15000	14575	101020	6
		50	54	0.93686	1353	15000	13647	216140	6
		39	53	0.9428	425	14084	13659	238810	6

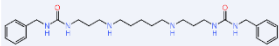
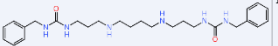
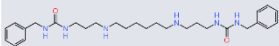
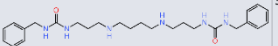









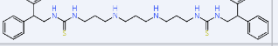




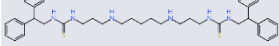
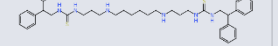
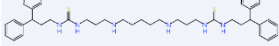

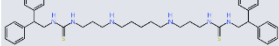
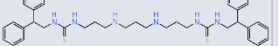
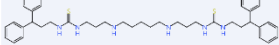
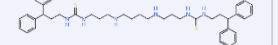
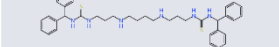
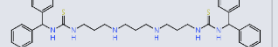
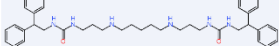
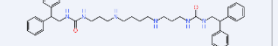
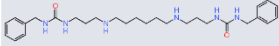
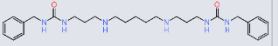

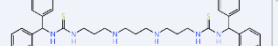

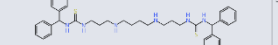

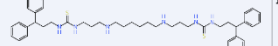






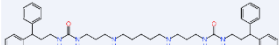
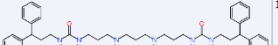
**Appendix Table 2B: Top 20% SALI summary MMP analysis of polyamine analogues separated based on internal substituents.**

Structure 1	Structure 2	ID 1	ID 2	Similarity	Activity 1	Activity 2	Delta Acti...	SALI	Internal
		13	52	0.99368	793	3475	2682	424100	O
		35	52	0.98783	339	3475	3136	257650	O
		31	43	0.99823	211	641	430	242360	S
		16	45	0.99679	30	637	627	195230	O
		34	49	0.99465	329	1316	987	184540	S
		14	46	0.99646	47	691	644	182060	O
		42	51	0.9949	528	1434	906	177750	S
		10	41	0.99753	40	436	396	160040	S
		11	51	0.99136	76	1434	1358	157250	S
		10	49	0.99094	40	1316	1276	140910	S
		11	42	0.99679	76	528	452	140740	S
		40	48	0.99438	433	1081	648	115270	S
		15	38	0.99663	28	408	380	112840	O
		13	35	0.9958	793	339	454	107980	O
		9	48	0.99049	68	1081	1013	106510	S
		9	40	0.99646	68	433	365	103190	S
		11	33	0.99764	76	310	234	99088	S
		9	43	0.99421	68	641	573	99015	S
		33	51	0.98743	310	1434	1124	89447	S
		10	34	0.99663	40	329	289	85915	S
		35	54	0.81758	339	15000	14661	80372	O
		16	44	0.99136	30	633	623	72140	O
		35	53	0.80911	339	14084	13745	72006	O

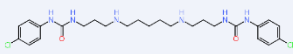
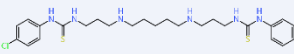

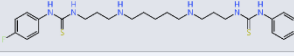

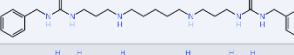
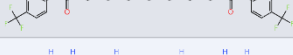
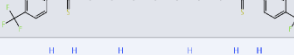








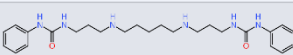
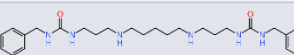
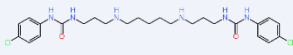
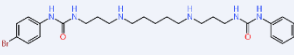
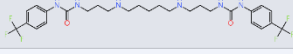





**Appendix Table 2B: Top 20% SALI summary MMP analysis of polyamine analogues separated based on internal substituents continued.**

Structure 1	Structure 2	ID 1	ID 2	Similarity	Activity 1	Activity 2	Delta Acti..	SALI	Internal
		32	51	0.98321	253	1434	1181	70352	5
		41	49	0.98683	436	1316	880	66828	5
		10	37	0.99448	40	405	365	66153	5
		31	48	0.98618	211	1081	870	62949	5
		9	31	0.9974	68	211	143	55064	5
		37	49	0.98242	405	1316	911	51820	5
		30	45	0.99002	144	657	513	51401	0
		29	46	0.98904	131	691	560	51082	0

**Appendix Table 2C: Top 20% SALI summary MMP analysis of polyamine analogues separated on terminal.**

Structure 1	Structure 2	ID 1	ID 2	Similarity	Activity 1	Activity 2	Delta Activity	SALI	Terminal
		13	52	0.99368	793	3475	2682	424100	benzyl
		35	52	0.98783	339	3475	3136	257650	benzyl
		31	43	0.99823	211	611	430	242360	diphenylmeth
		39	53	0.9428	425	14084	13659	238810	propyl
		50	54	0.93686	1353	15000	13647	216140	ethyl
		16	45	0.99679	30	657	627	195230	diphenylprop
		34	49	0.99465	329	1316	987	184540	diphenylethyl
		14	46	0.99646	47	691	644	182060	diphenylmeth
		42	51	0.9949	528	1434	906	177750	diphenylprop
		10	41	0.99753	40	436	396	160040	diphenylethyl
		11	51	0.99136	76	1434	1358	157250	diphenylprop
		10	49	0.99094	40	1316	1276	140910	diphenylethyl
		11	42	0.99679	76	528	452	140740	diphenylprop
		40	48	0.99438	433	1081	648	115270	diphenylmeth
		15	38	0.99663	28	408	380	112840	diphenylethyl
		35	13	0.9958	339	793	454	107980	benzyl
		9	48	0.99049	68	1081	1013	106510	diphenylmeth
		9	40	0.99646	68	433	365	103190	diphenylmeth
		11	33	0.99764	76	310	234	99098	diphenylprop
		9	43	0.99421	68	641	573	99015	diphenylmeth
		33	51	0.98743	310	1434	1124	89447	diphenylprop
		10	34	0.99663	40	329	289	85815	diphenylethyl
		16	44	0.99136	30	653	623	72140	diphenylprop

**Appendix Table 3: Top 20% SALI summary MMP analysis of polyamine analogues of the 3-5-3 backbone.**

Structure 1	Structure 2	ID 1	ID 2	Similarity	Activity 1	Activity 2	Delta Act.	SALI	Backbone
		E110	E115	0.95764	326	1175	849	2042	5
		E115	E155	0.95764	1175	417	758	17894	5
		8	13	0.95764	249	793	544	12842	5
		E170	E175	0.96519	710	1088	378	10860	5
		E125	E200	0.89385	1175	163	1012	95335	5
		E115	E150	0.8991	1175	439	736	7294.5	5
		F150	F200	0.95764	439	163	276	6515.5	5
		12	E115	0.81309	246	1175	929	4970.3	5
		E155	E175	0.86274	417	1088	671	4888.7	5
		12	13	0.88156	246	793	547	4618.5	5
		E110	E200	0.95764	326	163	163	3847.9	5
		E170	E200	0.85253	710	163	547	3709.2	5
		12	F170	0.83415	246	710	464	2797.7	5